DYNAMIC BEHAVIOUR OF COMPOSITE SANDWICH BEAMS AND PLATES WITH DEBONDS

A Thesis submitted by

Indunil Nayanakanthi Jayatilake

For the award of

Doctor of Philosophy

Centre for Future Materials
School of Civil Engineering and Surveying
Faculty of Health, Engineering and Sciences
University of Southern Queensland
Queensland, Australia

2017

DEDICATION

This thesis is dedicated to my beautiful daughter Venuri, who has been a constant source of support and encouragement throughout. Thanks for always being there for me and for your endless love!

ABSTRACT

Fibre Reinforced Polymer (FRP) composites are continuing to gain prominence in structural as well as non-structural applications all over the world due to their outstanding properties such as high strength to weight ratio, corrosion resistance, good thermal performance, anti-fire performance and reduction of carbon dioxide emissions both through its method of production and their effective thermal insulation qualities. The increased popularity and demand for FRP composites have spurred research efforts in both academia and civil construction industry.

A composite sandwich structural element can be made-up by attaching two thin and stiff skins to a lightweight and thick core, which serves as a building block for constructing laminated structural sandwich composites for civil engineering applications. A structural composite multilayer beam or plate can be manufactured by gluing two or more composite sandwiches together to form a laminated composite. An Australian manufacturer has fabricated a new generation structural Glass Fibre Reinforced Polymer (GFRP) sandwich panel made from E-glass fibre skin and a high strength modified phenolic core for civil engineering applications, the outstanding features of the sandwich material being high strength to weight ratio, good thermal insulation and termite resistance. These features offer the composite panel a wide range of applications in Australian construction industry as structural elements such as beams, slabs, bridge decks and railway sleepers.

While sandwich composite construction has some great benefits, the behaviour of sandwich structures containing damage is much more complex and one of the major factors limiting the optimum usage of the same. Although perfect bond between the skin and the core is a common assumption, an important issue that needs to be considered in using a composite beam or slab is the development of debonding between the skin and the core, which is a predominant damage mode of these sandwiches. Interlayer debonding or delamination is also a predominant form of damage phenomenon in laminated composites, which can often be pre-existing or can take place under service conditions. Debonding and delamination cause

significant changes in the vibration parameters, such as natural frequencies and mode shapes of structures leading to serviceability issues related to deflection limits. During the design stages of FRP composite structures, it is vital to identify how the global response of these structures will be affected by skin-core debonding and interlayer delamination.

Even though the dynamic behaviour of undamaged sandwich panels is the subject of extensive research, papers reported on the dynamic behaviour of sandwich panels with debonding are less presented in the literature. Specifically, knowledge on seismic behaviour of composites with debonds is severely limited. Further research is therefore needed into investigation of the dynamic behaviour of debonded composite structural elements to gain wider acceptance of composites by the structural composite field around the globe. Finite element method is particularly versatile and effective in the analysis of complex structural behaviour of the composite structures. The use of dynamic analysis methods helps the engineer to better understand the behaviour of a structure subjected to an earthquake.

This research deals with the investigation of the influence of debonding on the dynamic characteristics of novel GFRP beams and plates by finite element based numerical simulations and analyses using STRAND7 finite element (FE) software package. The research approach is to develop a three dimensional computer model and conduct numerical simulations to assess the dynamic behaviour. The FE model developed has been validated with published experimental, analytical and numerical results for fully bonded as well as debonded beams and slabs. Dynamic seismic response investigation of structures containing GFRP slab panels with debonds subjected to a probable earthquake loading is also incorporated. The influence of various factors such as debonding size, location of debonding, boundary condition of the structural member and the effect of multiple debonding has been delineated with the aid of an extensive parametric investigation and comparative analyses.

Generally it was evident from all the analyses that debonding and interlayer delamination cause reduction in magnitudes of natural frequency. Moreover, some vibration modes and accordingly the mode shapes are also noticeably changed. It is generally observed that higher natural frequencies and mode shapes are more influenced by the presence of debonding. Yet there are exceptions to this trend depending on how severely the local modes are affected by debonding. It is observed that the associated mode shapes explain the causes of these

inconsistencies. Furthermore, the results show that the presence of relatively small debonding or delamination has an insignificant effect on the natural frequencies and associated mode shapes. The results also suggest that fastening the delamination region is an effective corrective measure in decreasing the natural frequency variation, hence improving its dynamic performance compared to the delaminated panel.

To sum up, the results suggest that debonding and delamination predominantly leads to reduction of the natural frequencies and modifying the modes of vibrations thus altering the mode shapes as well, resulting in dramatic changes in dynamic characteristics when extents of debonding are large. The more the supports are restrained, the greater the influence on free vibration characteristics. Most importantly, the findings demonstrate the feasibility of non-destructive methods to detect debonding and delamination damage in practical composite structures. The results of the seismic study show that the seismic performance of the considered buildings is unresponsive to small percentages of debonding of the GFRP slab panels. An existence of extensive percentage of debonding causes a slight increase in the maximum vertical displacement and reduction of natural frequencies of the buildings due to loss of stiffness occurring due to debonding.

The results of this study will offer engineers and designers a better understanding of the influence of debonding and delamination on the dynamic performance of FRP composites in general, in addition to its direct application to Australian composite industry. Finally, the study provides valuable insights into the seismic behaviour of composite slabs with debonding thus facilitating the actual application of these findings in worldwide composite industry.

Certification of Thesis

This thesis is entirely the work of Indunil Nayanakanthi Jayatilake except where otherwise acknowledged. The work is original and has not previously been submitted for any other award, except where acknowledged.

Student and supervisors signatures of endorsement are held at USQ.

_____

Principal Supervisor

_____

Associate Supervisor

Acknowledgments

First, I would like to express my deepest gratitude and appreciation to my principal supervisor, Prof Karu Karunasena for giving me the opportunity, continuous guidance, encouragement, expert advice and continued support and also being patient and accessible for comments throughout the years of my doctoral study. He always had constructive suggestions, answered my frequent questions and made every effort to help me in completing my research project. I also wish to express my sincere gratitude to my associate supervisor Dr Weena Lokuge for her continuous help and guidance in numerous ways.

I would like to thank Dr Vasantha Abeysekera for his support to secure the scholarship for my studies. I also would like to thank Prof Amando Apan for his support and encouragement especially at the initial stages of my research project. I wish to acknowledge the financial support provided to me by USQ through the APA Scholarship during my study period. I would like to acknowledge the support of the Faculty of Health, Engineering and Sciences and the Centre for Future Materials. I greatly appreciate Associate Dean (Research and Research Training) Prof Thiru Aravinthan for his kind support and guidance. Appreciation is also extended to my confirmation committee for their time and suggestions. Special thanks to Nayana Kumarapeli and all the library staff at Springfield for their kindness and support throughout. I wish to express my deep appreciation to Mrs Juanita Ryan, Dr Mark Emmerson and Mr Lester Norris for kindly answering all my queries regarding administrative matters related to my studies and their immense support and clarifications.

My very special thanks go to Susantha for his wholehearted support in editing and proof reading. His immense patience and quick response whenever approached deserve warm appreciation. I am also much grateful to Jeff Miller and Elizabeth McCarthy for their kind support in formatting the thesis. From all my heart, I would like to thank my beautiful daughter Venuri for her endless love and continuous support without which this thesis would not have been possible. Your love, encouragement and endless support kept me going. My special thanks go to my husband Asoka for standing by my side when things were not going smoothly and encouraging me. I would also like to thank my son Ashan and sister Kumari for their love and continued support throughout. Finally, I wish to thank all those who have helped me to carry out this research successfully.

ASSOCIATED PUBLICATIONS

Journals

- Jayatilake, Indunil., Karunasena, Warna. & Lokuge, Weena. (2016). Finite element based dynamic analysis of multilayer fibre composite sandwich plates with interlayer delaminations. *Advances in Aircraft and Spacecraft Science,* 3 (1), 15-28.

- Jayatilake, I., Karunasena, W. & Lokuge, W. (2015). Influence of Single and Multiple Skin-Core Debonding on Free Vibration Characteristics of Innovative GFRP Sandwich Panels'. *International Journal of Mechanical, Aerospace, Industrial and Mechatronics Engineering*, 9(5), 723 - 727.

- Jayatilake, Indunil., Karunasena, Warna. & Lokuge Weena. (2013). Dynamic Behaviour of Debonded GFRP Composite Beams. *Journal of Multifunctional composites*, 1 (2), 113-122.

Refereed conference proceedings

- Jayatilake, Indunil N. and Karunasena, Warna and Lokuge, Weena (2014). Dynamic analysis of multilayer GFRP sandwich slabs with interlayer delaminations. In: 8th Australasian Congress on Applied Mechanics (ACAM 8), 24–28 Nov 2014, Melbourne, Australia.

- Jayatilake, Indunil and Karunasena, Warna and Lokuge, Weena (2014) Dynamic behaviour of fibre composite multilayer sandwich plates with delaminations.. In: 23rd Australasian Conference on the Mechanics of Structures and Materials (ACMSM23), 9-12 Dec 2014, Byron Bay, Australi

- Jayatilake, Indunil. Karunasena, Warna and Lokuge, Weena. (2013*).* Effect of skin-core debonding on the dynamic behaviour of GFRP composite beams. Fourth Conference on Smart Materials and Nanotechnology in Engineering 2013, 10-12 July 2013, Gold Coast, Australia

- Karunasena, W., Jayatilake, I. and Lokuge, W. (2013). Free vibration behaviour of fibre composite sandwich beams with debonds. In: 4th International Conference on Structural Engineering and Construction Management 2013 (ICSECM 2013), 13-15 Dec 2013, Kandy, Sri Lanka.

TABLE OF CONTENTS

LIST OF FIGURES

LIST OF TABLES

NOTATIONS

a	Debonding length
[A]	Membrane elasticity matrix
b	Width of the beam
[B]	Extensional/bending coupling matrix
[C]	Viscous damping matrix
C_h	Spectral shape factor
c_i, c_j	Damping coefficients of modes *i* and *j*
[D]	Bending stiffness matrix
DC	Damping coefficient
E	Elastic modulus
[F]	Dynamic load for the system
G	Shear modulus
h_{st}	Top skin thickness
h_{sb}	Bottom skin thickness
h_c	Core thickness
H	Height of the building
[K]	Stiffness matrix
$k_{F,i}$	Seismic distribution factor for level *i*
k_p	Probability factor
L	Length of the beam
[M]	Mass matrix
n	Number of levels in a structure
{N}	Resultant force vector
{P}	Resultant moment vector
[Q]	Lamina stiffness matrix
$[\overline{\mathbf{Q}}_k]$	Elasticity matrix for ply k
{R}	Load vector for a particular load case
{r}	Seismic direction vector
[S]	Lamina compliance matrix
S_p	Structural performance factor

S_i	Ordinate in the design spectrum at the frequency of i^{th} mode
s	Total response of the structure
[T]	Transformation matrix
{U}, {$\dot{U}$} & {$\ddot{U}$}	Node displacements, velocities, and accelerations
V	Base shear force
W_i	Seismic weight at level i
W_t	Seismic weight; the sum of seismic weight at each level (W_i)
{x}	Vibration mode factor
{y}	Modal coordinate vector
Z	Hazard factor
α and β	Stiffness and mass proportional damping constants
ζ	Modal damping
y_i	Modal displacement
r_i	Modal load
$\{\phi_i\}$	*i*-th mode shape vector
σ	Stress
ε	Strain
ν	Poisson's ratio
$\{\varepsilon^m\}$	Mid-plane membrane strain vector
$\{\boldsymbol{\kappa}\}$	Laminate plate curvature vector
$\{\phi_i\}$	i-th eigenvector
μ	Structural ductility factor
ω_{ni}, ω_{nj}	Angular natural frequencies of modes *i* and *j*

CHAPTER 1 INTRODUCTION

1.1 Background to the study

Fibre Reinforced Polymer (FRP) composites enjoy an array of applications ranging from aerospace, military and automotive to marine, recreational and civil industry due to their outstanding properties such as high strength to weight ratio, corrosion resistance, good thermal performance and reduction of carbon dioxide emissions both through its method of production and their effective thermal insulation qualities. FRP composites are increasingly being considered as a substitute and enhancement for infrastructure systems that are constructed of traditional civil engineering materials such as concrete and steel. Some disadvantages of FRP materials include brittleness and vulnerability to damage by ultraviolet light from exposure to sunlight, affecting their outdoor applications (Jain & Lee 2012). Although the relatively high production and material costs are considered as major drawbacks preventing FRP composites to be fully embraced for structural applications, when the cost of the structures is considered over its entire life cycle, the improved durability qualities of FRP material can make them the most cost-effective material in many instances (Gand et al. 2013).

Planners, developers, architects and builders are becoming more aware of the climate change impacts of construction materials and are increasingly including climate change considerations in their selection of materials for building projects (Buenett 2006). According to Mara et al. (2014), the energy consumption and carbon emissions of bridge constructions with FRP decks are usually less than those of bridges with conventional material. A study performed by the BECO Group (Netherlands) showed that the carbon emissions for a 12 m long road bridge composed of a Glass Fibre Reinforced Polymer (GFRP) composite superstructure were reduced by 48% compared with a concrete bridge as illustrated by Figure 1.1 (Mara et al. 2014). In the Figure 1.1 CFRP stands for Carbon Fibre Reinforced Polymer.

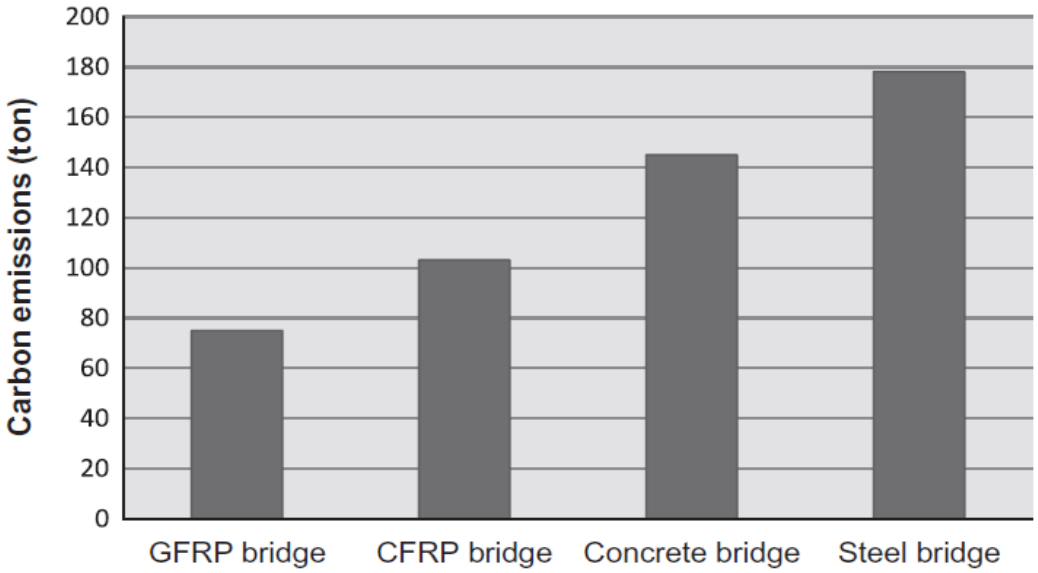

Figure 1.1 Comparison of carbon emissions for four bridges composed of different materials (Mara et al. 2014).

In the context that the development and use of new construction materials that are structurally efficient and environmentally green are becoming crucial in the reduction of carbon emissions, FRP building elements are proven a sustainable option. In the Australian context, there is an ever increasing demand for composites as an alternative to Australian hardwood that have been used for a wide range of applications including piles, railway sleepers and bridge components, due to the increasing cost, shortage and decline in quality of hardwood components.

Fibre-reinforced composites are made up of a combination of fibres in a matrix material. The fibres can be made of various materials including glass fibres which are the most commonly used due to its cost effectiveness, wide availability and history of good experience in service (Reinhart 1998). Glass fibre reinforced polymer composites are two phase materials with glass fibre acting as dispersed phase and polymer as the matrix. GFRP sandwiches are fabricated by attaching two stiff glass fibre skins (commonly known as face-sheets) to a thick core to form a single layer composite sandwich, which can be used for beam or slab type structural applications. A structural composite multilayer plate can be manufactured by gluing two or more composite sandwiches together to form a laminated composite.

A new generation composite sandwich made up of GFRP skins and high strength phenolic core material has been developed in Australia. Compared to the traditional sandwich panels, the new GFRP sandwich panel has a higher core density resulting in an improved structural behaviour (Awad et al. 2012a). The new panel composition comprises approximately 15 kg of polymer per square meter, and 65 % of this polymer is plant based, and it has a carbon foot print similar to timber making it environmentally sustainable, in addition to improved strength characteristics (Van-Erp 2010). Since a major percentage of the polymers used in the panel are plant-based, the atmospheric carbon absorbed by these plants during their growth becomes permanently locked into the panel during the manufacturing process, and, by recycling the panel at the end of its life this carbon will not be returned to the atmosphere, thus reducing the carbon footprint of the construction industry (Aravinthan 2008). Figure 1.2 illustrates the results of a study conducted to compare the energy consumption of the novel GFRP with four other common building material options (Aravinthan 2008). It is clear from Figure 1.2 that the novel GFRP uses significantly less energy than the traditional building materials.

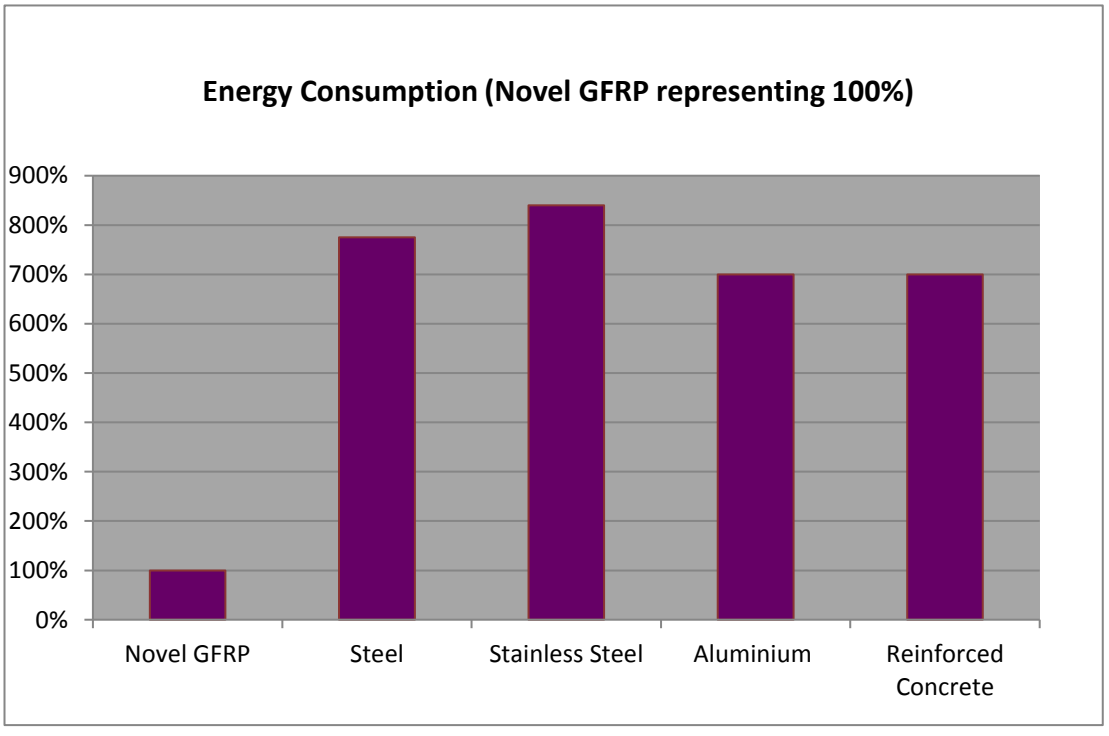

Figure 1.2 Comparison of energy consumption for novel GFRP and four common building materials (Aravinthan 2008).

The outstanding features of this sandwich material include high strength to weight ratio, good thermal insulation and termite resistance. These features offer the composite panel a wide range of applications in Australian construction industry as structural elements such as beams, slabs, bridge decks and railway sleepers. These applications require the panels to be manufactured from individual fibre composite sandwich panels (to form single layer beams or slabs consisting of 'skin-core-skin' glued together) or by gluing two or more of these layers of sandwich panels together to form a laminated composite. Figure 1.3 exemplifies samples of single layer and four layer (glue laminated) novel GFRP sandwich beams.

(a) Single GFRP sandwich beams (b) Four layer glue laminated GFRP sandwich beams

Figure 1.3 Samples of single layer and multilayer novel GFRP sandwich beams (Awad et al. 2012b).

According to Aravinthan and Manalo (2012), while fibre composites are reaching a point of commercial reality in the Australian construction industry, challenges faced by the structural designer include, the understanding of the behaviour of the fibre composite materials, its failure modes and applying available design guidelines to the local needs.

Although traditional construction materials such as concrete, steel, and timber are cheaper than the FRP materials, they have several drawbacks due to their low durability, and high self-weight adding much dead weight to the structure and significantly increasing the size of the members making it difficult during transporting and handling. These advantages of composites over the traditional structural materials have led to an increasing interest in the computational simulation

of such materials when designing composite structures. With the rapid growth in computer facilities, analysis of three-dimensional models with large degrees of freedom has been made possible. Most of these computer programs are based on the Finite Element Analysis (FEA) Method for discretizing the structure to produce a mathematical model that can be used within the context of numerical solution procedures. The FEA method is capable of dealing with the complex characteristics of fibre composite materials including their geometry and layout, material properties and their behaviour, and multi-layer (laminated) nature.

Earthquakes are normally considered to be among the worst natural disasters on Earth. Every year, earthquakes take the lives of thousands of people, and destroy property worth billions of dollars. Earthquakes of minor to moderate magnitude can affect virtually any urban area and may be associated with disasters in vulnerable areas. The Australian continent lies solely within the Indo-Australian Plate, and hence Australian earthquakes are typical examples of intra-plate type. The Newcastle mainshock of 28 December 1989 is one typical example of how an intra-plate earthquake with moderate magnitude can cause loss of life and extensive damage if it occurs close to a population centre (Sinadinovski et al. 2000). It is of utmost importance that structures are designed to resist earthquake forces, in order to reduce the loss of life.

Inertial forces are the product of mass and acceleration. Since the earthquake forces are inertial, an increase in the mass generally results in an increase in the force, hence the immediate virtue of the use of lightweight construction as a seismic design approach (Arnold & Reitherman 1982). In this context, the use of lightweight FRP slab panels to replace heavy weight reinforced concrete (R/C) slabs in a R/C building would be effective in improving seismic performance. The seismic performance evaluation is the most urgent issue for seismic hazard mitigation. The use of dynamic analysis methods helps the engineer to better understand the behaviour of a structure subjected to an earthquake. Without this understanding, the design may be less reliable.

Resonance is the tendency of a structure to respond at much higher amplitude when the frequency of its oscillation (working frequency) matches the system’s natural

frequency of vibration. If resonance is allowed to develop in a structure, it can result in an unacceptably high vibration and damage, which eventually can lead to structural failure. Hence avoiding resonance is a major concern in designing any structure. Normally structures are designed to resonate at a frequency that does not normally occur during its useful life. Especially buildings in seismic areas are designed taking into consideration the oscillating frequencies of predicted seismic ground motions.

While sandwich composite construction has some great benefits, the behaviour of sandwich structures containing damage is much more complex and one of the major factors limiting the optimum usage of them. Due to complex manufacturing methods, composite sandwiches can contain a variety of defects. A composite sandwich is basically made of three components; a top skin, a middle core and a bottom skin. Sandwich structure relies on the adhesive bond between the skins (also called face-sheets) and core for its overall stability and consistency. A region where there is no bond is called a debond. Skin-core debonding (hereinafter called 'debonding') arises as a result of manufacturing defects when a small region between the face sheet and the core has not been adequately bonded or during handling or under service conditions such as impact loading. In real structures, depending on the loading conditions, this debond may propagate creating larger debonding areas, and in fibre composite beams, this can result in debonding occurring across the full width of the beam, which may cause changes to the free vibration behaviour in addition to the strength degradation. When the natural frequency of the debonded structure is close to its working frequency, resonance could happen, which may lead to excessive vibrations and failure of the structure. Debonds are inherent potential cause for the structural failures in adhesively bonded composite structures (Abrate 1997). It can cause failure of the sandwich structure under loads significantly lower than those for a fully bonded one.

Interlayer debonding (hereinafter called 'delamination', to distinguish from skin-core debonding) which happens due to loss of adhesion between adjacent layers, is a predominant form of damage phenomenon in laminated composites, which can often be pre-existing or can take place during service life (Kim et al. 2003a). It occurs in a multilayer laminated sandwich material, leading to split-up of the layers in the

sandwich, which in turn can severely affect the structural integrity of the laminated multilayer composite panel. Figure 1.4 illustrates the delamination (between the bottom skin of layer 1 and the top skin of layer 2) of a two layer composite sandwich.

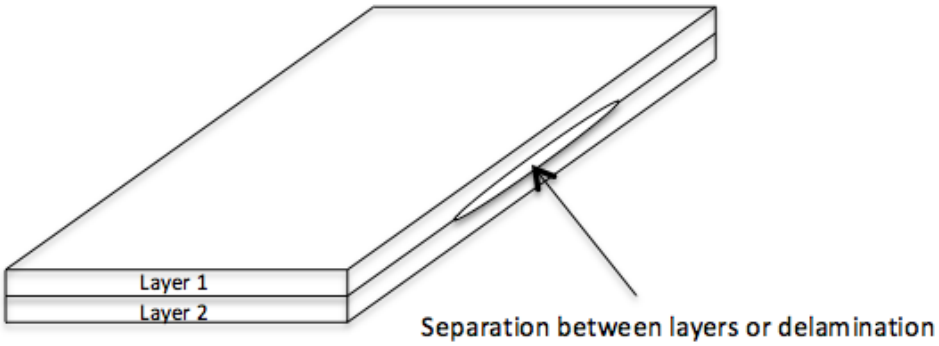

Figure 1.4 Delamination between the layers of a two layer laminated sandwich

The natural frequencies of a delaminated composite plate will decrease because of the loss in stiffness caused by the presence of delamination (Ju et al. 1995). Since the natural frequencies and vibration modes change considerably with respect to the undamaged material, they can indeed be used to develop methods for damage detection and evaluation (Gallego et al. 2013). Hence it is vital to predict the changes in natural frequencies and mode shapes due to delamination with respect to developing damage detecting techniques for practical composite beams and slabs. While the analysis and design of undamaged composites have comparatively well progressed, less advancement has been made towards understanding of damaged structural elements. This may lead to the use of large safety factors in design resulting in higher costs. Hence, to reach design optimization, a deeper understanding on the damage behaviour is vital.

Although the use of fibre composite and sandwich structures has increased tremendously, there are still several aspects concerning the dynamic behaviour of these materials that are not clearly understood. Free vibration behaviour, and forced vibration behaviour due to probable dynamic loadings of these sandwiches are considered as key aspects to be considered in this context. Although much research

has been carried out to investigate dynamic behaviour of fully bonded composites, research on this aspect for debonded composites is scarce. Specifically, knowledge on seismic behaviour of composites with debonds is severely limited. Further research is therefore needed into investigation of the dynamic behaviour of debonded composite structural elements to gain wider acceptance of composites particularly by the Australian industry, and more importantly by the wider structural composite field around the globe.

1.2 Objective

Though sandwich construction has numerous benefits it also has downsides such as a wide variety of failure modes and complexity of analysis. Unless a better understanding of the potential damages of sandwiches is developed, it will rigorously limit its structural applications. Compared to homogeneous structural materials, there is little understanding of the dynamic behaviour of sandwich composites. This understanding is even less for sandwich composites containing debonding. The dynamic behaviour of sandwich structure comprising debonding damage is much more complex and one of the key factors limiting the prime usage of sandwich panels for structural applications. Particularly, the current understanding on the dynamic earthquake performance of composites with debonds is rigorously limited.

Hence the current research, which aims at filling the knowledge gap by developing a deeper understanding of the dynamic failure behaviour of sandwich structures with regard to debonding and interlayer delamination. This has been carried out by means of investigating the free vibration behaviour of debonded composite beams and slabs initially, and then moving in to exploring the dynamic behaviour of debonded composite structures subjected to a probable seismic loading. A typical R/C office building upgraded with GFRP slab panels has been used to investigate the dynamic seismic response with regard to debonding. The variation in free vibration behaviour in terms of alteration of natural frequencies, mode shapes and dominant modes are to be analysed and conclusions made.

1.3 Significance and contribution

There is a lack of information regarding the realistic dynamic behaviour of debonded and delaminated fibre composite structural elements. In this context an attempt is

made to explore the influence of debonds and delaminations on the dynamic performance of GFRP beams and plates.

The fundamental contribution of this research is to fill the knowledge gap and acquire a deeper understanding on dynamic behaviour of GFRP beams and slabs with debonding, and their effects on seismic behaviour. This allows generalizations and correlations to be arrived at, which would be useful in design stage. Hence, the research will facilitate developing improved design and construction guidelines with regard to fibre composite structural elements.

1.4 Scope of the study

The study concentrates on understanding the dynamic behaviour of fibre composite sandwich beams and slabs with debonds. During the progress of the study, specific consideration is given to the following: Review of existing knowledge on fibre composites in general, and influence on debonding on the dynamic behaviour of fibre composites, in particular.

(a) Review the existing knowledge and research on the novel GFRP composite sandwich developed in Australia.
(b) Review the existing knowledge and research on probable earthquake loading on structures and appropriate methods of seismic analyses.
(c) Investigation of the free vibration behaviour of the debonded novel GFRP composite beams.
(d) Investigation of the free vibration behaviour of the debonded novel GFRP composite slabs.
(e) Examination of the free vibration behaviour of laminated GFRP composite multilayer slabs with delaminations between layers.
(f) Investigation of dynamic seismic response of R/C buildings containing GFRP slab panels with debonds subjected to a probable earthquake loading.

The following issues are not considered in the study to limit its scope, in view of facilitating deeper insight in to the topics of critical concern described above.

(a) Non- linear behaviour of composite sandwiches
(b) Propagation of debonding during the free vibration period

(c) Non-linear behaviour of structures under seismic loading
(d) Influence of dynamic loadings other than seismic loading
(e) Dynamic behaviour of debonded composite sandwich walls
(f) Stress analysis to account for stress concentrations due to fastening delamination regions

1.5 Approach

The research approach was to develop a finite element (FE) models for fully bonded and debonded GFRP beams and slabs, and conduct numerical simulations using FE software program STRAND7. Clearly an experimental approach would be very difficult if not virtually impossible. Where possible, the developed models for fully bonded as well as debonded beams and slabs have been validated using published results. Then a parametric investigation is carried out to assess the influence of critical parameters of concern with respect to dynamic behaviour of debonded composite sandwiches. Critical parameters identified to be studied are as follows.

(a) The length and width of the debond
(b) Location of debond
(c) Number of debonding regions and their sizes
(d) Sizes of GFRP beams and slabs
(e) Support conditions of the structural elements under consideration

Moreover, change in dynamic behaviour of a six story reinforced concrete building with fully bonded and debonded GFRP slab panels when subjected a probable earthquake loading was examined. Different building configurations were generated by replacing the concrete slabs with GFRP slabs at locations of interest, and extent of debonding was varied and dynamic response spectrum analyses were carried out to assess the relative performance with and without debonding. The seismic response was assessed in terms of variation in natural frequency and mode shapes, top displacements and interstorey drifts, taking into consideration the relevant gravity and seismic load combinations according to AS1170.4 (2007).

1.6 Outline of the thesis

Chapter 1 **Introduction**: Presents the background and the introduction to the study, highlights the gaps in knowledge, states the objective and outlines the approach used in the research.

Chapter 2 **Literature Review**: Covers the relevant literature on the topics of interest. It also covers a review of previous literature published in connection to the research area and highlights gaps in knowledge.

Chapter 3 **Methods and Materials**: Demonstrates the methods implemented in developing the finite element model, relevant theory, the materials used and a description of the overall methodology adopted in chapters 4, 5 and 6.

Chapter 4 **Free vibration behaviour of debonded composite beams**: Presents the investigation of dynamic response of debonded GFRP beams including the results of the analyses and also the discussion and chapter conclusions.

Chapter 5 **Free vibration behaviour of debonded and delaminated composite plates**: Emphasises on the dynamic behaviour of debonded single layer slabs and delaminated multilayer slabs and presents the results of the analyses including discussion, evaluation and conclusions.

Chapter 6 **Dynamic behaviour of debonded composite plates subjected to seismic loading:** Examines the relative performance of buildings with fully bonded and debonded GFRP Slab panels, evaluates results and makes conclusions.

Chapter 7 **Conclusions and Recommendations:** Highlights the major conclusions derived from the results of Chapters 4, 5 and 6 and makes recommendations for further research.

CHAPTER 2 LITERATURE REVIEW

2.1 Fibre composites

2.1.1 Introduction

Construction industry has made use of the concept of gluing thinner elements to produce thicker structural members to support higher loads. Composites are made by combining two physically distinct and mechanically separable components where one forms a continuous matrix while the other provides the reinforcement. These two components are combined to achieve optimum properties, which are superior to the properties of each individual component. Sandwich structure achieves this by bonding high-density, high-strength material to either side of a low-density core material. Fibre reinforcements are generally preferred since most materials are much stronger in fibre form than in their bulk form. Over the last few decades, fibre composite materials have been increasingly considered for structural applications by the civil engineering construction industry and have also been recognized as a viable and competitive alternative for rehabilitation and retrofit of existing civil structures.

2.1.2 Properties, applications and limitations

FRP composites are made up of a combination of fibres in a matrix material. The mechanical properties of the fibres and matrix in a composite are the core elements influencing the strength and stiffness of the component. The fibres carry the main loads and these are surrounded by a matrix, which binds the fibre together, transfer loads and protects them from physical impact (Cripps 2002). Depending on the type of fibres, type of matrix material, the proportion of fibre-matrix and the type of manufacturing process, the properties of fibre composites can be custom-made to achieve the desired end product (Ticoalu et al. 2010).

According to Cripps (2002), the main advantages provided by FRP composites for new construction are:

- High strength-to-weight ratio
- Resistance to weathering
- Impact resistance

- Flexibility of appearance
- Potential for rapid installation
- Low maintenance

All these advantages encourage engineers to use these materials in numerous structural forms. According to Karbhari (2004), a major disadvantage of FRP, to date, has been the tendency to use these materials in one-to one replacement of existing steel or concrete components, thereby negating its intrinsic advantages of the anisotropy and tailorable nature and the use these materials for primary structural elements in new construction. This is mainly due to limited data on long-term structural response and durability and the absence of appropriate guidelines, codes and standards (Karbhari 2004). Currently there are no standard codes that stipulate or cover the full range of sections of composite members including available sections properties and allowable strength.

The use of composites in the area of seismic retrofit is fairly well advanced with established principles of design and analysis, while their use is vital for the seismic retrofit of historic structures wherein the use of conventional materials would result in a dramatic change in configuration and other architectural features (Karbhari 2004). The intrinsic advantages of FRPs pose them as a more reliable candidate for seismic retrofitting of R/C buildings when compared to traditional methods such as external bracing or steel jacketing (Ronagh & Eslami 2013).

Today, FRP composites are used in a variety of applications ranging from replacements for steel reinforcement, jackets for retrofit of columns and externally bonded reinforcement for the rehabilitation of weakening structural systems and all composite structures such as building frames and even bridge decks (Karbhari 2004). A few examples of FRP applications are shown in Figure 2.1.

FRP Slab Bridge over Bennetts Creek New York, USA (Stewert 2011)

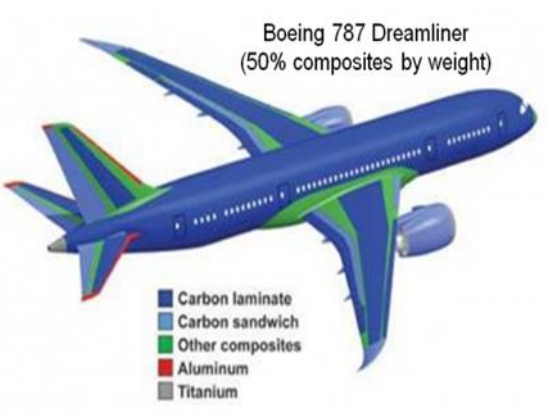

Boing 787 Dreamliner (Margetan 2011)

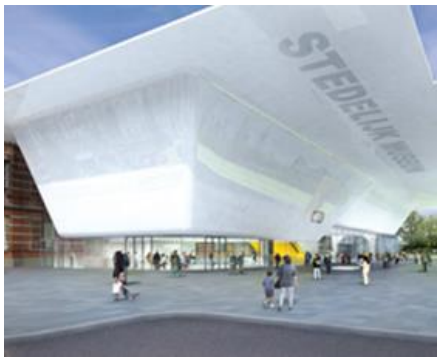

Stedlijk Museum in Amsterdam (Stewert 2011)

Fibre composite Waler, Australia (Aravinthan 2012)

Figure 2.1 Some applications of composites around the world

2.1.3 Glass fibre reinforced polymer composites

One of the outstanding FRP composite materials is glass fibre reinforced polymer. They are two-phase materials with glass fibre acting as dispersed phase and polymer as continuous phase called matrix. According to Bunsell and Renard (2005), glass fibres, first commercially manufactured in the USA in early 1930s, were the first artificial fibres with a reasonably high modulus of elasticity. Glass fibres make up a significant portion of the composites used in the construction industry today as it offers low cost and ease of use, which facilitates manufacturing. Glass reinforced plastics represent more than 90% of the overall composite world market (Bunsell & Renard 2005).

E- Glass, also known as 'electrical glass' because of its high electrical resistivity, is used to produce the vast majority of glass fibre used in FRP products for structural

applications. A-Glass (window glass) and C-Glass (alkaline resistant glass) are used in the production of specialized products in structural applications. S- Glass or 'high strength glass' is used to produce high performance fibres used mainly in the aerospace industry (Bank 2006).

2.1.4 Fastening methods of fibre composite structural elements

Mechanical fasteners (like bolts, rivets and pin-connectors) are commonly used in composite laminates for structural applications in transferring loads between the structural components. Such fasteners are extensively used mainly because they are easy to assemble or disassemble (Pisano & Fuschi 2011). Depending on the requirements, both mechanical and bonded joints are used for fastening fibre composites, and mix joints combining the two are often used (Cripps 2002). In cases such as joining of thick composite components, and damage repair in laminated composites, mechanically fastened joints are preferred over adhesive joints.

Manalo and Mutsuyoshi (2012) investigated the mechanical behaviour and the applicability of bolted joints in fibre composite beams for civil engineering applications experimentally and it was revealed that the combination of bolts and epoxy adhesives could provide a reliable connection method for fibre reinforced composite beams.

2.2 Research and applications of GFRP composites in Australia

An Australian manufacturer has fabricated a new structural GFRP composite sandwich panel (Figure 2.2) made from E-glass fibre skin and a modified phenolic core for the civil engineering applications such as floors, pedestrian bridges and railway sleepers (Awad et al. 2012a).

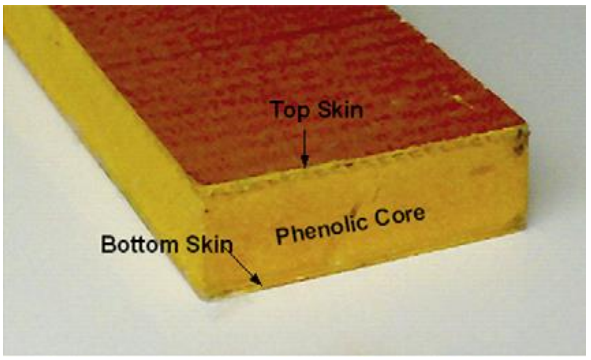

Figure 2.2 Novel GFRP sandwich panel (Awad et al. 2012a)

The top and bottom skins of this sandwich structure is made up of two plies of stitched biaxial (0/90) E-CR glass fibre fabrics manufactured by Fiberex Corporation, and the phenolic foam core comes from natural plant products derived from vegetable oils and plant extracts and chemically bonded within the polymer resin (Manalo et al. 2013). The LOC Composites Pty Ltd, Australia, has made this novel fibre composite sandwich panel available for structural applications (see Figure 2.3).

Figure 2.3 Novel GFRP panels (produced by LOC composites) ready to be transported to site (Aravinthan 2008)

The new GFRP sandwich panel is produced with a nominal thickness of 18 mm, the top and bottom skin is made of 3 mm and the middle core is made of 12 mm thickness as shown in Figure 2.4.

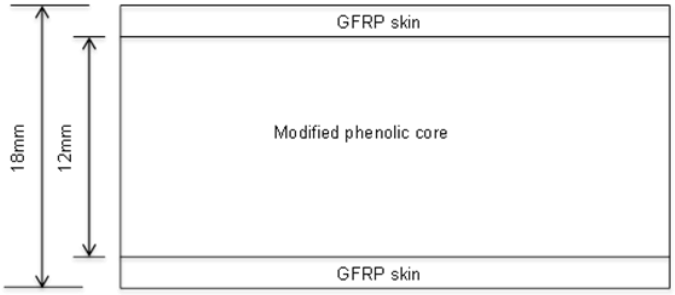

Figure 2.4 Cross-section of the single layer new GFRP composite sandwich panel

Table 2.1 gives the effective mechanical properties of the GFRP skin and modified phenolic core of the novel GFRP composite material, extracted from Manalo et al. (2010b).

Table 2.1 Effective mechanical properties of fibre composite skin and core material of the novel GFRP (Manalo et. al. 2010b)

Property	Skin	Core
Young's modulus along long direction (MPa)	15380	1150
Young's modulus in transverse direction (MPa)	12631	1150
Poisson's ratio	0.25	0.30
Density (kg/m^3)	1366	855

By using the new plant based resin technology for both the skins and the core, the novel composite panel offers unprecedented performance at a price that is comparable to traditional building materials (Van Erp & Rogers 2008). The panel is manufactured as glass fibre composite skins co-cured onto the modified phenolic core material with the use of a toughened phenol formaldehyde resin through an automated production line, and this panel has been classified as a waterproof member grade 1 and a fire testing rating of class 1 (Awad et al. 2012a, 2012b). The difference between the innovative GFRP sandwich panel and the traditional sandwich panel is that the former has a higher core density to improve its structural behaviour (Awad et al. 2012a). Outstandingly, this sandwich structure uses less than 1/7th of the energy to produce, creates 1/10th of the volume of polluted water and about 1/5th of the air pollution, compared to the production of concrete and steel (Manalo et al. 2013). Although the bending stiffness and strength of these composite panels can be controlled by changing the skin thickness (h_s) and the core thickness (h_c), presently they are produced in limited thicknesses due to cost effectiveness and efficiency. The satisfactory performance in several building and residential projects and the flexibility of this innovative composite sandwich panel have shown a high possibility in using this material in the development of structural beams (Manalo et al. 2010a). Since its development, there has been an increased use of this fibre composite sandwich panel in structural applications such as floor slabs, structural beams, pedestrian and bridge decks. These structural components are manufactured from

individual fibre composite sandwich panels or by gluing several layers of sandwich panels together to satisfy the strength and serviceability requirements. A structural composite multilayer beam or slab can be manufactured by gluing two or more of these composite sandwiches together to form a multilayer laminated composite sandwich.

According to Aravinthan (2012), during the past 16 years, there has been substantial activity in the research and development of fibre composites in the Australian construction industry incorporated in bridge systems, replacement of hardwood girders, marine structures and strengthening of existing structures. Australia's experience has shown that it is possible to develop fibre composite expertise for the civil infrastructure market, which provides end users with the performance, and cost structure they are pursuing (Van Erp et al. 2005). The Centre of Excellence in Engineered Fibre Composites (CEEFC) at the University of Southern Queensland (USQ) played a leading role in these developments. One of the earliest technologies developed by CEEFC at USQ is a composite railway sleeper (Figure 2.5) that can replace timber, steel and concrete sleepers in existing or new railway tracks (Manalo et al. 2010a).

Figure 2.5 Sleeper made of polymer concrete and fibre composites (Manalo et al. 2010a)

Several new and innovative structural systems using composites are becoming a reality within the Australian market, and the continuing development of these composite structural systems in combination with national programs providing engineers with necessary design guidance will gain an increasing foothold in the Australian civil engineering market (Van Erp et al. 2005).

2.3 Debonding and delamination in composites

According to Reid and Zhou (2000), there are five basic mechanical failure modes that can occur in a composite after initial elastic deformation. They are:

- Debonding between the skin and the core
- Delamination of adjacent plies in a laminate
- Fibre failure and fracture
- Resin crazing, micro cracking and gross fracture
- Fibre pull out from the matrix and stress relaxation

Debonding refers to the separation of skin from the core of an adhesively bonded composite. It is well known that debonding between the core and the face sheet is the predominant mode of failure for sandwich composite structures (Mousa & Uddin 2012). This may happen during fabrication or during service.

According to Burlayenko and Sadowski (2010), causes of debonding include:

- The manufacturing defects such as incomplete wetting or entrapped air pockets into resin-dominant layer, which may result in non-uniform adhesion between the face sheets and the core.
- The local separation of the principal sandwich layers in isolated area can appear as a consequence of accidental tool drops during maintenance operations.
- The local separation of layers due to low velocity impact by foreign objects.
- The partial interface degradation of the sandwich structure caused by water absorption ability of cellular cores.
- Debonding induced at the weakest point of the skin-to-core interface due to overloading.

The structural integrity of a composite panel can be severely affected by the skin-core debonding. The key problem with debonding failure is that it is sub surface, which makes it difficult to detect and can therefore grow to a critical size before being detected, and as a result, mechanical properties of sandwich materials can be severely degraded (Idriss et al. 2013).

The presence of debonding is of great concern not only because it severely affects the strength but also it modifies the dynamic behaviour of the structure. Debonding causes significant changes in the vibration parameters, such as natural frequencies and mode shapes of structures. Specifically, debonding could reduce the natural frequency and if the reduced natural frequency reaches the working frequency of the beam, resonance may occur, leading to serviceability issues related to deflection limits.

According to Burlayenko and Sadowski (2010), in addition to reducing the overall stiffness and strength and affecting the dynamic responses, debonding can also propagate and trigger new damage modes such as face sheet wrinkling, face sheet delamination and core shear cracks, as shown in Figure 2. 6.

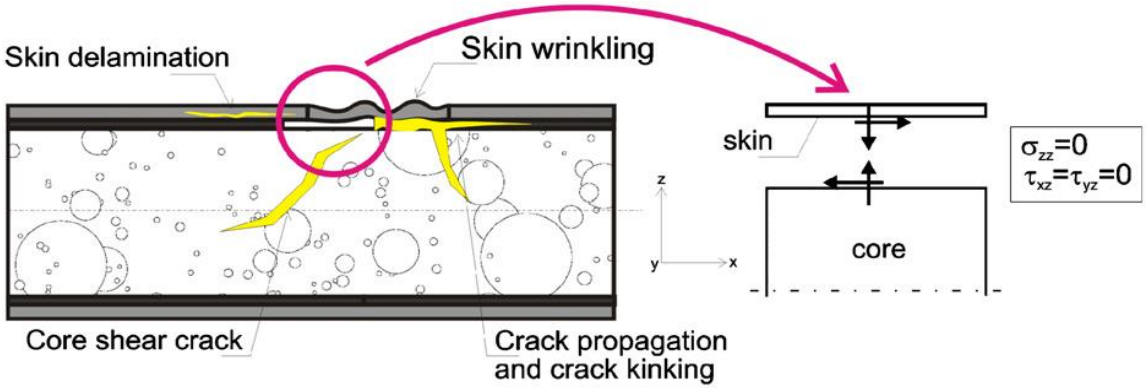

Figure 2.6 A section of a debonded sandwich plate (Burlayenko & Sadowski 2010)

Islam and Aravinthan (2010) carried out experimental tests on the innovative composite sandwich panels under point load and observed debonding between the sandwich core and the skins observed at the edge of the wrinkled part as shown in Figure 2.7.

Figure 2.7 Debonding failure between sandwich core and skins (Islam & Aravinthan 2010)

According to Burlayenko and Sadowski (2010), debonding in sandwich structures is analogous to delamination in laminated composite structures. A lamina or ply is a typical sheet of composite material and a fibre-reinforced lamina consists of many fibres embedded in a matrix material (Reddy 2003). A laminate is a group of laminae stacked to achieve the anticipated stiffness and thickness, and these laminae can be stacked so that the fibres in each lamina are oriented in the same or in different directions as shown in Figure 2.8 (Reddy 2003).

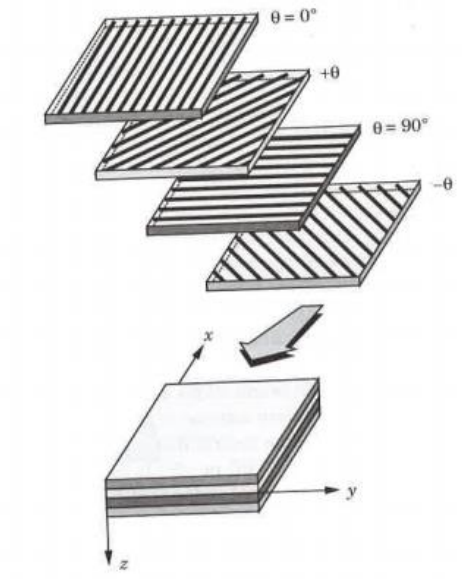

Figure 2.8 A schematic diagram of a laminate made up of laminae with different fibre orientations (Reddy 2003)

Delamination occurs in a laminated material, often a composite, which leads to separation of the layers. It can grow in size under an increasing load and render the laminate structurally useless, triggering failure of the structure (Bunsell & Renard 2005). According to Shanmugam et al. (2013), delamination between plies is the most common failure mode in composite laminates and it happens due to the presence of matrix cracks, free edges like holes and notches in a laminate. Delamination is one of the major failure modes, which endanger the reliability of composite structures. Its modelling can be done accurately at a mesoscopic level, and then, the lamina are discretised using standard finite elements, while the delamination is modelled in a discrete manner using interface elements (Borst & Remmers 2006).

2.4 Assumptions and theories

The usual assumptions used in analysis of sandwich panels are that the face-sheets carry all bending and membrane forces as tensile and compressive stresses, whereas the core carries all of the transverse forces as shear stresses (Zenkert 1991).

Modelling and detection of delaminations in composite plate have been studied mainly with classical lamination theory (CLT) and first order shear deformation theory (FSDT) where CLT completely ignores transverse shear deformations and FSDT accounts for them through shear correction factors (Karunasena 2010).

The classical laminate theory is found to be suitable for most applications where the thickness of the laminate is small by two orders of magnitude compared to in-plane dimensions (Reddy & Miravete 1995). According to Agarwal et al. (2006), in classical lamination theory, the bond between two lamina in a laminate is assumed to be perfect, infinitesimally thin and not shear deformable, yet for real structures this analysis can only be used when the laminate is subjected to constant in-plane forces and moments. However practical laminates are often subjected to transverse loads. According to Reddy and Miravete (1995), when CLT is not applicable, FSDT, which accounts for the transverse shear strains through the thickness, is used. Shear deformation laminate theories do not neglect these out-of-plane stresses (Bunsell & Renard 2005). In other words, the CLT completely ignores transverse shear deformations while FSDT accounts for them through shear correction factors. Hu et

al. (2008) did a comprehensive study on the Analysis and assessment of the various theories used for the modelling of sandwich composites.

2.5 Earthquakes

2.5.1 Introduction

The earthquake is among the most feared of all natural disasters, demanding a devastating toll on human life. Earthquakes pose a direct threat to humans when they cause major landslides or tsunamis. For instance, the 26th December 2004 tsunami that hit many Asian countries killed more than 250,000 people, making it the deadliest tsunami in recorded history.

The magnitude of an earthquake is a measure of the amount of strain energy released by an earthquake, and is usually defined as the logarithm (base 10) of the maximum amplitude, measured in micrometres, of the earthquake record obtained by a Wood-Anderson seismograph, corrected to a distance of 100 km, and quoted as the Richter scale magnitude (Thambiratnam 1997).

Earthquakes are caused mainly by the fracture of the crust of the earth or by the sudden movement along an already existing fault. According to the theory of plate tectonics, the earth is divided into about seven major plates, subdivided into a number of smaller plates all in constant motion relative to one another. Most of the geological features - faults, mountains, volcanoes and earthquakes are due to different types of interaction at plate boundaries. Most earthquakes around the world occur on well-defined tectonic plate boundaries (see Figure 2.9), and are known as inter-plate earthquakes. Some earthquakes also occur within the plate itself away from the plate boundaries and these are called intra-plate earthquakes. They occur less frequently.

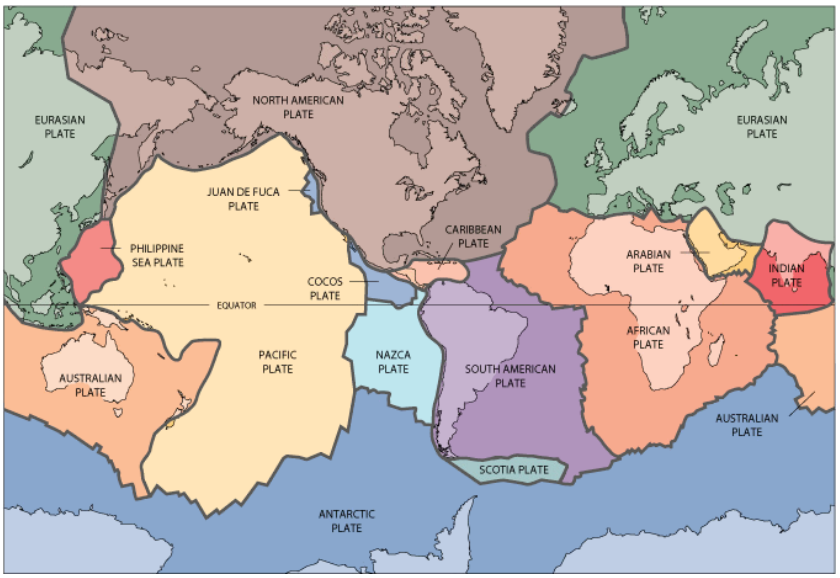

Figure 2.9 Tectonic plates and plate bounaries (Alden 2013)

Australia lies in the middle of the Indo-Australian plate, and for this reason, the type of earthquakes experienced in Australia is of the type intra-plate. One example of the intra-plate type earthquake is the one which hit the city of Newcastle situated on the eastern coast of Australia on 28th December 1989, killing twelve people and causing extensive damage to the infrastructure in the city (Thambiratnam 1997). Newcastle NSW was the worst earthquake disaster in Australia in the last 200 years (Sinadinovski et al. 2000). Seismological information suggests that a similar event to the Newcastle earthquake could occur in the other parts of Australia (Thambiratnam 1997).

According to McCue et.al (1995), over the past 100 years, Australia has been subjected to one earthquake occurrence exceeding magnitude 5 every year and one event exceeding magnitude 6 every 5 years, on average. Table 2.2 lists the major earthquakes occurred in Australia in the last sixty years.

Table 2.2 Recent Australian earthquakes (Thambiratnam 1997)

Location	Year	Magnitude (Richter scale)
Adelaide	1954	5.5
Meckering	1968	6.8
Picton	1973	5.5
Marryat Ck	1986	5.8
Tennant Ck	1988	6.7
Newcastle	1989	5.6

For the majority of earthquakes, ground shaking is the predominant cause of damage. The shaking can cause straight damage to buildings, roads, bridges and other man-made structures, which generates fires, landslides, tsunamis and other damaging phenomena. Buildings experience horizontal deformation when subjected to seismic motion, and when these distortions become large, the resulting damage can be catastrophic. During the Northridge earthquake, around 1000 single houses were 'red-tagged' (rendered not fit to live in), and around 6000 were 'yellow tagged' (restricted entry) in the Los Angeles area (Hall 1996).

2.5.2 Earthquake Design Techniques

Seismic analysis of any structure has now become a mandatory requirement for design of structures (Mittal & Prashanth 2012). In this context, understanding and familiarising with the seismic analysis of structures is a challenging and vital element in the field of civil engineering. The response of structures to earthquake loading is dynamic in nature due to its variation with time. The design seismic forces acting on a structure as a result of ground shaking are usually determined by one of the following methods:

- Static analysis, using equivalent seismic forces obtained from response spectra for horizontal earthquake motions.
- Dynamic analysis, i.e. either modal response spectrum analysis or numerical integration time history analysis using earthquake records.

Until recently, seismic design of most structures was based on a static analysis using a set of lateral forces assumed to represent the actual (dynamic) earthquake loading.

In the absence of commercial software appropriate for dynamic analysis of three-dimensional structures as well as of the expertise for using whatever software of this type was available, most codes of practice clearly promoted the simpler static procedure (Kappos 2002). However, the last two decades were marked by a massive introduction of more advanced software packages running on increasingly more powerful hardware. As a consequence, in modern codes such as EC8, dynamic analysis is adopted as the reference method, and its application is compulsory in many cases of practical interest (Kappos 2002).

2.5.2.1 Static Analysis Procedure

Although earthquake forces are of dynamic nature, equivalent static analysis procedures can be adopted for the majority of buildings. These have been developed on the basis of considerable amount of research conducted on the structural behaviour of structures subjected to base movements. In this approach, the structure is designed to resist a static lateral force, which is supposed to be equivalent to the lateral force exerted by a designated earthquake. The typical procedure in the equivalent static analysis method is the determination of an appropriate value of the base shear in terms of the structure mass and the design earthquake intensity, properly reduced for inelastic effects. The base shear is then used for estimating a set of lateral forces distributed along the structure following the fundamental mode of vibration. Since the base shear itself is also calculated on the basis of the fundamental period, it is clear that the application of the equivalent lateral force method should be restricted to structures whose dynamic response is governed by the fundamental mode (Kappos 2002).

The natural frequency, which is the reciprocal of natural period, can be calculated using the following formulae (Smith & Coull 1991) as given in Table 2.3.

Table 2.3 Formulae to calculate the fundamental natural frequency of a building (Smith & Coull 1991).

Formula	**Notation**	**Type of lateral load resisting system**
$N_o=D^{1/2}/0.091H$	D = base dimension in the direction of motion in meters. H = height of the building in meters	Reinforced concrete shear wall buildings and braced steel frames
$N_o = 10/N$	N = number of storeys	Moment resisting frame
$N_o = 1/C_TH^{3/4}$	C_T= 0.035 for steel structures, 0.025 for concrete structures H = height of the building in feet	Moment resisting frame is the sole lateral load resisting system.
$N_o = 46/H$	H = height of the building in meters	For any type of building

Some of the earthquake design techniques available are the methods presented in Uniform Building Code (1985), Standards Australia (AS1170.4 2007) and National Building Code of Canada (1990). A summary of the first two methods is presented.

(1) Uniform Building Code (UBC 1985) method.

The equivalent base shear force is given by:

$$V = ZIKCSW \qquad (2.1)$$

where:

V = Total lateral force or shear at the base, which will be distributed appropriately at each floor level to determine the lateral response of the building.

Z = Seismic probability zone factor which determines the probability of occurring an earthquake.

For many countries, there are seismic risk maps from which the designers can obtain the appropriate risk factor depending on the location of the building.

Following values have been recommended:

In zone zero where no seismic damage is expected,

Z = 0.125

In zone one where minor seismic damage can be expected,

Z = 0.1875

In zone two where moderate seismic damage can be expected,

Z = 0.375

In zone three where major seismic damage can be expected,

Z = 0.75

In zone four where the location is close to a major fault,

Z = 1.0

I = Occupancy importance factor

For essential facilities such as hospitals, fire and police stations,

I = 1.5

For any building where the primary occupancy is for assembly use for more than 300 persons in one room,

I = 1.25

For all other cases

I = 1.0

K = Building type factor which has to be considered as 1.33 for load bearing brick wall structures, 0.67 for ductile moment resisting space-frames, and 0.80 for ductile moment resisting space frame plus shear walls and 1.0 for all other systems.

C = Seismic coefficient which takes account of the dynamic characteristics of the building. It is given by the following equation, where *T* is the fundamental natural period. The fundamental natural period is equal to the reciprocal of natural frequency.

$$C = 1/(15\ T^{1/2}) < 0.12 \quad \text{and} \quad CS < 0.14 \qquad (2.2)$$

S = Soil structure interaction factor. This factor takes account of the way that the vibrations can be amplified due to the response of the soil to earthquake vibrations. It takes values of:

1.0 for rocklike formations or stiff soil conditions overlaying rock at a depth of less than 60 m

1.2 for deep cohesionless or stiff clay soil conditions overlaying rock at a depth less than 60 m

1.5 for soft to medium stiff clay and sands 10 m or more deep, or if the soil profile is unknown

W = Total dead load and appropriate portions of the live loads.

(2) Standards Australia (AS1170.4 2007) method

According to Clause 6.2.1 of AS1170.4 (2007), the horizontal equivalent base shear force is given by

$$V = \left[k_p Z C_h(T_1) \frac{S_p}{\mu}\right] W_t \qquad (2.3)$$

where:

V = Base shear force

k_p = Probability factor (Table 3.1) that depends on annual probability of exceedance (P).

Z = Hazard factor and it is taken from Table 3.2

$C_h(T_1)$ = Spectral shape factor calculated from Table 6.4

μ = Structural ductility factor taken from Table 6.5

S_p = Structural performance factor selected from table 6.5.

W_t = Seismic weight taken as the sum of seismic weight at each level (W_i) for all levels as given in Clause 6.2.2

Distribution of base shear force is performed according to the formula:

$$F_i = k_{F,i} V = \frac{w_i h_i^k}{\sum_{j=1}^{n} (w_j h_i^k)} \left[k_p Z C_h(T_1) \frac{S_p}{\mu}\right] W_t \qquad (2.4)$$

$k_{F,i}$ = Seismic distribution factor for level *i*

W_i and W_j = Seismic weight at levels *i* and *j* respectively

h_i, h_j = Height of levels *i* and *j* respectively above the base of the structure, in metres

n = Number of levels in a structure

2.5.2.2 Response spectrum analysis

An earthquake excitation of the ground can be given in the form of a time history of the ground acceleration, or in the form of a response spectrum. The response spectrum approach is more common, and it is used by almost every modern design code (STRAND7 2010). It is a procedure for dynamic analysis of a structure subjected to earthquake excitation as it uses dynamic characteristics of the ground motion through its design spectrum (Chopra 1995). According to Wilson (2002), there are numerous computational advantages in using the response spectrum technique of seismic analysis for predicting displacements and member forces in structural systems. The response spectrum analysis is the most popular technique of dynamic analysis adopted by design engineers due to the convenient usage of computers, user-friendly software and the availability of response spectra for most earthquake regions in the design codes (Thambiratnam 1997). Response spectra provide a very convenient tool for engineers to measure the demands of earthquake ground motion on the capacity of buildings to resist earthquakes (Freeman 2007).

The response spectrum of an earthquake is a diagram whose ordinates present the maximum amplitude of one of the response parameters (e.g. relative displacement, relative velocity and acceleration) as a function of the natural period of the single degree of freedom system (Penelis & Kappos 1997). Response spectra form the basis for much modern seismic analysis and design, and are normally presented for 5% of critical damping (Scawthorn & Chen 2002). Figure 2.10 shows the displacement, velocity and acceleration response spectra for the ground motion recorded at El Centro, California during the Imperial Valley, California earthquake of May18, 1940.

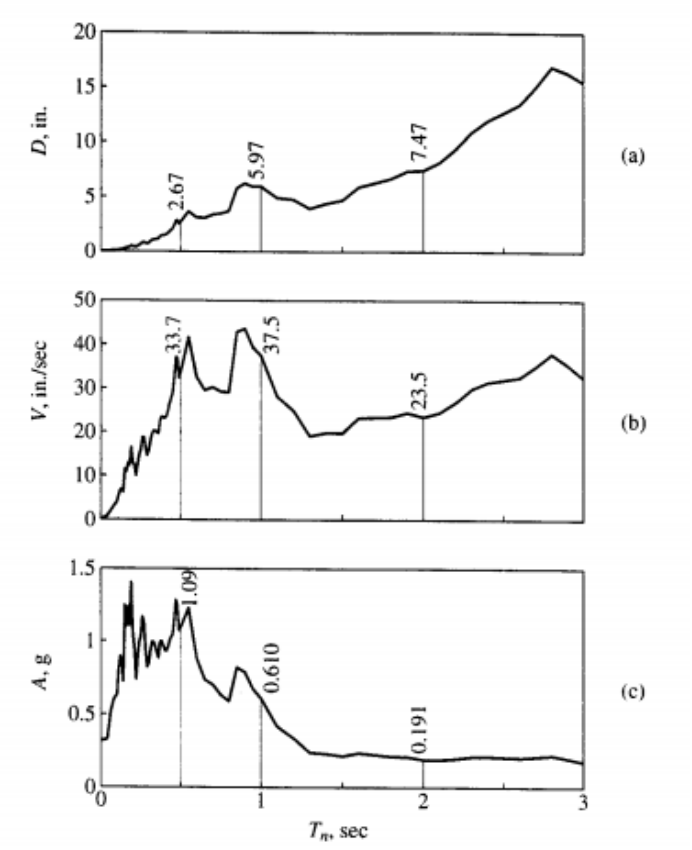

Figure 2.10 Response spectra for El Centro ground motion (a) displacement response spectrum (b) Velocity response spectrum (c) Acceleration response spectrum (Scawthorn & Chen 2002)

Response spectra suitable for intra-plate regions such as Australia differ in shape from the familiar response spectral shapes resulting from early accelerograms from inter-plate regions (Sinadinovski et al. 2000). Figure 2.11 illustrates the 5% damping and normalised acceleration response spectra for the synthetic Newcastle mainshock plotted for reference against the recommended spectra for Australia (Sinadinovski et al. 2000).

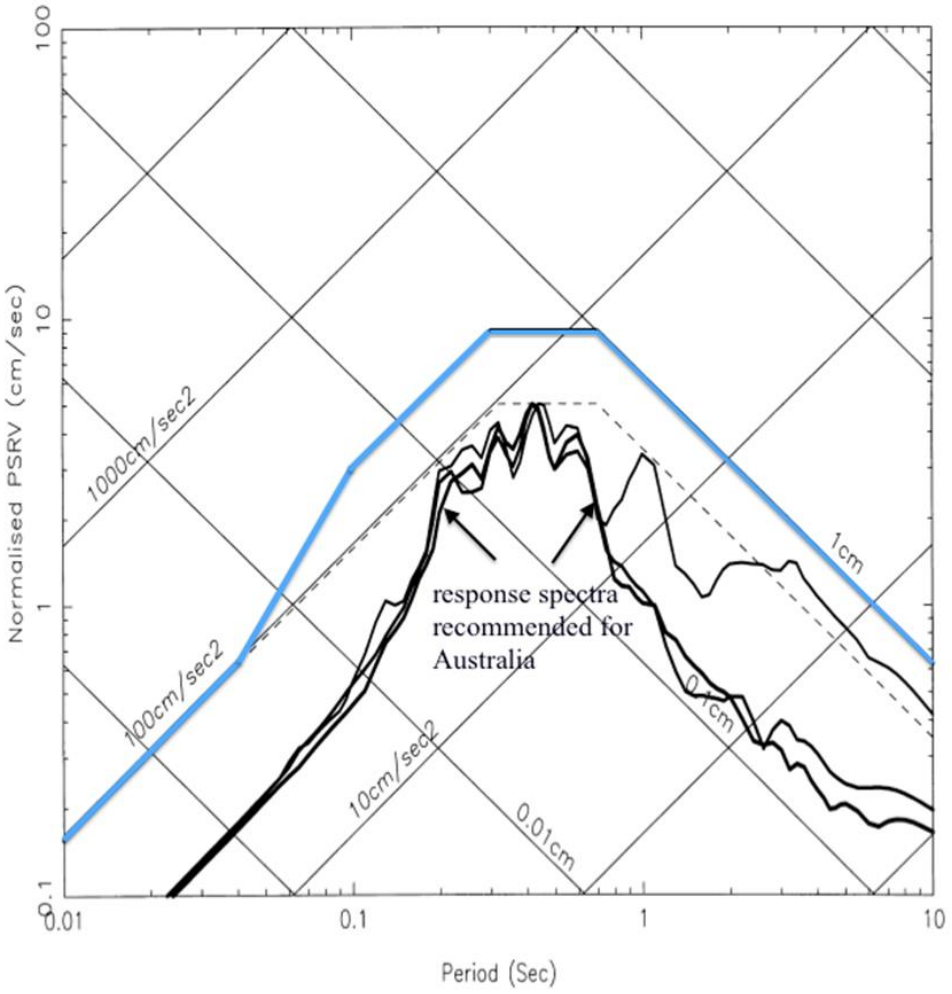

Figure 2.11 Acceleration spectra of the synthetic Newcastle event in comparison with the recommended Australian response spectrum (Sinadinovski et al. 2000)

The response spectrum method calculates the maximum response of a structure to an earthquake design spectrum by means of an estimate of the structure's fundamental period and damping ratio. Since the response spectra give the maximum response of a structure, the maximum response values for each mode are to be obtained and superimposed to give the total response. The most common approaches of superimposing modal responses are Complete Quadratic Combination (CQC) and Square Root of Sum of Square (SRSS) methods. Both these techniques are available in STRAND7. Standard Australian Code Response Spectrums (both AS1170.4-1993 & AS1170.4-2007) are included in STRAND7 installation (STRAND7 2010).

2.5.2.3 Time history analysis

Time history analysis is a method to solve the equation of motion of the system using successive numerical computations, and can be used for linear or nonlinear systems. Here, the total response of the system is calculated at the end of every small time step and the analysis proceeds step by step using the end conditions for one step as initial conditions for the next one (Penelis & Kappos 1997). There are two categories of this method, namely, direct integration and modal superposition. Modal superposition is only suitable for linear analysis while direct integration can also be used for nonlinear analysis. Time history analysis method has the advantage over the linear-elastic response spectrum method in that it may be used to analyze the response of highly non-linear structures (AS 1170.4 1993).

2.5.3 Damping

According to Chopra (1995), the process by which free vibration steadily reduces in amplitude is called damping. All structural dynamic systems contain damping to some degree, but the effect might not be significant if the load duration is short and only the maximum dynamic response is of interest (Biggs 1964).

Real structures dissipate energy while undergoing vibratory motion. The most common and practical method for considering this dissipation of energy is to assume that it is due to viscous damping forces. These forces are assumed to be proportional to the magnitude of the velocity but acting in the direction opposite to the motion. The factor of proportionality is called the viscous damping coefficient. Damping varies with the materials used, the form of the structure, the nature of the subsoil and (the nature of) the vibration (Dowrick 1977). Most building codes do not recognize the variation in damping with structural materials; typically a 5% damping ratio is implicit in the code-specified earthquake forces and design spectrum (Chopra 1995). Hence 5% damping is assumed in the response spectrum analysis procedure described in Chapter 6.

2.6 Dynamic behaviour

The initial step in the dynamic analysis of a structural model is the calculation of the three-dimensional mode shapes and natural frequencies of vibration (Wilson 2002). A mode shape is a set of relative nodal displacements for a particular mode of free vibration for a specific natural frequency. The first or the fundamental mode of a structural system corresponds to the longest natural period. There are as many modes as there are degrees of freedom in the system. Associated with each mode are a natural period and a characteristic shape (Biggs 1964).

2.7 Numerical modelling

With the rapid development of computer technology, many problems that could not be computed or could only be computed by simplified methods can now be simulated on the computer, and the cost and workload are much lower than experimental research. Fast progress in numerical modelling has made analysing three-dimensional models with large degrees of freedom possible. Most of these computer programs are based on the Finite Element Method (FEM) for discretising the structure to produce a mathematical model, which can then be used within the context of numerical solution procedures.

The finite element method is today the most powerful numerical tool available for the analysis of structures (STRAND7 2010). The versatility of the FEM for solving complex topological and multi-physical problems has made it a popular technique in investigations of debonded sandwich panels (Burlayenko & Sadowski 2014). From the point of view of accuracy, the best approach in terms of FE modelling of sandwich panels is to utilise three-dimensional elements for each sandwich layer. In modelling debonded sandwich plates, taking the contact conditions into consideration is very important to properly model their dynamic behaviour (Burlayenko & Sadowski). The finite element software used to model and analyse the free vibration behaviour, and forced vibration behaviour due to seismic loading of fully bonded, debonded and delaminated composites is the software code STRAND7. It is capable of modelling the laminate behaviour of FRP's through the laminate option in STRAND7. Moreover the contact conditions of the debonding region can properly be modelled through the use of master-slave links (by selecting appropriate degrees of

freedom) in STRAND7. Additionally, Standard Australian code response spectrum (AS1170.4-2007 response spectrum), which is to be employed for seismic analysis (Chapter 6) for the present study is available in STRAND7 installation. All these reasons justify the use of STRAND7 for the present study.

2.8 Salient research done in the area of study

Kulkarani and Frederick (1971) were among the first to examine the problem of delamination in laminated composite structures, and in their study the effect of delamination was considered as a reduction in bending rigidity. However, later studies revealed that such modelling overestimates the reduction in bending stiffness due to delamination and hence give erroneous results (Mujumdar & Suryanarayan 1988). Ramkumar et al. (1979) modelled a beam with a full width delamination assuming four Timoshenko beams connected at delamination ends. The anticipated natural frequencies obtained with the use of their model were constantly lower than the results reported in experimental studies. The authors suggested that this disagreement is due to the contact between the delaminated `free' surfaces during vibrations and proposed that the presence of the effect of contact might improve the analytical results. Wang et al. (1982) presented an analytical model, referred to as 'free model', which is also known as 'without-contact model', consisting of four separate Euler-Bernoulli beam segments joined together with appropriate boundary and continuity conditions to get the response of the beam. In their model, it was assumed that delaminated layers deform freely and have different transverse deformations. Although their numerical results were in reasonable agreement with experimental results, they included physically unreal overlapping at the delamination. Mujumdar and Suryanarayan (1988) supposed that the appearance of the open modes in a dynamic response is not possible because of probable overlap between the delaminated sublaminates. To avoid this incompatibility, two delaminated segments of the beam were constrained to have transverse displacements along the whole length of the beam under consideration. Their model was called 'the constrained model', which is also referred to as 'with-contact model' or 'contact model' in the literature. Their analytical results were in very good agreement with experimental results, and it was shown that the contact model is simple and accurate for analysing vibration characteristics of delaminated composites. Later, a comparable analytical model was proposed by Tracey and Pardoen (1992) to study the effects of

delamination. Duggan and Ochoa (1992) suggested that the natural frequencies are sensitive to the size and shape of delamination in structural components. The contact model was later extended by Hu and Hwu (1995) for sandwich beams by including the effects of transverse shear deformations and rotary inertia, and by Shu and Fan (1996) for bi-material beams.

Chattopadhyay and Gu (1994) developed a refined higher order theory (HOT), which was shown to be accurate for delamination modelling in moderately thick composite plates. Later, Chattopadhyay et al. (2000) further extended this theory where HOT results were compared with experimental results and 3D finite element results using NASTRAN software package. Ju et al. (1995) carried out a 2D finite element analysis based on the Mindlin theory to investigate the free vibration behaviour of delaminated composite plates. They found that mode shapes are not significantly affected but delamination effects on natural frequencies are mode dependent and some frequencies may be significantly affected. Krueger and Shell (1999) presented a 3D shell modelling technique using ABAQUS finite element software package for analysis of delaminated composite plates. Kwon and Lannamann (2002) used a finite element analysis with surface-to-surface contact model to predict the dynamic behaviour of a debonded cantilever sandwich beam subjected to an impact load at the free end. Kim et al. (2003a, 2003b) presented an improved layerwise theory for dynamic analysis of delaminated composites. In their analysis, they used delaminated elements with additional nodal unknowns to model delamination effect.

Della and Shu (2005, 2007) conducted studies on free vibration of beams with double delaminations and also on delaminated bimaterial beams. Qiao et al. (2007) used ANSYS finite element (FE) software to study the dynamic behaviour of delaminated composite beams. They used bi-linear contact elements with tension only option for modelling the delamination contact conditions. The model proposed by Mujumdar and Suryanarayan (1988) was extended also by Grouve et al. (2008) for anisotropic laminated composite beams, to study the effect of delamination on the resonance frequencies. Schwarts et al. (2008) presented a high-order analytical approach for the free vibration analysis of fully bonded and debonded unidirectional sandwich panels with a transversely flexible core. In their method, compressibility and shear deformability of the core as well as ‘with’ and ‘without’ contact conditions at the

debonding between skin and core were taken into account. Same authors reported a modified Galerkin method to tackle the same problem (Schwarts et al. 2007). They verified their results against those from finite element analysis with ANSYS code.

Mendelsohn (2006) studied the progressive failure of debonding in a sandwich plate by using the Dugdale-Barenblatt cohesive zone model. Chakrabarti and Sheikh (2009) did a dynamic analysis of a debonded sandwich plate by using a linear spring model in the interfacial region. Burlayenko and Sadowski (2010) investigated influence of debonding on free vibration behaviour of foam and honeycomb cored sandwich plates using finite element (FE) package ABAQUS and found that core types of the sandwich plates strongly affected their dynamic response. Moreover, the same authors (Burlayenko & Sadowski 2011) reported their findings on dynamic characteristics of honeycomb and PVC foam core sandwich plates containing skin/core debonding by FE modelling with ABAQUS, and revealed that natural frequencies are poorly sensitive to the number of debonding zones. Furthermore the same two authors (Burlayenko & Sadowski 2012) developed a finite element model for analysing the dynamic response of sandwich plates with partially damaged face sheet and core using three-dimensional FE modelling using the software package ABAQUS. It was revealed from the study that, the contact phenomenon within the debonded region need be taken into account for an accurate simulation of dynamics of debonded sandwich plates. Newly, the same authors (Burlayenko & Sadowski 2014) carried out a nonlinear dynamic analysis of a rectangular simply supported sandwich plate with a central penny shaped debonded zone under harmonic loading using FE analysis within the ABAQUS code. The predictions made by them showed that the finite element model they applied would be useful for non-destructive evaluation of defects in composite sandwich plates.

As yet only a few investigations of dynamic behaviour of composites under earthquake loading have been performed. Roeder (1998) did a study on the use of composite structural systems for seismic design. An experimental study was done by Zhoudao et al. (2011) on the seismic behaviour of concrete beam-column joints strengthened by basalt fibre reinforced polymer (BFRP) and found that seismic performance of joints damaged by cyclic loads and reinforced by BFRP can be improved significantly. Alhaddad et al. (2012) carried out experiments and FE

analyses with ANSYS code for FRP and textile reinforced mortar (TRM) upgraded reinforced concrete beam-column exterior joints for predicting their seismic performance under simulated earthquake loading and found that FE model can accurately predict the seismic behaviour and response through comparison with experimental results. Meftah et al. (2012) did a parametric investigation to study the influence of the boundary conditions at the top of a one-story sandwich box column under seismic load. Abeysinghe et al. (2013) explored the dynamic performance of an innovative Hybrid Composite Floor Plate System composed of Polyurethane core, outer layers of Glass–Fibre Reinforced Cement and steel laminates at tensile regions using experimental testing and FE modelling with ABAQUS, to verify its applicability in residential and office floors. It was concluded that this lightweight floor system would provide significant economic benefits in the design of the supporting system and have favourable response under seismic loads.

It is vital to review the research carried out so far on the novel GFRP composite sandwich. Although dynamic behaviour of debonded sandwiches has been done only in two studies (Karunasena et al. 2009, Karunasena 2010), several authors as detailed below have investigated free vibration behaviour for the full bonded case. The experimental study of this innovative GFRP sandwich panel was carried out by Manalo et al. (2010b) to find the bending behaviour of a simply supported GFRP sandwich beam. In that study, the authors investigated the experimental behaviour of the GFRP sandwich beam in the flat-wise and edge-wise positions. Islam and Aravinthan (2010) examined the behaviour of this innovative GFRP sandwich floor panel as two-span continuous floor panel and found that the panel shows a similar behaviour under point load and distributed load and also that there is no major effect of the type of fixity on the overall behaviour. It was also specified that there is a necessity to conduct a parametric study to have a better understanding of such composite sandwich panels in flooring systems. Investigation of the free vibration behaviour of the fully bonded GFRP sandwich by experimental and numerical methods was carried out by Awad et al. (2012a). The investigation was done on the novel GFRP sandwich floor panels by varying panel span, fibre orientation and restraint type. It was found that simply restraint panels had the lowest natural frequency while glue restraint panel had the highest frequency. Although the design engineers have accepted the innovative GFRP sandwich panel to be used as a

structural member due to its good mechanical properties, there is a lack of information about the free vibration behaviour of the GFRP sandwich floor panel (Awad et al. 2012a). A study on the free vibration behaviour of debonded novel sandwich plates using a 2D model was done by Karunasena (2010). The author examined the deviations in natural frequency due to various amounts of debonding along the glue line in a four layer laminated fibre composite sandwich plate structure using 2D finite element modelling. Karunasena et al. (2009) did a study on the vibration of delaminated beams constructed from four layers of sandwich plates using numerical analyses. It was revealed that the mid-plane glue-line debonding causes a higher reduction in frequencies than the bottom glue line.

While the dynamic behaviour of undamaged sandwich panels is the subject of extensive studies, papers reported on the dynamic behaviour of sandwich panels with debonding are less presented in the literature (Burlayenko & Sadowski 2014).

2.9 The way forward

Generally it can be seen that the majority of research carried out has been concerned about the delamination of laminated structures. However, skin-core debonding in a single layer beam or slab has received relatively minor attention. Furthermore, it is revealed that research done on multilayer structures having multiple delaminations is undeniably very limited.

In the Australian context, although experimental and numerical research has been conducted on the examination of the free vibration behaviour of the fully bonded GFRP sandwich floor panel, there has been no investigation on the free vibration behaviour of the debonded GFRP sandwich floor panels except the study done by Karunasena (2010) using 2D models. Clearly, any published papers have not addressed dynamic behaviour of the debonded novel single layer sandwich beams. Furthermore, any study in which finite-element analysis for dynamic behaviour of both debonded FRP structural elements and delaminated multilayer FRP laminates are presented together is not reported in the literature.

In fact, no experimental or numerical study on dynamic behaviour of composites with debonds subjected to earthquake loading could be found in the approachable

references. Filling this gap in research and lack of understanding on dynamic behaviour of debonded composites under seismic loading is also a motivation of this study.

To address the gap in knowledge as described above, a comprehensive research project investigating dynamic behaviour using finite-element modelling and analysis is presented for predicting the influence of debonding on the free vibration behaviour, and seismic performance of debonded GFRP single layer slabs used in practice. Additionally, dynamic behaviour of delaminated multilayer GFRP slab panels have been investigated. It is aimed at carrying out a comprehensive parametric investigation with different debonding lengths, widths and locations for single layer beams and slabs. For multi-layer GFRP slab panels, location of delamination would also be considered as a parameter in addition to debonding size. Finally, this research addresses the influence of debonding on the dynamic behaviour due to a probable earthquake loading in buildings with debonded GFRP slab panels using response spectrum method of analysis to fill the gap in knowledge on seismic behaviour of debonded composites.

CHAPTER 3 METHODS AND MATERIALS

3.1 Introduction

This chapter describes the research approach and detailed methodology to be adopted in different scenarios such as debonding in single layer beams, interlayer delamination in multilayer slab panels and seismic analysis procedures for debonded slab panels. It gives details of the model development and material properties selected for each case.

3.2 Approach

The research approach is to develop a computer model and conduct numerical simulations to assess the dynamic behaviour of debonded and delaminated composite sandwich beams and slabs. Developed models for fully bonded and debonded beams and slabs have been validated using results from literature. In order to achieve the research goals, a parametric investigation is carried out to assess the influence of various parameters of concern including length and width of the debond, location of debond, size and support conditions of the structural element on the free vibration behaviour at the outset and then examine the change in dynamic behaviour of the debonded structural elements when subjected to a probable earthquake loading.

Small test beams and slabs are first used and modelled for the verification and initial modelling, and these test specimen sizes are extended to larger sizes of beams and slabs for full scale modelling. Initial selection of test specimens expedites the validation of the developed models with the published experimental results (Awad et al. 2012c) in addition to facilitating the in depth investigation of influence of debonding on the parameters of interest with efficient use of computational time. Thereafter practical beam and slab panel sizes are selected for full scale modelling for further investigations. Important parametric investigations done for the test specimen sizes have been repeated for full scale beams and slabs in order to further confirm the main findings for generalisation and to arrive at final conclusions.

After completing the analyses of single layer beams and slabs, multilayer sandwich slabs with interlayer delaminations are analysed. Finally earthquake response spectrum analyses have been carried out for a probable earthquake loading for a typical six-story R/C office building having GFRP slab panels in different floor locations. The focus of this investigation is to do a parametric analysis to assess the relative performance of the building with fully bonded and debonded GFRP slab panels. Different configurations of the building models were created by replacing the concrete slabs with GFRP slabs at various locations of the building to assess the relative performance with and without debonding.

3.3 Materials and properties

3.3.1 Selection of Novel GFRP beam sections

Manalo et al. (2010b) did a comprehensive experimental study of the flexural behaviour of this novel GFRP sandwich test beams with a nominal thickness of 20 mm in flatwise and the edgewise positions. The fibre composite skin of this novel GFRP sandwich is made up of two plies of stitched bi-axial (0/90) E-CR glass fibre fabrics, and the modified phenolic foam core is a proprietary formulation by LOC Composites Pty. Ltd., Australia (Manalo et al. 2010b). The composite sandwich panel has a nominal thickness of 20 mm and has an overall density of approximately 1000 kg/m^3. The effective mechanical properties (extracted from Manalo et al. 2010b) of the fibre composite skin and the modified phenolic core material were given in Chapter 2 Table 2.1.

The 300 mm long novel GFRP test beam used by Manalo et al. (2010b) for his experimental study (comprising of 2 mm top and bottom skins and a 16 mm middle core) has been selected for the initial investigation of the effect of skin-core debonding on the dynamic characteristics. Figure 3.1 shows the preparation of these glue-laminated novel sandwich beams.

(a) Gluing of sandwich panels (b) Cutting of sandwich beams

Figure 3.1 Preparation of glue-laminated composite sandwich beams (Manalo et al. 2010c)

There have been some developments in the sandwich structure used in the production of full-scale glue-laminated sandwich beam specimens, and the new sandwich panel is only 18 mm thick with 3 mm thick top and bottom skins and 12 mm thick core (Manalo 2011).

3.3.2 Selection of Novel GFRP slab panel sections

Awad et al. (2013) conducted an experimental study of the behaviour of the new GFRP sandwich panels with nominal thicknesses 15 mm and 18 mm (see Figure 3.2).

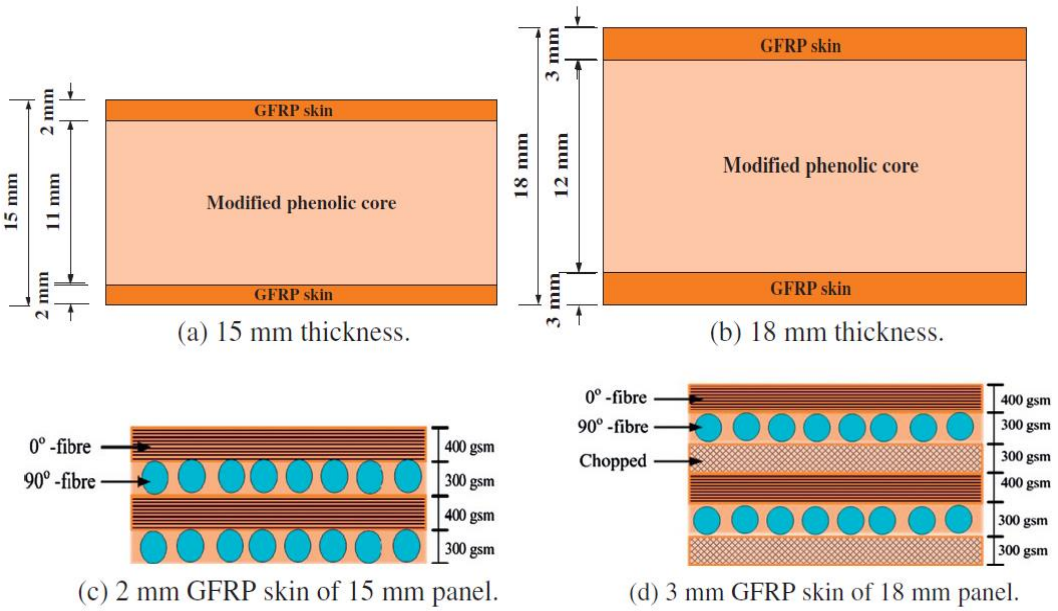

Figure 3.2 New GFRP sandwich panel cross sections (Awad et al. 2013)

The slab panel section having overall thickness of 18 mm (illustrated in parts (b) and (d) of Figure 3.2) used by Awad et al. (2013) have been selected for the present analysis of slab panels. At first, top and bottom skins were modelled as laminates consisting of 6 plies as shown in Figure 3.2 (d) using ply property input and laminate option in STRAND7 to verify whether the resultant properties of the laminated plate are matching with the experimental skin properties reported in Awad et al. (2013). The effective properties of the skin plate are automatically calculated within STRAND7 using classical laminate theory, and the data were in agreement with the effective skin properties reported. After the justification, the effective skin properties tabulated in Table 2.1 were used for modelling the skin for the subsequent models.

3.4 Finite element modelling

Finite element method (FEM) discretises a structure into a mesh of elements, and these elements are joined together by nodes. Finite element method involves dividing the structure into an equivalent system of finite elements with associated nodes, selecting the most appropriate element type to model closely the actual physical behaviour, formulating the equations for each finite element and combining them to obtain the solution of the whole structure (Logan 2012). FEM is especially versatile and efficient for the analysis of complex structural behaviour of the composite laminated structures. The formation of delamination is a complicated process and the problem is three dimensional in nature (Senthil et al. 2013). Hence numerical simulations are carried out using 3D finite element models of the structures. The fineness of the finite element mesh is critical to the outcome of a FE analysis (Zenkert 1997). Therefore, a convergence study has been carried out by refining mesh size to obtain accurate results. Before the simulations are done, it is needed to develop the numerical model, and then to compare the model with published results for a known problem for the verification of the developed model used in the analyses.

3.5 Software used

The computer program employed in this research to develop the model, analyse and investigate the responses is the finite element software package STRAND7 comprising pre-processor, solvers and post-processors. The STRAND7 structural analysis program offers specially the following features of interest and many more (STRAND7 2005).

Static Analysis**:**

- Linear Static
- Linear Buckling

Dynamic Analysis:

- Natural Frequency
- Harmonic Response
- Spectral Response

3.6 Development of the model

3.6.1 General

The first task in the research is the development of the numerical model using available techniques by innovatively selecting the suitable elements to diligently represent their actual behaviour.

According to Zenkert (1997), shear deformation in the core of a sandwich has to be considered, be it static or dynamic, and the user has to select elements that do so for adequate sandwich analysis and design. Due to the geometry and material properties of the core, using a solid element is the suitable option for core modelling because solid element uses a 3-dimensional state of stress. In modelling composites, building core using brick elements gives higher accuracy stress output in the core, and more accurate interaction between the core and facesheets. In view of the above facts, 3D brick element (Hexa 8) shown in the Figure 3.3, which takes care of shear deformations, is selected for modelling the phenolic core of the composite sandwich.

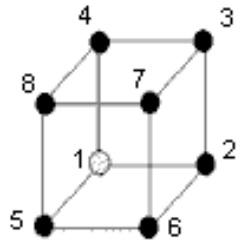

Figure 3.3 8-node hexahedral element (STRAND7 2010)

GFRP skins are meshed using 4-node Quadrilateral (Quad4) elements, developed based on thin shell theory. In Quad4 element there is a complete set of spatial degrees of freedom, $\lfloor u \;\; v \;\; w \;\; \theta_x \; \theta_y \; \theta_z \rfloor$ at each node (as shown in Figure 3.4), which makes the element easy to connect to space beams without causing local singularity (STRAND7 2005).

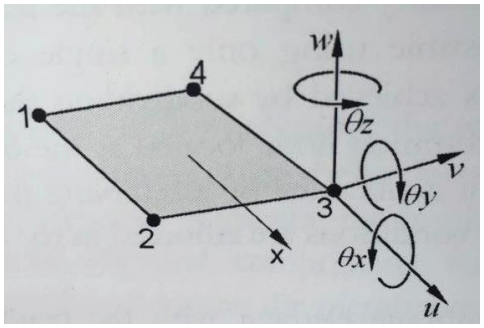

Figure 3.4 Nodal degrees of freedom for a 4-node plate element (STRAND7 2005)

It is noted that skins can be modelled using higher order plate elements such as 8-noded or 9-noded elements. In that case, core needs to be modelled with corresponding higher order elements to ensure compatibility. Since the skins of both the beams and slab panels used in this study satisfy the criteria for ‘thin plates’ according to linear classical thin plate theory (length and width are at least ten times higher than the plate thickness), it is appropriate to use 4-node plate element (Quad4) for skin. It should be noted thin plate theory has been incorporated into the formulation of Quad4 element in STRAND7. The matching 3D brick element (Hexa

8) which takes care of shear deformations is suitable for modelling the core. Hence, in this study, Quad4 and Hexa8 elements are used for skins and core, respectively.

The skins are bonded to the core using rigid link elements. Rigid links in STRAND7 provides an infinitely stiff connection between two nodes. Rigid link also provides restraints to the nodal rotations, in addition to the translational displacements (STRAND7 2010).

3.6.2 Model development for beams

In this study, a composite sandwich beam with core bounded by top and bottom skins with a finite debonding between the top skin and the core is considered (see Figure 3.5). The geometric dimensions of the beam and the debonding length and location are as defined in Figure 3.5.

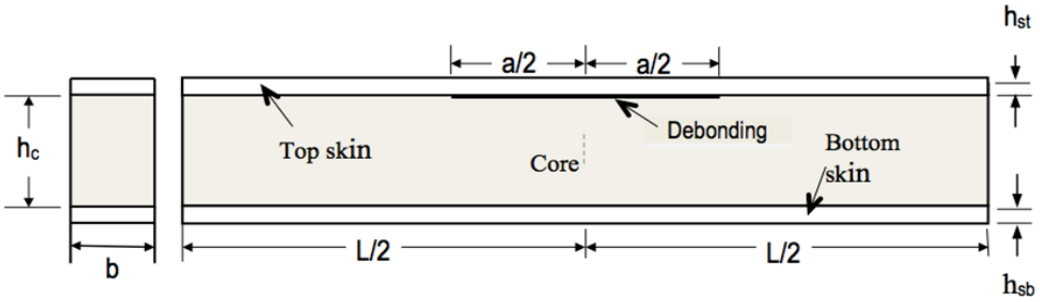

Figure 3.5 Longitudinal and cross sections of the sandwich beam with a central Debonding

The beam cross-section is rectangular with a width of b. Top and bottom skin thicknesses are h_{st} and $h_{sb,}$ respectively, and the length of the beam is L. Materials in each of the skins are assumed to be orthotropic and linear elastic. It is possible to have different materials for top and bottom skins. The plate element mesh for each skin lies at the horizontal plane at the mid-thickness level of the respective skin. Core material is assumed to be linear elastic, homogeneous and isotropic. Debonding is assumed to be an artificial flaw of zero thickness, embedded between top skin and core. It is assumed that debonding exists before vibration commences and stays constant without propagation during the vibration. Debonded surfaces (of skin and

core) are in contact vertically but can slide in the horizontal plane (as per the contact model).

The links for the sandwich beams are of length $h_{st}/2$ where h_{st} is the thickness of the top skin. These rigid links are used for the fully bonded regions to ensure that there is no gap or sliding between the top skin and the core. In a similar manner, bottom skin is connected to the bottom surface of the core using rigid links of length $h_{sb}/2$.

According to Mujumdar and Suryanarayan (1988), in the analysis of dynamics of delaminated beams, 'free model' is of limited significance, and 'contact model' is simple and accurate. Contact model is of importance to prevent the interacting fragments from overlapping each other and, consequently, the modelling of the contact behaviour is necessary to properly represent the global dynamic response (Burlayenko 2012). Hence master slave links are used in the finite element model to allow for sliding between interfaces of skin and core in the horizontal directions while keeping skins in contact with the core in the vertical direction to effectively simulate a debonded beam according to 'contact model'. The FE model for the debonded beam is obtained by simply converting the rigid links within the debonded region to 'master slave links' in STRAND7 with appropriate degrees of freedoms. A master-slave link defines relations between two nodes so that the displacement of the selected components will be of the same magnitude (STRAND7 2005). These links will allow for sliding between interfaces of skin and core in the horizontal directions yet keeping skins in contact with the core in the vertical direction. This process effectively embeds an artificial zero thickness debond into the intact plate to mimic a debonded plate to represent the constrained or contact model.

A number of preliminary models were created and analysed before the final form described above was settled upon. The final refined model for a debonded beam is shown schematically in Figure 3.6.

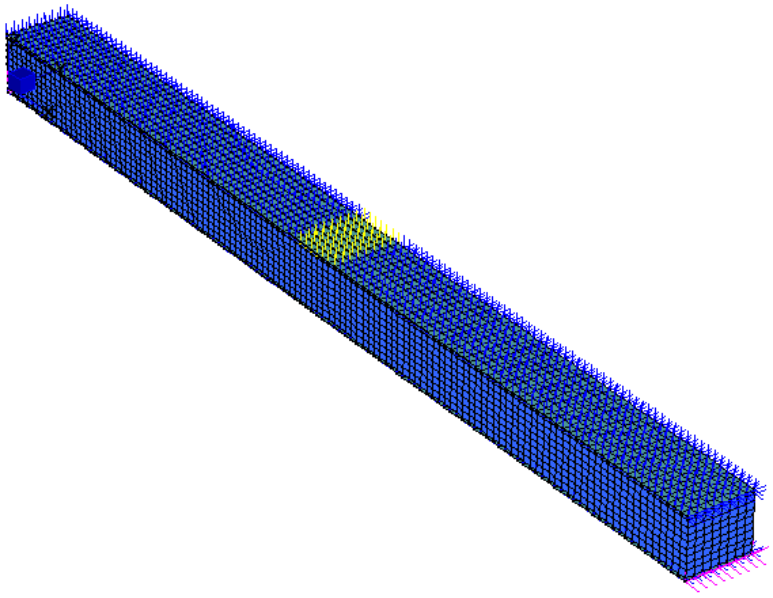

Figure 3.6 FE model for a simply supported beam with 30 mm full width debonding

The final form of the model developed has the features explained below.

1. Linear elastic orthotropic top and bottom skins are modelled using 4-noded rectangular (Quad4) plate elements. The plate element mesh for each skin lies at the horizontal plane at the mid-thickness level of the respective skin.
2. Core is modelled using isotropic 3D brick elements (Hexa8). These elements take care of any shear deformations happening in the thick core.
3. Core 3D FE mesh is generated by extruding the Qaud4 plate element mesh using the 'extrude' command in STRAND7. This ensures that a vertical line through corresponding plate nodes in the top and bottom skins will pass through corresponding brick nodes in the core.
4. The structural integrity between top skin and core is assured by connecting plate nodes with corresponding brick nodes at the top surface level of the core through vertical 'rigid link' elements. Rigid link provides restraints to the nodal rotations, in addition to the translational displacements (STRAND7 2010).

5. The Finite element model for the debonded beam is obtained by converting the rigid links within the debonded region to ‘master slave links’ in STRAND7, thus innovatively assigning the proper degrees of freedom.

After the FE model has been created, the appropriate eigenvalue problem can be solved to obtain natural frequencies and corresponding mode shapes. As usual in the conventional finite element method, more elements will ensure better convergence and, therefore, appropriate numerical studies are carried out to get a reasonably converged solution by refining the mesh.

In order to compare the effect of degree of contact at the debonded interface on the free vibration behaviour, a spring model in STRAND7 has been utilized. By the use of spring elements, ‘Free Model’ and ‘Contact Model’ were simulated (as described below) and natural frequency variation due to similar debonding is compared for the two models.

To simulate the contact model using spring elements, a spring model is implemented between the skin and the core of debonded single layer beams by removing the master slave links and replacing them with spring damper elements in STRAND7. Firstly the axial stiffness of the spring was increased until the analysis give similar frequency values as accomplished for the constrained model with master-slave links described above. Then, a free model is simulated by assigning zero stiffness for these spring elements.

3.6.3 Model development for slabs

Development of the model for single layer and multilayer slabs has been done accordingly with plate elements for skins and brick elements for cores to represent their actual behaviour. After developing the model, validation of the model for slabs is carried out using published experimental and numerical results.

A mesh refinement procedure and a convergence study were conducted for slabs as well, in order to determine the appropriate mesh density required for the finite element modelling.

After the validation with a small slab size (400 mm × 400 mm), the model is extended to

(a) Single layer 800 mm square slab
(b) Two layer 1000 mm square slab
(c) Single layer 3000 mm square slab

To maintain consistency in the selected skin and core thicknesses, thicknesses of skins and cores in 800 mm square slab were scaled by eight to get the corresponding thicknesses for 3000 mm square slab. Accordingly, the top and bottom skin thicknesses of the 3 m slab are 24 mm each and the core thickness is 96 mm.

Different configurations of debonding and regions are considered to examine the critical locations and sizes of debonding with respect to change in dynamic behaviour. For this purpose, single layer and multilayer slabs considered are divided in to nine regions (of equal size) as shown in Figure 3.7, and, single as well as multiple debonding in the middle of these regions are analysed to examine the influence of size and location of debonding on the dynamic characteristics.

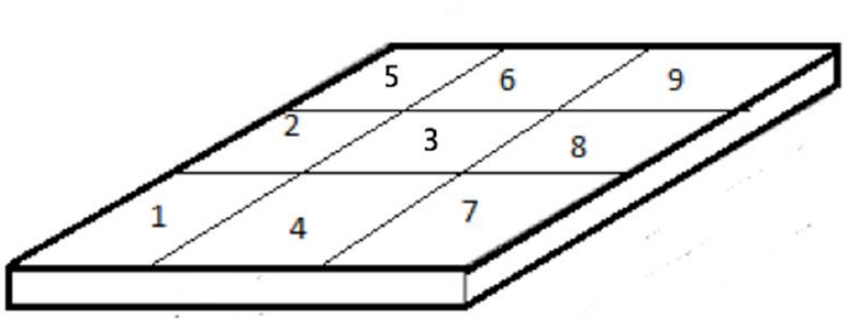

Figure 3.7 Division of a typical single layer slab in to nine regions for parametric analysis

Debonding positions 1, 2 and 3 considered (located in the middle of regions 1, 2 and 3 respectively as illustrated by Figure 3.7) are shown in Figure 3.8.

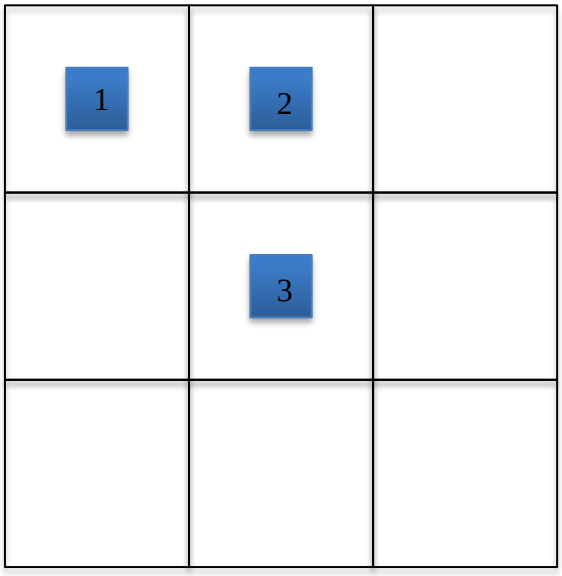

Figure 3.8 Debonding positions 1, 2 and 3 considered

Four different types of end conditions for the slabs are considered, namely, two opposite ends simply supported and the other two ends free (S-S-F-F), all four ends simply supported (S-S-S-S), two opposite ends clamped and the other two ends free (C-C-F-F) and all four ends clamped (C-C-C-C). For C-C-C-C and S-S-S-S end conditions, only three distinct regions or positions, namely 1, 2 and 3 need to be considered, because regions 5, 7 & 9 have similar conditions as region 1, and regions 4, 6 & 8 are having identical conditions as position 2 (see Figure 3.7).

Figure 3.9 shows the FE models developed for 1% debonding (by area of the slab) in positions 1 and 2 for 3000 mm slab panel with C-C-C-C end condition.

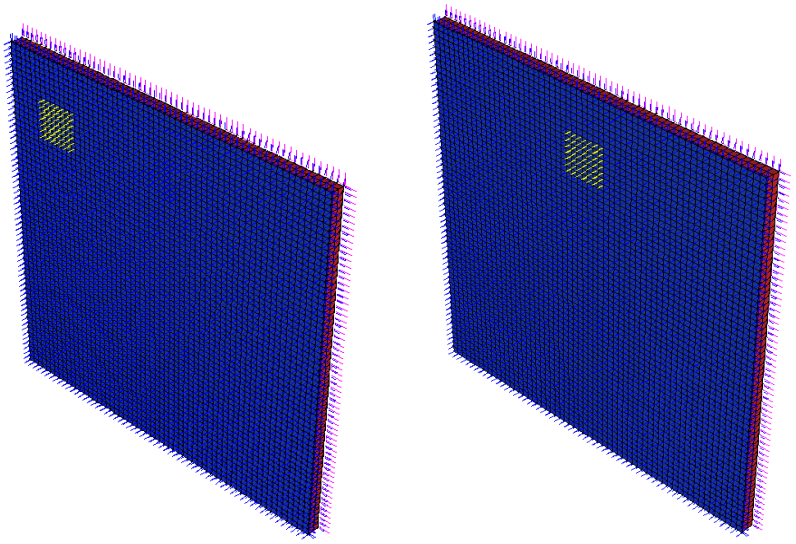

(a) Debonding position 1 (b) Debonding position 2

Figure 3.9 Developed models for 1% debonding in positions 1 and 2 for 3000 mm C-C-C-C slab panel

Single and multiple delaminations between layers in the middle and edge positions across the thickness of two layer slab panels have been considered for parametric analysis in multilayer slab panels. A typical single delamination on the middle position in the middle layer (between bottom skin of layer 1 and top skin of layer 2) of the two layer laminate is shown in Figure 3.10 (a) and the positions of delaminations considered are shown in Figure 3.10 (b).

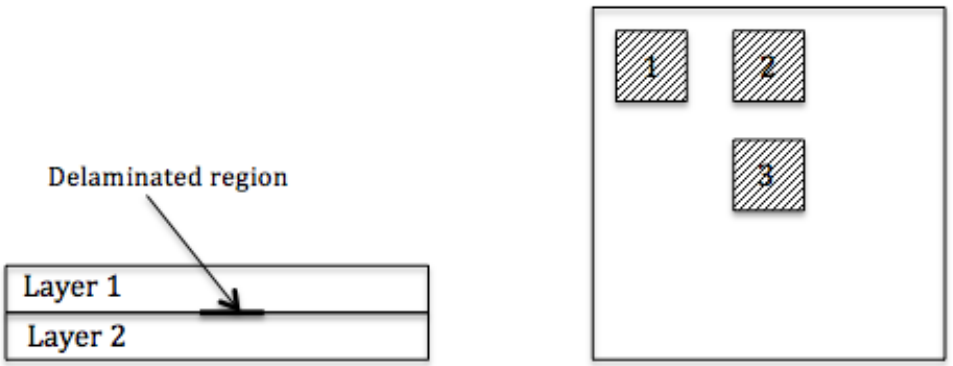

(a) Two layer plate used (b) Positions of delamination considered

Figure 3.10 Two layer laminated composite sandwich used and the positions of delamination considered

After developing the models, model validation has been carried out using published experimental and numerical results. Model verification details for beams and slabs are reported in Chapter four and five, respectively, under the relevant headings.

For seismic response spectrum analysis described in Chapter 6, the single layer 3000 mm GFRP slab, having 96 mm core thickness and 24 mm skin thicknesses (as described above) has been selected for the comparative parametric investigation.

3.7 Dynamic analysis procedure

3.7.1 Introduction

A dynamic load is one whose magnitude, direction, or point of application varies with time. The most basic pieces of information needed for dynamic analysis are the natural period, which is a function of the structure's mass and stiffness, and the amount of available damping (Kappos 2002).

3.7.2 Free vibration analysis

Free vibration is the natural vibration of a structure released from initial condition and subjected to no external load or damping. The solution gives natural frequencies, associated mode shapes and an insight to the dynamic behaviour and response of the structure. Free vibration analysis forms a vital aspect in the total investigation of a structure or a structural system (Thambiratnam & Zhuge 1996).

3.7.3 Modal analysis

The dynamic response of a multi-degree-of-freedom system to external forces can be computed by modal analysis. The frequencies at which vibration naturally occurs, and the modal shapes, which the system assumes, are properties of the system, and can be determined analytically using modal analysis. In modal analysis method, the responses in the normal modes are determined separately and then superimposed to provide the total response. The applicability of the modal method of analysis is limited to linearly elastic systems and to cases in which all forces applied to the structure have the same time variation. When these conditions are not met, numerical analysis must be used (Biggs 1964).

3.7.4 Response spectrum analysis

The response spectrum analysis (RSA) method enjoys wide acceptance as an accurate method for predicting the response of a structural model to earthquake excitations. Generally, building codes require a dynamics based procedure for specific categories of structures, and the RSA method satisfies this dynamics requirement. It is easier, faster and more accurate than the static method of earthquake analysis. RSA method of earthquake analysis involves the calculation of the maximum values of the displacements and member forces in each mode using smooth design spectra that are the average of several earthquake motions (Wilson 2002).

3.8 Governing equations

3.8.1 Free vibration analysis

Using the concept of dynamic equilibrium, for forced vibration with damping, the equation of motion can be written as:

$$[M]\{\ddot{U}\} + [C]\{\mathring{U}\} + [K]\{U\} = [F]\,(t) \qquad (3.1)$$

Here [M] is the mass matrix, [C] is the viscous damping matrix, [K] is the stiffness matrix and [F] is the dynamic load for the system of structural elements. The time dependent vectors {U}, {$\mathring{U}$} and {$\ddot{U}$} are the absolute node displacements, velocities, and accelerations, respectively.

For free vibration, ignoring damping, equation (3.1) becomes

$$[M]\{\ddot{U}\} + [K]\{U\} = 0 \qquad (3.2)$$

The natural frequency Solver in STRAND7 is used to calculate the natural frequencies and corresponding vibration modes of an undamped structure. The natural frequency analysis problem is formulated as the following eigenvalue problem (STRAND7 2005):

$$[K]\,\{x\} = \omega^2\,[M]\,\{x\} \qquad (3.3)$$

where

$\{x\}$ = Vibration mode vector

ω = Circular frequency (radians/sec) and natural frequency = $\omega/2\pi$ (Hertz)

In STRAND7, the subspace iteration method is used to solve the generalised eigenvalue problem. Subspace iteration is a very effective and efficient method for solving an eigenvalue problem in a situation where the model is large (as is the case for most practical problems) but only a relatively small number of the eigenvalues and corresponding eigenvectors are of interest (STRAND7 2005).

3.8.2 Damping and mass participation factors

According to STRAND7 (2005), damping can be modelled through two viscous damping models: Rayleigh damping and modal damping.

Rayleigh damping is one of the most common models of damping in finite element analysis. In STRAND7 (2005) damping is assumed to be a linear combination of the stiffness and mass matrices of the following form:

$$[C] = \alpha [M] + \beta [K] \qquad (3.4)$$

α and β are called the stiffness and mass proportional damping constants. The damping matrix as a linear combination of mass and stiffness matrices, shares a common property of the two matrices, it also is an orthogonal matrix of the free vibration modes (STRAND7 2005).

Modal damping is also a commonly used damping model and it allows the modal damping ratio to be defined independently for each vibration mode used in any analysis based on the modal technique, including the harmonic response, spectral response and superposition linear transient solvers (STRAND7 2005).

The modal damping value for vibration mode *i* is often denoted by ζ_i and with modal damping included, the modal equilibrium equation is normally put in the format given below.

$$\{\ddot{y}_i\} + 2\zeta\omega_i\{\dot{y}_i\} + \omega_i^2\{y_i\} = r_i \quad (3.5)$$

where $\{y_i\}$ is the modal displacement, ω_i is the frequency, and r_i is modal load.

The calculated damping coefficients can be used in further dynamic analysis in either the spectral, harmonic response or transient solvers. The mass participation factor is calculated using the following equation (STRAND7 2005):

$$P.F. = \frac{\left(\{\phi_i\}^T[M]\{E\}\right)^2}{\{E\}^T[M]\{E\}} \quad (3.6)$$

where:

$\{E\}$Global displacement vector, determined by the excitation direction

$\{\phi_i\}$ *i*-th mode shape vector

The effective damping coefficients for each mode can be found by:

$$DC = \frac{\sum_{j=1}^{n}\{\phi_{ij}\}^T DC_j[k_j]\{\phi_{ij}\}}{\{\phi_i\}^T[K]\{\phi_i\}} \quad (3.7)$$

where:

$\{\phi_{ij}\}$ Mode shape vector of element *j* of *i*-th mode

$[k_j]$ Stiffness matrix of element *j*

DC_j Damping coefficient of element *j*

3.8.3 Laminate theory

As the properties of top and bottom skins of the GFRP beams and slabs are input in STRAND7 as a laminate material using 'laminate' option, it is worthwhile examining the governing equations relevant to laminate theory used in STRAND7.

When the thickness of the laminates in a laminated composite is small, the Classical Lamination Theory (CLT), based on the same hypotheses of the Classical Plate Theory can be effectively used (Treviso et al. 2017). However, in thick laminates, the

transverse stresses are no longer negligible and refinements are required to correctly capture the structure behaviour (Gibson 2012). In STRAND7 (2005), the laminate engineering properties and the characteristic matrices are calculated based on standard laminate theory. The laminate relations used are expressed in matrix form. The fundamental relationships are defined below (STRAND7 2005).

The lamina stiffness matrix [Q] defines the relationship between stresses and strains in the material axes:

$$\begin{Bmatrix}\sigma_1\\ \sigma_2\\ \tau_{12}\end{Bmatrix} = [\mathbf{Q}]\begin{Bmatrix}\varepsilon_1\\ \varepsilon_2\\ \frac{1}{2}\gamma_{12}\end{Bmatrix} = \begin{bmatrix}\frac{E_1}{1-v_{12}v_{21}} & \frac{E_2 v_{12}}{1-v_{12}v_{21}} & 0\\ \frac{E_2 v_{12}}{1-v_{12}v_{21}} & \frac{E_2}{1-v_{12}v_{21}} & 0\\ 0 & 0 & 2G_{12}\end{bmatrix}\begin{Bmatrix}\varepsilon_1\\ \varepsilon_2\\ \frac{1}{2}\gamma_{12}\end{Bmatrix} \quad (3.8)$$

where σ, ε and υ denote stresses, strains and Poisson's ratio, respectively, and

G_{12} = in-plane shear modulus

γ_{12} = in-plane shear strain

τ_{12} = in-plane shear strength

The corresponding lamina compliance matrix [S] relates strain to stress in material axes,

where $[S] = [Q]^{-1}$ is:

$$\begin{Bmatrix}\varepsilon_1\\ \varepsilon_2\\ \frac{1}{2}\gamma_{12}\end{Bmatrix} = [\mathbf{S}]\begin{Bmatrix}\sigma_1\\ \sigma_2\\ \tau_{12}\end{Bmatrix} = \begin{bmatrix}\frac{1}{E_1} & \frac{-v_{21}}{E_2} & 0\\ \frac{-v_{12}}{E_1} & \frac{1}{E_2} & 0\\ 0 & 0 & \frac{1}{2G_{12}}\end{bmatrix}\begin{Bmatrix}\sigma_1\\ \sigma_2\\ \tau_{12}\end{Bmatrix} \quad (3.9)$$

The terms above are a result of compacting the tensor relationship (a 6 x 6 matrix relation). This is because the thickness of the ply is so small relative to its planar dimensions that no stress is generated through its thickness and thus plane stress is assumed (STRAND7 2005).

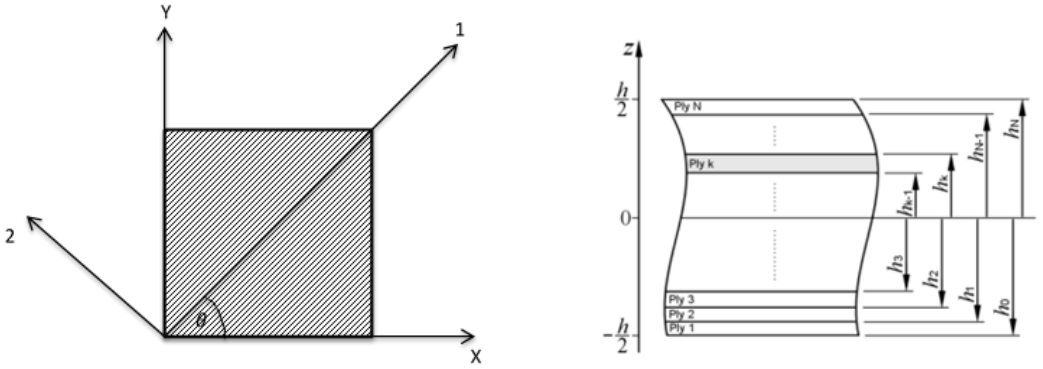

(a) Element x-y axes and fibre 1-2 axes (b) Plies in a laminate

Figure 3.11 Element x-y-axes, fibre 1-2-axes and plies in a laminate (STRAND7 2005)

Laminate stresses and strains (in structural axes) are related to lamina stresses and strains (in material axes) by the following transformations, as shown in Figure 3.11.

$$\begin{Bmatrix} \sigma_1 \\ \sigma_2 \\ \tau_{12} \end{Bmatrix} = [\mathbf{T}] \begin{Bmatrix} \sigma_x \\ \sigma_y \\ \tau_{xy} \end{Bmatrix} \tag{3.10}$$

$$\begin{Bmatrix} \varepsilon_1 \\ \varepsilon_2 \\ \frac{1}{2}\gamma_{12} \end{Bmatrix} = [\mathbf{T}] \begin{Bmatrix} \varepsilon_x \\ \varepsilon_y \\ \frac{1}{2}\gamma_{xy} \end{Bmatrix} \tag{3.11}$$

where the transformation matrix [T] is given by

$$[\mathrm{T}] = \begin{bmatrix} \cos^2\theta & \sin^2\theta & 2\cos\theta\sin\theta \\ \sin^2\theta & \cos^2\theta & -2\cos\theta\sin\theta \\ -\cos\theta\sin\theta & \cos\theta\sin\theta & \cos^2\theta - \sin^2\theta \end{bmatrix} \tag{3.12}$$

Note here that equation 3.11 (the tensor relationship for strain) is of a different form to the standard engineering definition of strain. Using this definition of strain, it conveniently turns out that the stress and strain transformations matrices are identical.

The stress/strain relationship in xy-axes is:

$$\begin{Bmatrix}\sigma_x\\ \sigma_y\\ \tau_{xy}\end{Bmatrix} = [\mathbf{Q}']\begin{Bmatrix}\varepsilon_x\\ \varepsilon_y\\ \frac{1}{2}\gamma_{xy}\end{Bmatrix} \tag{3.13}$$

where

$$[\mathbf{Q}'] = [\mathbf{T}^{\mathbf{T}}][\mathbf{QT}] \tag{3.14}$$

Equation (3.13) can be further expressed as

$$\begin{Bmatrix}\sigma_x\\ \sigma_y\\ \tau_{xy}\end{Bmatrix} = [\overline{\mathbf{Q}}]\begin{Bmatrix}\varepsilon_x\\ \varepsilon_y\\ \gamma_{xy}\end{Bmatrix} \tag{3.15}$$

The matrix $[\overline{\mathbf{Q}}]$ can be determined by comparing (3.15) with (3.13).

With perfect bond between the plies, the strain distribution along the thickness direction of the laminate can be assumed to be;

$$\begin{Bmatrix}\varepsilon_x\\ \varepsilon_y\\ \gamma_{xy}\end{Bmatrix} = \varepsilon^m + z\mathrm{S} = \begin{Bmatrix}\varepsilon_x^{\boldsymbol{m}}\\ \varepsilon_y^{\boldsymbol{m}}\\ \varepsilon_{xy}^{\boldsymbol{m}}\end{Bmatrix} + z\begin{Bmatrix}\mathrm{K}_x\\ \mathrm{K}_y\\ \mathrm{K}_{xy}\end{Bmatrix} \tag{3.16}$$

where z is the coordinate in the direction normal to the mid-plane with z=0 at the mid-plane, ε^m is the mid-plane membrane strain vector and S is the laminate plate curvature vector.

The constitutive equation for the total laminate plate is described by

$$\begin{Bmatrix}\mathbf{N}\\ \mathbf{P}\end{Bmatrix} = \begin{bmatrix}\mathbf{A} & \mathbf{B}\\ \mathbf{B} & \mathbf{D}\end{bmatrix}\begin{Bmatrix}\boldsymbol{\varepsilon}^{\boldsymbol{m}}\\ \mathbf{S}\end{Bmatrix} \tag{3.17}$$

where

$$\{\mathbf{N}\} = \begin{Bmatrix}N_x\\ N_y\\ N_{xy}\end{Bmatrix} = \int_{-k/2}^{k/2}\begin{Bmatrix}\sigma_x\\ \sigma_y\\ \tau_{xy}\end{Bmatrix}dz = \sum_{k=1}^{N}\int_{h_{k-1}}^{h_k}\begin{Bmatrix}\sigma_x(z)\\ \sigma_y(z)\\ \tau_{xy}(z)\end{Bmatrix}dz \tag{3.18}$$

is the resultant force vector, which has units of force per unit length, and

$$\{\mathbf{P}\} = \begin{Bmatrix} P_x \\ P_y \\ P_{xy} \end{Bmatrix} = \int_{-k/2}^{k/2} \begin{Bmatrix} \sigma_x \\ \sigma_y \\ \tau_{xy} \end{Bmatrix} z\, dz = \sum_{k=1}^{N} \int_{h_{k-1}}^{h_k} \begin{Bmatrix} \sigma_x(z) \\ \sigma_y(z) \\ \tau_{xy}(z) \end{Bmatrix} z\, dz \tag{3.19}$$

is the resultant moment vector, which has units of moment per unit length.

[A] is the extensional stiffness matrix (membrane elasticity matrix) defined by

$$[\mathbf{A}] = \sum_{k=1}^{N} (h_k - h_{k-1})[\overline{\mathbf{Q}}_k] \tag{3.20}$$

[D] is the bending stiffness matrix defined by

$$[\mathbf{D}] = \frac{1}{3} \sum_{k=1}^{N} (h_k^3 - h_{k-1}^3)[\overline{\mathbf{Q}}_k] \tag{3.21}$$

and [**B]** is the extensional/bending coupling matrix defined by

$$[\mathbf{B}] = \frac{1}{2} \sum_{k=1}^{N} (h_k^2 - h_{k-1}^2)[\overline{\mathbf{Q}}_k] \tag{3.22}$$

where $[\overline{\mathbf{Q}}_k]$ is the elasticity matrix for ply *k* (see Figure 3.11(b)), and the matrices [**C]** and [**D]** are symmetric.

Using the above definitions, it is possible to determine the ply stresses and/or ply strains (as explained in equations 3.13-3.15) resulting from the applied stress resultants and applied moment resultants or by applied mid-plane strains and curvatures, in the absence of thermal strains.

3.8.4 Response spectrum analysis

According to STRAND7 (2005), an improved understanding about how spectral analysis works comes from the details of its numerical implementation. Once the natural frequencies and mode shapes have been calculated, it is possible to decouple the equation of motion into single oscillators:

$$\{\ddot{y}\} + [S]\{y\} = [L] \tag{3.23}$$

where

{y} = Modal coordinate vector; and

[S] = Diagonal normalized stiffness matrix.

At this stage the damping is added to each of the equations and the external force taken from the design spectrum corresponding to the equation's frequency. If the design spectrum is defined in terms of acceleration, the right hand side will have the following expression:

$$[L_i] = [\phi_i^T][M]\{r\}[S_i] \quad (3.24)$$

where

$[\phi_i]$ = The i-th eigenvector;

[M] = Mass matrix;

{r} = Seismic direction vector; and

$[S_i]$ = Ordinate in the design spectrum at the frequency of the i-th mode.

If the spectrum has been normalized then the peak value is included in the direction vector r. If the spectrum is defined in terms of an external load and not ground acceleration, then the following right hand side applies:

$$[L_i] = [\phi_i^T]\{R\} \quad (3.25)$$

where

{R} = Load vector for a particular load case.

The decoupled equations are solved and the solution transformed back to physical coordinates.

$$x_i = [\phi_i]y_i \quad (3.26)$$

3.8.5 Modal combination rules

In RSA method modal responses are calculated and combined appropriately to get the total response.

STRAND7 provides two of the most common methods for combining modal responses; the square root of the sum of square (SRSS) method and the complete quadratic combination (CQC) method.

The SRSS method calculates the total response of the structure (s) using the following equation (STRAND7 2005):

$$s = \left(\sum_{i=1}^{n} s_i^2\right)^{\frac{1}{2}} \quad (3.27)$$

where s_i is one of the n corresponding modal values ($i = 1, 2, \ldots n$).

The CQC method uses the following equation.

$$s = \left(\sum_{i=1}^{n} \sum_{i=1}^{n} \rho_{ij} s_i s_j\right)^{\frac{1}{2}} \quad (3.28)$$

$$\rho_{ij} = \frac{8(\zeta_i \zeta_j)^{\frac{1}{2}}(\zeta_i + \beta\zeta_j)\beta^{\frac{3}{2}}}{(1-\beta^2)^2 + 4\zeta_i\zeta_j\beta(1+\beta^2) + 4\left(\zeta_i^2 + \zeta_j^2\right)\beta^2} \quad (3.29)$$

and

$$\zeta_i = \frac{c_i}{2\omega_{ni}} \quad (3.30)$$

$$\zeta_j = \frac{c_j}{2\omega_{nj}} \quad (3.31)$$

$$\beta = \frac{\omega_{nj}}{\omega_{ni}} \quad (3.32)$$

In the equations, c_i, c_j, ω_{ni} and ω_{nj} denote damping coefficients and angular natural frequencies of modes i and j.

According to (Chopra 1995), SRSS provides accurate response estimates only for structures with well-separated natural frequencies while CQC is applicable to a wider class of structures, as it overcomes the limitations of SRSS rule.

3.9 Earthquake analysis methods according to AS1170.4 (2007)

Australian Standard (AS 1170.4, 2007) offers three types of analysis procedures for structural systems. These are;

1. Simple static check
2. Static analysis
3. Dynamic analysis

Figure 3.12 (adopted from Figure 2.2 of AS1170.4-2007) summarises the design procedure for earthquake actions depending on the Earthquake Design Category (EDC).

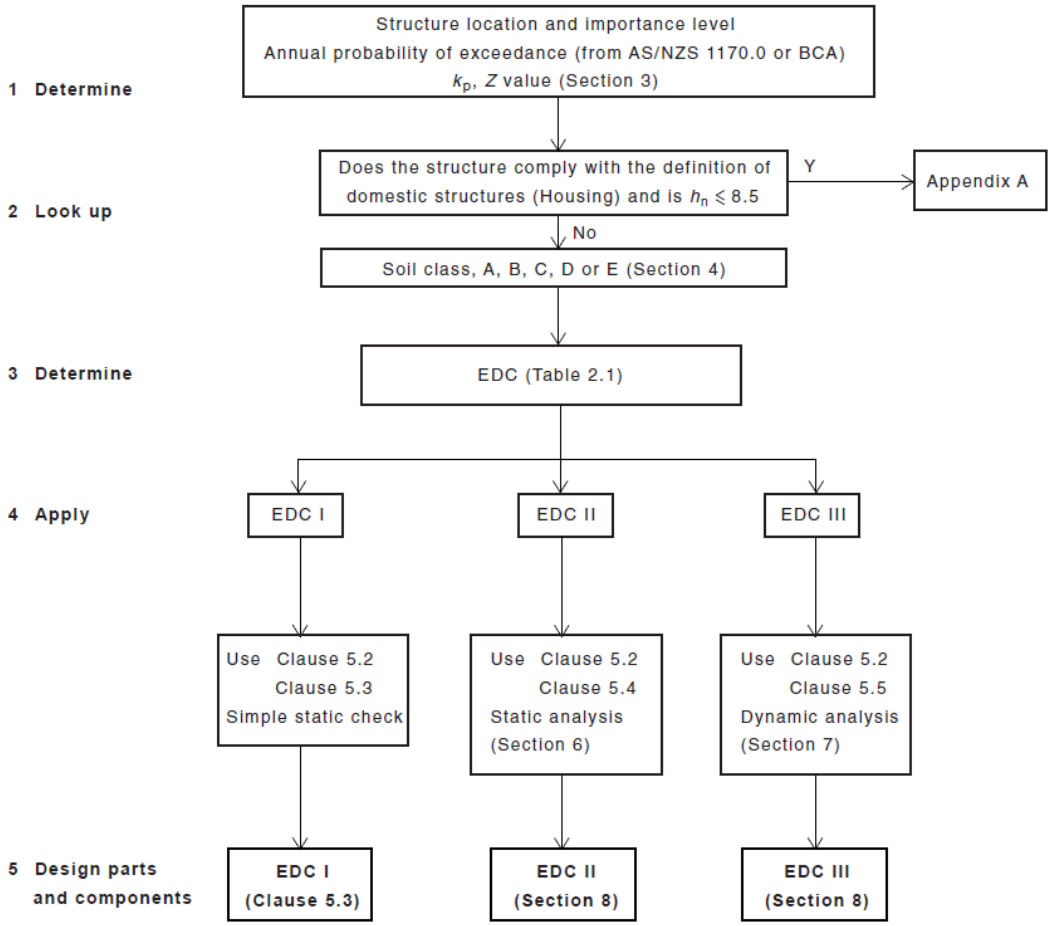

Figure 3.12 Seismic design procedure- Flow diagram (AS1170.4: 2007)

The Earthquake analysis has been carried out in accordance with specifications and recommendations stipulated in Australian Standard (AS1170.4 2007), and the step-by-step procedure is described in Chapter 6.

CHAPTER 4 FREE VIBRATION BEHAVIOUR OF DEBONDED COMPOSITE BEAMS

4.1 Introduction

Fibre reinforced polymer composites have an extensive array of applications ranging from structural applications such as beams, girders and slabs, to aircraft industry and recreational use. While sandwich composite construction has some great benefits, the behaviour of sandwich structures containing damage is much more complex and one of the major factors limiting the effective usage of sandwich structures.

An experimental study of the innovative GFRP sandwich (developed in Australia) was carried out by Manalo et al. (2010b) to find the flexural behaviour of a simply supported GFRP sandwich beam. In that study, the authors investigated the experimental behaviour of the GFRP sandwich beam in the flat-wise and edge-wise positions. According to Aravinthan and Manalo (2012), while fibre composites are reaching a point of commercial reality in the Australian construction industry, challenges faced by the structural designer includes, the understanding of the behaviour of the fibre composite materials, its failure modes and applying available design guidelines to the local needs.

One of the main concerns in sandwich composites is that their load carrying capacity may be significantly reduced by local damage (debonding) between the face sheet and the core (Rizov et al. 2005). This could be due to manufacturing defects like incomplete wetting or entrapped air pockets in the adhesive layer between the core and skins. Debonding could also be caused by local separation of skin due to accidental dropping of tools during construction and maintenance of the composite structure (Burlayenko & Sadowski 2010, Guedra 1977). Water absorption, overloading and elevated temperature levels can also cause debonding (Manalo et al. 2010c). Debonding has considerable effects on the vibration parameters, such as natural frequencies and mode shapes of the beam. Therefore, it is important to make accurate predictions of changes in natural frequencies in such structures. Moreover,

having accurate predictions for the changes of free vibration parameters is very useful for non-destructive detection of invisible defects such as debonding in sandwich construction. This chapter concentrates on investigating the dynamic behaviour of fibre composite sandwich beams with debonds.

4.2 Research approach

The research approach embraced in the analysis is finite element based modelling and analysis using three-dimensional models of composite beams to accurately simulate the actual behaviour. A parametric investigation is carried out to assess the influence of various parameters of concern including length and width of the debond, location of debond, size and support conditions of the beam on the free vibration behaviour of novel GFRP sandwich beams. Small test beams are first used to model and analyse the free vibration behaviour, and then these test specimen sizes are extended to a practical size. The parametric approach adopted here enables comparisons to be made among different debonding configurations, in order to support design decisions. The commercial finite element software package STRAND7 (2010) is used for modelling by giving due consideration to bonded and debonded interfaces between skin and core using rigid and master-slave link elements as appropriate.

4.3 Modelling and assumptions

4.3.1 Contact model using master-slave links

Development of the model for beams has been described in Chapter 3, using a ‘constrained ‘or ‘contact’ model to simulate debonding phenomenon. Hence master slave links are used in the finite element model to allow for sliding between interfaces of skin and core in the horizontal directions while keeping skins in contact with the core in the vertical direction to effectively simulate a debonded beam according to ‘contact model’. After the FE model has been created, the appropriate eigenvalue problem can be solved to obtain natural frequencies and corresponding mode shapes. As usual in the conventional finite element method, more elements will ensure better convergence and, therefore, the mesh size was suitably refined to get the required convergence, to obtain natural frequencies as accurately as possible with the minimum number of elements, to save computational effort. The finally

established finite element mesh for the test beam consists of 11979 nodes with 1920 plates (8x120 in each of the skins), 7680 bricks (8x8x120 in the core) and 2178 links (2x9x121 from plate nodes to top and bottom surface nodes in the core).

4.3.2 Modelling contact and free models using spring elements

According to Schwarts et al. (2007), the contact conditions (either ‘contact’ or ‘free’) at the debonded surfaces have a significant influence in cases involving large debonded zones or stiff core materials. To investigate the influence of degree of contact on the dynamic behaviour of debonded composite beams, a ‘spring model’ in STRAND7 is employed. A free model and a contact model have been simulated using spring elements to compare the natural frequency results for the two models, to justify the use of contact model for the present study. Note here that, in the contact model, the interfaces of debonding are assumed to be in contact (in vertical direction) throughout the motion while the free model assumes that the interfaces are always open and free. To simulate the contact model using spring elements, a spring model is implemented between the skin and the core of debonded single layer beams by removing the master slave links and replacing them with spring damper elements in STRAND7. Initially the axial stiffness of the spring was increased until the analyses give similar frequency values as accomplished for the contact model with master-slave links described above. Assigning zero stiffness for these spring elements simulates a free model, and comparisons were made between contact and free models.

4.3.3 Assumptions made for the contact model

Assumptions made in the FE simulation are listed below.

1. Debonding is assumed to be an artificial flaw of zero thickness, embedded between top skin and core.
2. Debonding exists before vibration starts and stays constant without propagation during the period of vibration.
3. Debonded surfaces (of skin and core) are assumed to be in contact vertically but can slide in the horizontal plane (similar to contact or constrained model).

4.4 Verification for the beam model

4.4.1 Materials and procedure

Primarily, the numerical model is verified by comparing model results with published results by Burlayenko and Sadowski (2011) and Schwarts et al. (2007, 2008) for a foam core sandwich panel. Natural frequencies of intact (fully bonded) and debonded foam cored sandwich beams were obtained by Burlayenko and Sadowski (2011) using ABAQUS FE code, and by Schwarts et al. (2007, 2008) using a higher order analytical approach (Modified Galerkin Method) and using ANSYS FE package. Figure 4.1 shows a diagram of longitudinal and cross sections of the foam cored beam used for the verification. The beam is 300 mm long and 20 mm wide with a 19.05 mm thick foam core. Top and bottom skin thicknesses are 0.5 mm and 1.0 mm respectively. All dimensions shown in Figure 4.1 are in millimetres (mm).

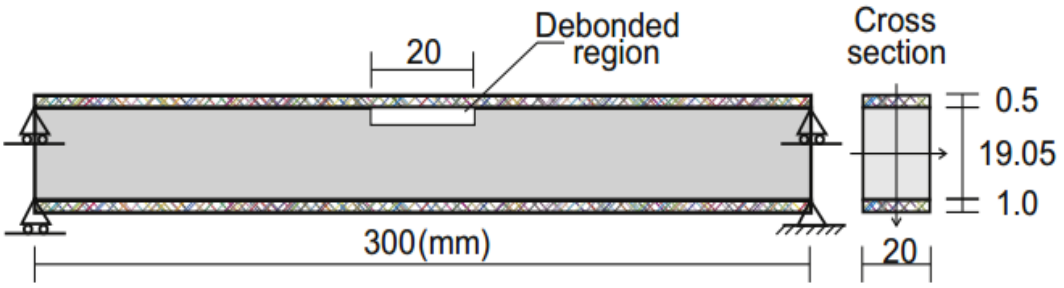

Figure 4.1 Longitudinal and cross sections of the debonded sandwich beam with foam core (Burlayenko & Sadowski 2011)

The debonding considered in these studies is 20 mm long, centrally located at the interface between top skin and core, extending through the full width of the beam. The beam is simply supported at the ends of both top and bottom skins as shown in Figure 4.1. The core is assumed to be linear elastic orthotropic while the skin is isotropic (Schwarts et al. 2007).

Table 4.1 gives material properties of the foam core sandwich beam used by both Burlayenko and Sadowski (2011) and Schwarts et al. (2007, 2008) for their studies, extracted from Burlayenko and Sadowski (2011).

Table 4.1 Material properties of foam cored sandwich beam (Burlayenko and Sadowski 2011)

Property	Skins	Core
Type	Isotropic	Isotropic
Young's modulus E (MPa)	36000	50
Poisson's ratio, ν	0.3	0.19
Density ρ (kg/m^3)	4400	52

The natural frequencies from the proposed model (developed by STRAND7) for the foam core sandwich beam are obtained and compared with results reported by Burlayenko and Sadowski (2011) and Schwarts et al. (2007, 2008).

4.4.2 Model verification results

A comparison of the numerical results of natural frequencies from the developed model with those from Burlayenko and Sadowski (2011) and Schwarts et al. (2007, 2008) is presented in Table 4.2 and Table 4.3. Table 4.2 gives results for the intact beam whereas Table 4.3 is for the debonded beam.

Table 4.2 Comparison of natural frequencies (Hz) for the fully bonded foam cored sandwich beam

Mode Number	ABAQUS Burlayenko and Sadowski (2011)	ANSYS Schwarts et al. (2007)	Modified Galerkin Method Schwarts et al. (2007)	Present analysis with STRAND7
1	293.46	290.76	289.18	293.52
2	707.09	710.67	708.29	722.96
3	1106.70	1117.70	1114.24	1139.51
4	1495.80	1515.30	1511.14	1545.91
5	1818.70	1907.09	1902.25	1863.62

Table 4.3 Comparison of natural frequencies (Hz) for the debonded foam cored sandwich beam

Mode	ABAQUS Burlayenko and Sadowski (2011)	Modified Galerkin Method Schwarts *et al.* (2008)	Present Analysis with STRAND7
B1	293.07	288.98	293.52
L1	433.67	383.38	360.81
T1	-[b]	-[b]	540.79
B2	-[b]	-[b]	710.75
B3	1093.2	1093.2	1139.31
T2	1132.0	1146.9	1146.32
T3	-[b]	-[b]	1394.31
B4	-[b]	-[b]	1520.84
B5	1769.9	1771.3	1861.72
B6	2080.2	1842.2	1948.35

b – Not reported in reference (Burlayenko and Sadowski 2011)

B – Bending mode; L – Lateral mode; and T – Twisting mode

It can be clearly seen that the presented results from STRAND7 show a good agreement with the results reported in the literature thus validating the developed model for the beam.

4.5 Influence of skin-core debonding on dynamic behaviour of GFRP beams

4.5.1 Selection of parameters for the analysis

Composite sandwich beams with core bounded by top and bottom skins with a finite debonding between the top skin and the core are considered (see Figure 3.5) to investigate the dynamic behaviour.

Three boundary conditions for the beam, namely, both ends simply supported (S-S), clamped-clamped (C-C) and clamped-free (C-F) are used in the analyses. Two debonding positions (debonding near end or corner and at centre) are considered for C-C and S-S beams whereas three positions (debonding near fixed end, at centre and near free end) are used for C-F beams. Figure 4.2 explains the three debonding positions considered for C-F beams.

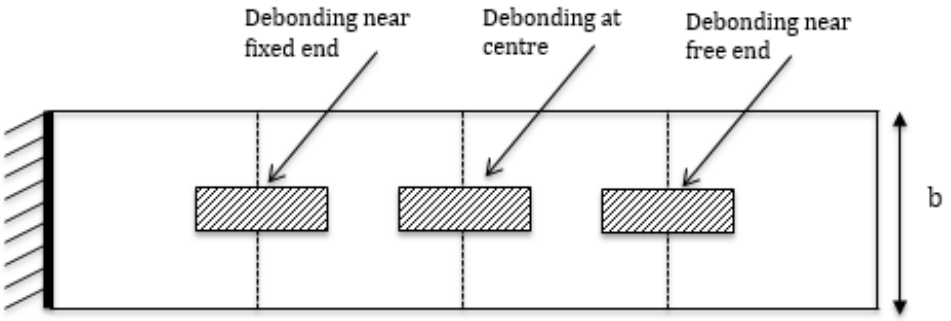

Figure 4.2 Debonding positions considered for C-F beams

The relevant dimensions for the novel composite sandwich beam are (see Figure 3.5):

(a) For the test beam

L = 300 mm, b = 20 mm, h_c = 16 mm and $h_{sb} = h_{st}$ = 2 mm.

(b) For the full scale beam

L = 3m, b = 200 mm, h_c = 160 mm and $h_{sb} = h_{st}$ = 20 mm.

Debonding length ‘a’ varies from

(a) 30 mm to 270 mm in steps of 30 mm for the test beam model, and

(b) 30 cm to 270 cm in steps of 30 cm for the full scale beam model

The debonding is located centrally along the length of the beam and extends through the full width of the beam for case 1 (referred to as full width debonding), and only

middle half width for case 2 (denoted as half width debonding). Each beam presented here is a new generation sandwich composite structure mentioned in the introduction of this chapter and consists of a rigid core bonded to the top and bottom glass fibre composite skins.

Typical 3D finite element models created with STRAND7 for the beams with different end conditions are shown in Figure 4.3.

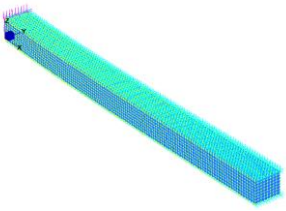

(a) C-F beam (fully bonded)

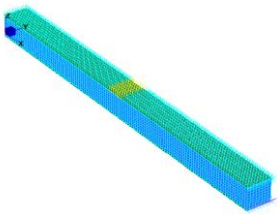

(b) S-S beam 30mm debond length (full width debonding)

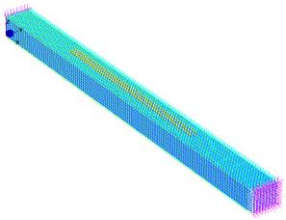

(c) C-C beam 150mm debond length (half width debonding)

Figure 4.3 Typical 3D Finite element models of (a) C-F, (b) S-S and (c) C-C beams with STRAND7

4.5.2 Mechanical properties used for the GFRP sandwich beams

The mechanical properties used by Manalo et al. (2010b) for the innovative GFRP beam have been employed for the present study and were listed in Table 2.1. Materials in each of the skins are assumed to be orthotropic and linear elastic. Core material is assumed to be linear elastic, homogeneous and isotropic. The beam longitudinal and cross sections have been defined in Figure 3.5.

4.6 Results and Discussion

4.6.1 Results for the 300 mm test beam

4.6.1.1 Influence of debonding size and end conditions of the beam

Free vibration frequencies for the first five modes for the novel composite sandwich test beam with full width, half width and various lengths of debonding along the length of the beam are presented in this section.

Frequency results for case 1(full width debonding) for the test beam are listed in Table 4.4, 4.5 and 4.6. Table 4.4 presents results for a beam with simply supported (S-S) ends while Tables 4.5 and 4.6 show results for C-C and C-F end conditions, respectively. Similarly, Tables 4.7, 4.8 and 4.9 illustrate case 2 results for half width debonding. The debonding length (a/L) = 0 corresponds to the fully bonded or intact beam.

Table 4.4 First five frequencies (in Hz) of a simply supported (S-S) novel sandwich beam with full-width debonding

Debond length, a/L	Mode 1	Mode 2	Mode 3	Mode 4	Mode 5
0	289.78	1015.26	1580.87	2103.39	3152.96
0.1	289.78	1004.14	1577.27	2102.16	3068.59
0.2	289.72	954.04	1561.91	2085.11	2818.74
0.3	289.43	864.98	1537.75	2011.43	2660.67
0.4	288.48	768.90	1505.78	1866.39	2636.19
0.5	286.15	689.94	1442.13	1737.26	2610.09
0.6	281.56	633.54	1347.37	1686.34	2477.64
0.7	273.87	597.35	1270.42	1675.93	2288.38
0.8	262.72	577.46	1230.09	1666.79	2137.18
0.9	247.91	569.99	1218.40	1629.04	2062.35

Table 4.5 First five frequencies (in Hz) of a clamped- clamped (C-C) novel sandwich beam with full-width debonding

Debond length, a/L	Mode 1	Mode 2	Mode 3	Mode 4	Mode 5
0	592.28	1421.21	2440.31	3535.90	3559.82
0.1	592.25	1401.74	2438.94	3444.76	3537.24
0.2	591.71	1320.98	2413.64	3138.73	3537.09
0.3	588.71	1203.55	2301.44	2974.30	3533.40
0.4	579.16	1110.95	2097.59	2954.38	3501.87
0.5	557.67	1065.27	1916.46	2920.99	3395.82
0.6	521.33	1055.28	1826.33	2776.32	3288.57
0.7	473.15	1051.72	1810.52	2629.06	3227.69
0.8	420.10	1018.48	1795.04	2586.58	3152.76
0.9	368.58	942.71	1706.80	2563.78	3044.52

Table 4.6 First five frequencies (in Hz) of a clamped- free (C-F) novel sandwich beam with full-width debonding

Debond length, a/L	Mode 1	Mode 2	Mode 3	Mode 4	Mode 5
0	106.69	609.16	1517.53	1772.36	2609.95
0.1	106.57	609.09	1492.06	1772.05	2603.27
0.2	105.95	608.36	1386.67	1771.12	2553.26
0.3	104.48	604.98	1234.81	1770.03	2407.51
0.4	101.95	595.15	1110.89	1768.60	2174.50
0.5	98.31	574.55	1038.25	1765.15	1972.93
0.6	93.73	541.74	1007.44	1755.18	1870.65
0.7	88.51	500.08	999.21	1735.34	1848.44
0.8	82.97	455.31	991.19	1703.66	1840.11
0.9	77.42	412.31	965.71	1659.41	1794.04

Table 4.7 First five frequencies (in Hz) of a simply supported (S-S) novel sandwich beam with half-width debonding

Debond length, a/L	Mode 1	Mode 2	Mode 3	Mode 4	Mode 5
0	289.78	1015.26	1580.87	2103.39	3152.96
0.1	289.78	1013.84	1580.40	2103.13	3142.35
0.2	289.77	1012.07	1579.71	2100.98	3133.75
0.3	289.75	1010.81	1578.96	2095.76	3132.53
0.4	289.70	1010.16	1578.14	2088.93	3130.09
0.5	289.62	1009.97	1577.27	2083.35	3119.68
0.6	289.51	1009.94	1576.38	2080.78	3105.48
0.7	289.37	1009.70	1575.51	2080.43	3096.71
0.8	289.20	1008.95	1574.64	2079.41	3095.27
0.9	288.98	1007.32	1573.77	2074.04	3091.62

Table 4.8 First five frequencies (in Hz) of a clamped- clamped (C-C) novel sandwich beam with half-width debonding

Debond length, a/L	Mode 1	Mode 2	Mode 3	Mode 4	Mode 5
0	592.28	1421.21	2440.31	3535.90	3559.82
0.1	592.27	1418.73	2439.96	3534.49	3546.90
0.2	592.19	1415.88	2436.47	3529.26	3541.22
0.3	591.95	1414.32	2428.36	3527.88	3540.82
0.4	591.47	1413.94	2418.92	3526.55	3536.15
0.5	590.72	1413.85	2412.84	3514.43	3532.35
0.6	589.71	1412.84	2411.36	3499.77	3531.80
0.7	588.47	1409.90	2410.77	3495.16	3531.59
0.8	587.06	1404.69	2405.30	3493.64	3531.38
0.9	585.56	1397.65	2392.18	3479.51	3531.26

Table 4.9 First five frequencies (in Hz) of a clamped-free (C-F) novel sandwich beam with half-width debonding

Debonds length, a/L	Mode 1	Mode 2	Mode 3	Mode 4	Mode 5
0	106.69	609.16	1517.53	1772.36	2609.95
0.1	106.68	609.15	1514.29	1772.32	2608.90
0.2	106.65	609.07	1510.53	1772.26	2603.95
0.3	106.63	608.85	1508.41	1772.20	2593.81
0.4	106.61	608.42	1507.80	1772.15	2582.62
0.5	106.59	607.78	1507.72	1772.09	2575.68
0.6	106.57	606.96	1506.90	1772.03	2573.93
0.7	106.55	606.00	1504.48	1771.96	2573.19
0.8	106.53	604.99	1500.43	1771.90	2568.32
0.9	106.51	603.98	1495.48	1771.84	2558.35

Comparison of corresponding natural frequencies for the fully bonded beams with the three end conditions reveals that beam with C-C end condition has the highest natural frequency values whereas the C-F beam has the lowest. This is due to the fact that C-C beam has the highest restraint conditions and hence highest stiffness.

It is observed that, in general, the extent of natural frequency variation with respect to debonding length increases with the order of the natural frequency, giving the least variation for the first frequency. The results for the two cases indicate that the natural frequency response is significantly affected by full width debonding whereas half width debonding has only a slight influence on natural frequencies.

A normalized form of the frequency results of first three natural frequencies for full width debonding with regard to the three end conditions considered is shown in Figure 4.4. It shows frequency variation (w/w_0) with debonding length as a ratio of beam length (a/L) for the composite beam with full width debonding for (a) S-S, (b) C-C and (c) C-F end conditions. Note here that w_0 is the frequency of the virgin beam and w is the frequency of debonded beam for the corresponding mode.

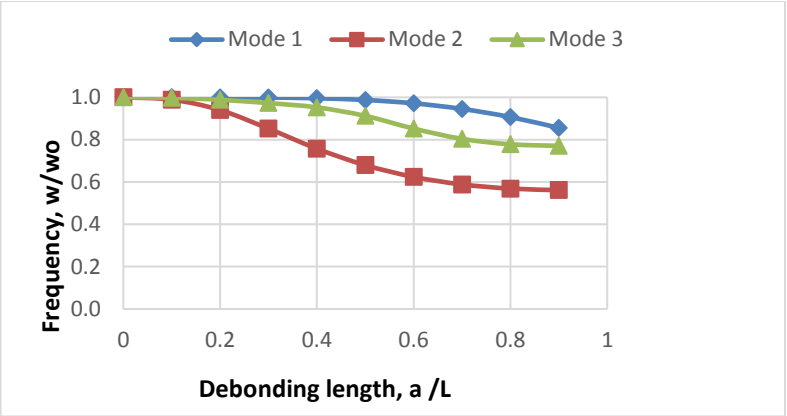

(a) S-S beam

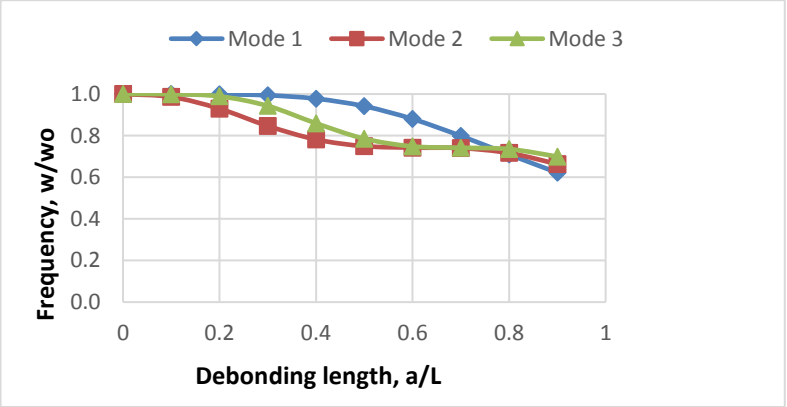

(b) C-C beam

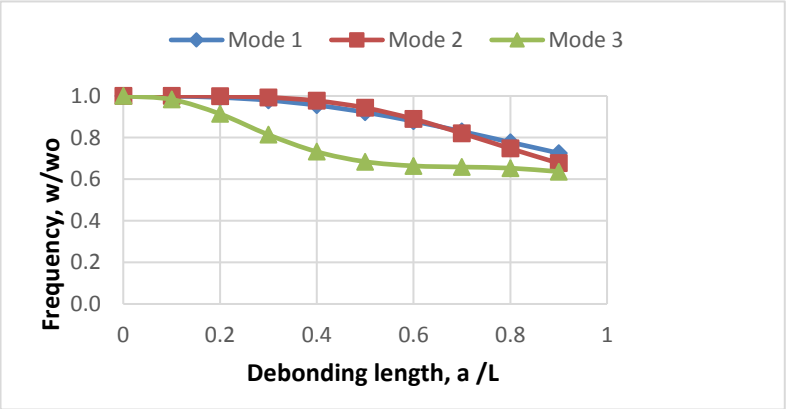

(c) C-F beam

Figure 4.4 Comparison of frequency variation (w/w_0) with debonding length for the composite beam with full width debonding for (a) S-S, (b) C-C and (c) C-F end conditions.

Comparison of frequency variations for the three end conditions illustrated in Figure 4.4 reveals that first natural frequency has the least effect on debonding for the case of full width debonding. Careful observation of Tables 4.8, 4.9 and 4.10 further reveals that this is true for half width debonding as well. It is interesting to note from Figure 4.4 that debonding does not have much effect on the first frequency when debonding length, a/L, is less than 0.4 for all three end conditions considered in the analysis. In fact, second mode frequency is the most sensitive frequency to debonding length for both S-S and C-C end conditions, with the only exception occurring at C-C beam which shows a sharp drop for first natural frequency for debonding length of 0.9L, giving it the least value out of the three modes. On the contrary, for C-F beam, third mode dominates with regard to sensitivity to debonding length. In addition, mode 1 and 2 frequencies of the C-F beam show nearly the same sensitivity to debonding length in contrast to the substantial difference shown by S-S and C-C beams for the same. This is an interesting observation which reveals that the end conditions of the beam is a governing factor dictating which modes are more affected. It is also interesting to observe that the first natural frequency is unaffected when a/L is less than 0.3 for all three end conditions. It is also seen that the maximum reduction in natural frequencies is close to but always below 50% of virgin beam frequencies for all three end conditions, namely S-S, C-C and C-F end conditions even when the debonding is right through the full length of the composite beam. This is important as this confirms that if the working frequency of the beam is kept away from the range 50% to 100% of the virgin beam there is no possibility of resonance happening due to debonding in the beam considered.

Comparison of percentage reduction in natural frequency when compared with fully bonded beam for case 1 and case 2 for S-S, C-C and C-F boundary conditions are illustrated graphically in Figure 4.5 (a), (b) and (c), respectively.

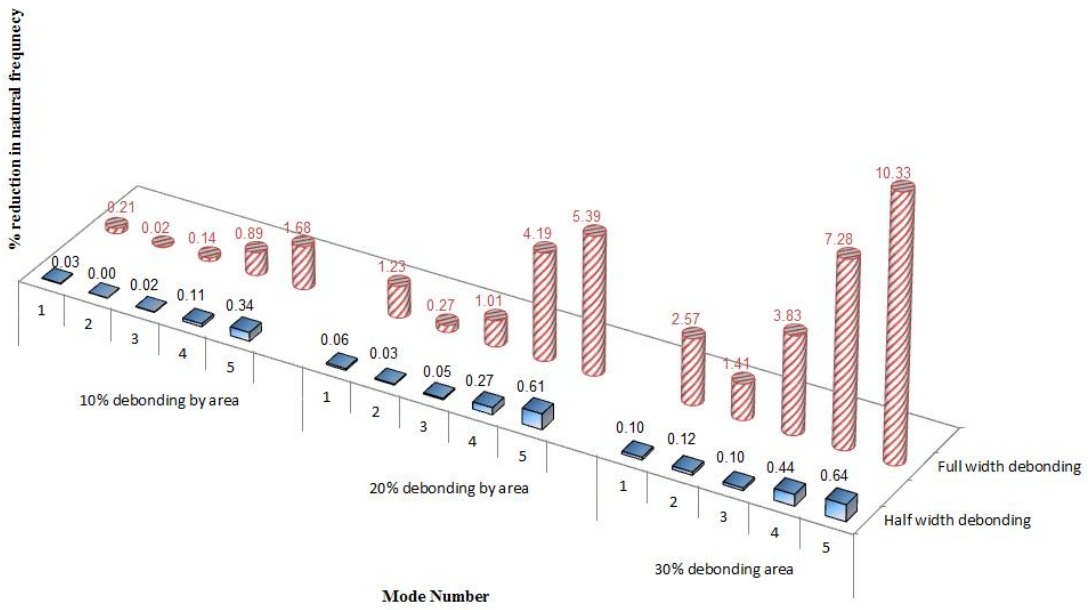

(a) Comparison of half width and full width debonding near end :S-S beam

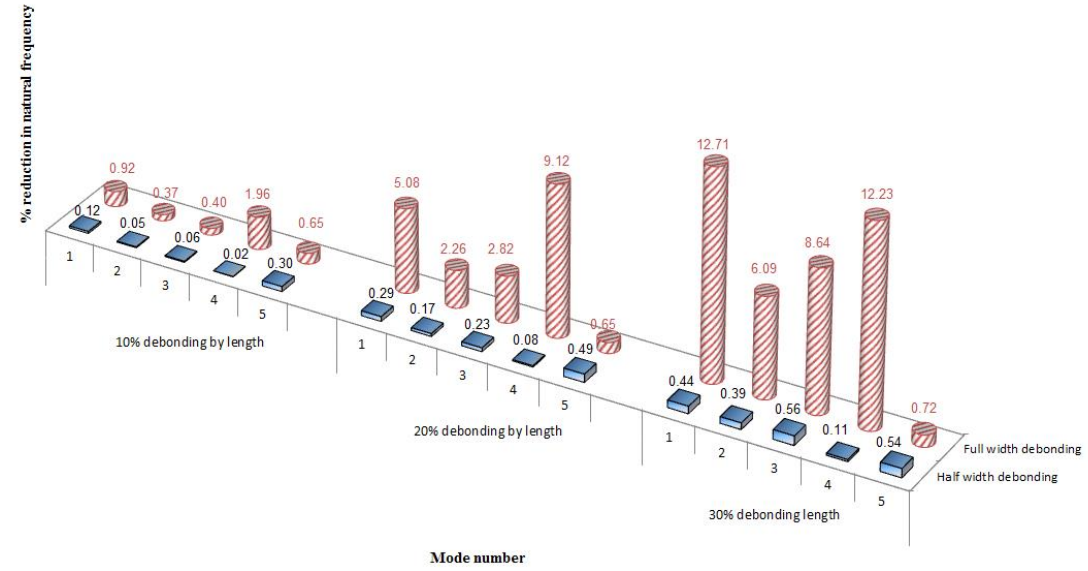

(b) Comparison of half width and full width debonding near end: C-C beam

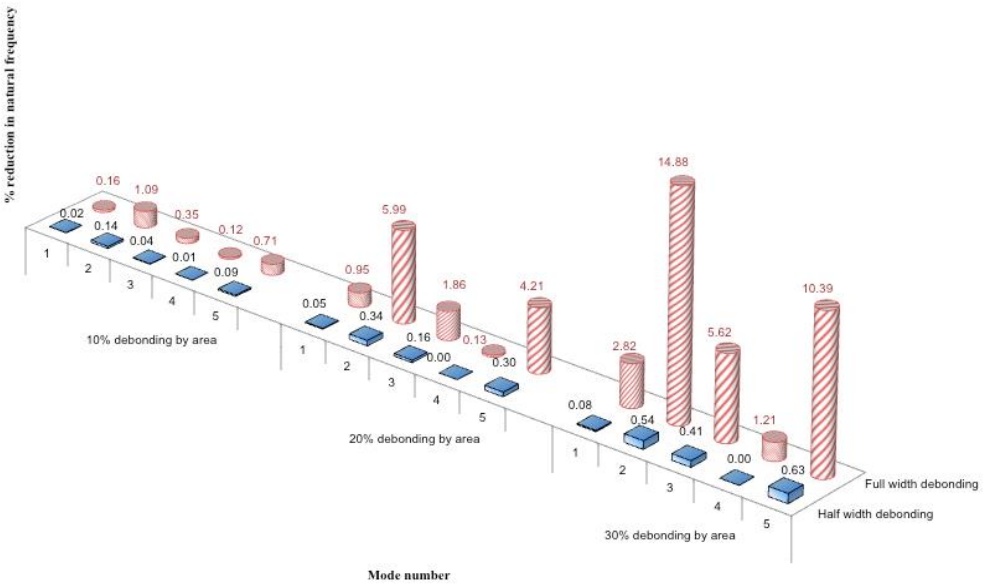

(c) Comparison of half width and full width debonding near end C-F beam

Figure 4.5 Comparison of half width and full width debonding for (a) S-S, (b) C-C and (c) C-F beams

It is interesting to observe that percentage of natural frequency reduction is significantly dependent on the boundary conditions of the beam and, furthermore, it is rigorously dependent on whether the debonding is half width or full width. Generally, it is seen that C-C boundary condition gives highest reduction in natural frequency whereas C-F gives lowest variation. It is clear from all three boundary conditions that full width debonding causes severe reduction in natural frequency compared to half width debonding. Although there is a general tendency that the extent of natural frequency variation with respect to debonding increases with the mode number for S-S beams, this does not show the same trend for other two boundary conditions. Thus it can be concluded that the effect on debonding does not always exhibit an increasing trend as the mode number increases, but follows different trends depending on the boundary condition, extent of debonding and location of the debond. It is of special practical interest to observe in all three boundary conditions that when the extent of debonding is small, its effect on natural frequency reduction is negligible. Thus it is revealed that when the extent of debonding is not more than 10% of the top area of the beam (this is the case with 10% debonding by length and half width debonding), the natural frequency reduction is negligible for all three end conditions considered in the present analysis.

It is interesting to compare some noticeable mode shapes of half width debonding and full width debonding in three end conditions considered in the simulation and analyses. One such comparison is illustrated in Figure 4.6 for the three end conditions of the beam for full width and half width debonding having 30 mm debond length.

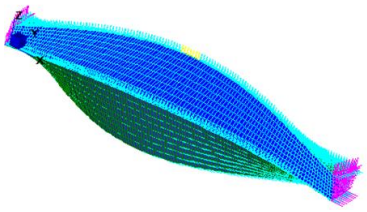

Mode 3 (full width debonding for C-C case)

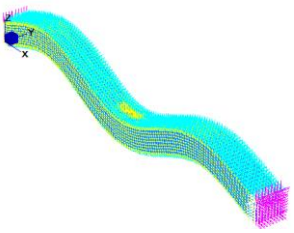

Mode 3 (half width debonding for C-C case)

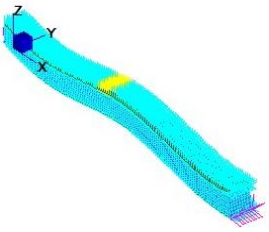

Mode 3 (full width debonding for S-S case)

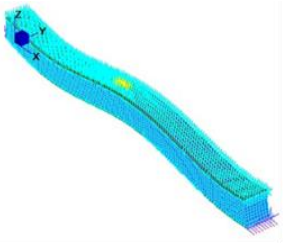

Mode 3 (half width debonding for S-S case)

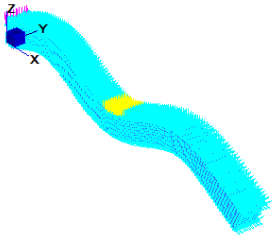

Mode 3 (full width debonding for C-F case)

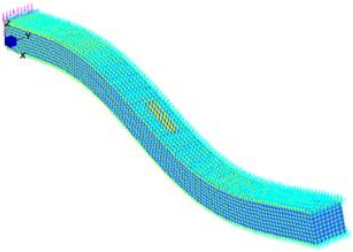

Mode 3 (half width debonding for C-F case)

Figure 4.6 Comparison of prominent mode shapes for C-C, S-S, and C-F end conditions for full-width and half-width debonding (for 30 mm debond length)

It is fascinating to witness here that bending modes prevalent in 3rd mode in half width debond case are replaced by twisting modes for full width debond, for the C-C end condition. This is attributed to increased participation of rotational or twisting modes in full width debonding case compared to half width debonding situation for the C-C case. This reveals that full width debonding leads to increased participation of twisting modes, specifically for clamped-clamped end condition. Such transition is not seen in the cases of S-S beam or C-F beam as illustrated in Figure 4.6.

Similar transition from bending mode to twisting mode was observed in the comparison of mode 6 as well, only in the case of C-C beam (Figure 4.7).

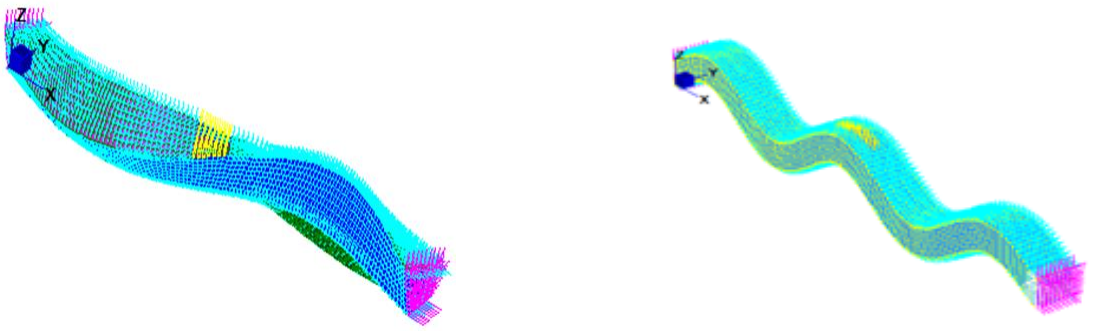

Mode 6 (full width debonding) Mode 6 (half width debonding)

Figure 4.7 Comparison prominent of mode shapes for C-C beam for full-width and half-width debonding (for 30 mm debond length)

Thus it can be concluded that full width debonding attributes to increased participation of twisting modes.

4.6.1.2 Effect of location of debonding

To investigate the effect of location of debonding on the natural frequency variation, similar extents of debonding are compared for two debonding locations, namely, near the end of the beam and at the centre. In the case of centre debonding, the debonding is located centrally along the length of the beam and extends through the middle half width of the beam for case 1, and through full width for case 2 (as illustrated in

Figure 4.8). Debonding near ends of the beam too contains two cases for half width and full width debonding as described. Typical 3D finite element models created with STRAND7 for the beams with C-F and S-S end conditions to investigate the influence of debonding location are shown in Figure 4.8.

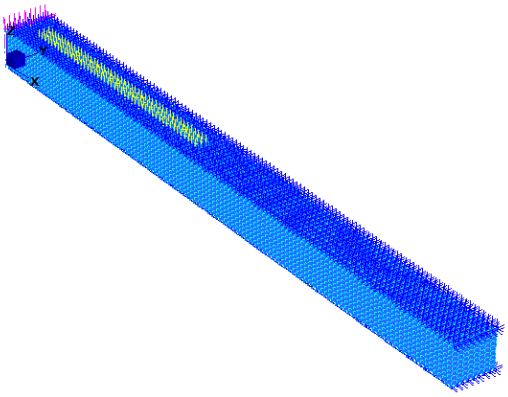

(a) C-F beam 120 mm debond length (Half width debonding near fixed end)

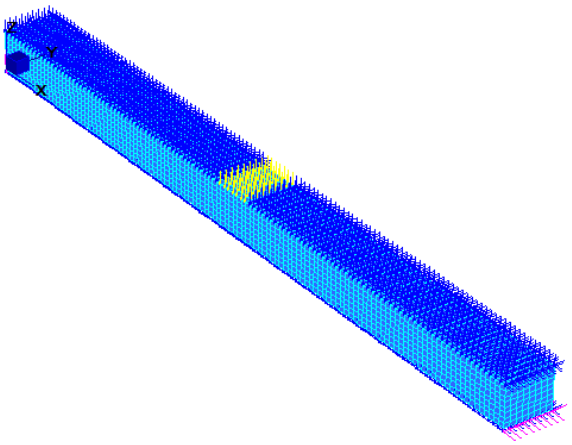

(b) S-S beam 30 mm debond length (Full width debonding at centre)

Figure 4.8 Typical 3D Finite element models of (a) C-F and (b) S-S and beams with STRAND7

Figure 4.9 shows the comparison of natural frequency reduction due to debonding near end and at centre for 150 mm long half width debonding (50% of debonding by length for case 2) for all three boundary conditions. Note here that for the C-F boundary condition, debonding near the fixed end of the beam (which gives higher

reduction in natural frequency compared to debonding near free end) has been selected for comparison.

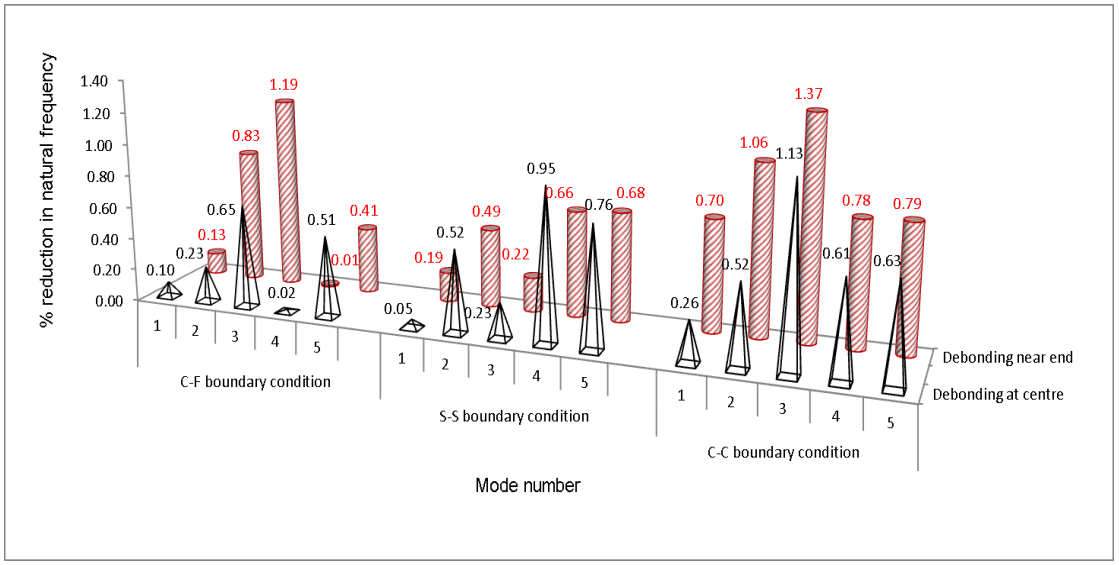

Figure 4.9 Comparison of debonding near end and at centre for the three boundary conditions

A general reflection through all these variations is that for similar extents of debonding, free vibration behaviour changes depending on the location of debonding along the beam. It is seen that for C-F and C-C end conditions, debonding near end generally gives higher extent of natural frequency reduction compared to centre debonding. On contrary, for S-S boundary condition, there is a general tendency that centre debonding gives higher reduction in natural frequency.

The cantilever beam (C-F) has a special situation with regards to debonding near the end, due to the difference in boundary conditions prevailing in the beam (one end is free and the other end is fixed). This has been investigated by simulating debonding near fixed end and free end separately and the results are shown in Figure 4.10.

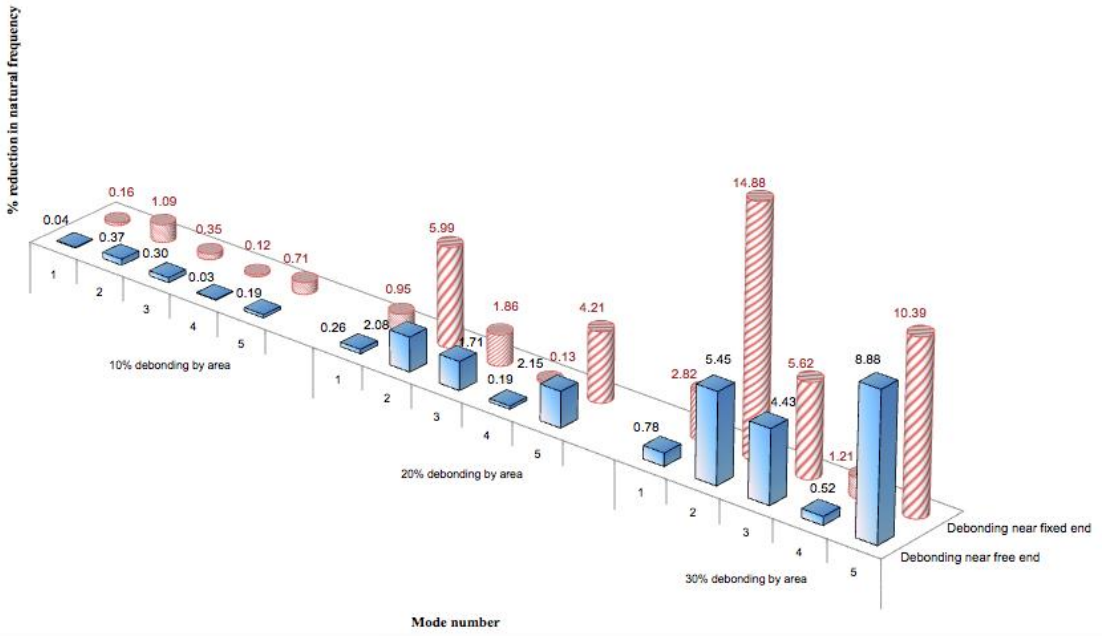

Figure 4.10 Comparison of debonding near fixed end and free end for cantilever (C-F) beam

It is interesting to observe that debonding near fixed end gives much higher reductions in natural frequency compared to debonding near the free end of the beam for similar extents of debonding. This is the case for all the extents of debonding considered in the present analysis. This it can be concluded that the influence of debonding on natural frequency can be lessened by keeping the debonding damage away from the fixed end of the beam.

4.6.1.3 Effect of multiple debonding

For the investigation of effect of multiple debonding on the free vibration characteristics, single and multiple debonding for some prominent cases are compared in this section. Figure 4.12 shows the comparison of the percentage reduction in natural frequency for single and multiple debonding for a beam with S-S boundary condition. Here the debonding considered is 10% by length and half width debonding (30 mm length of debonding for case 1) as illustrated in Figure 4.11.

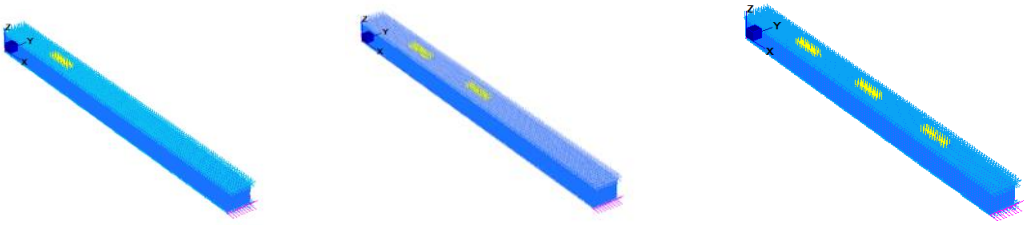

Single debonding (near one end) Double debonding (near one end and at centre) Triple debonding (near two ends and at centre)

Figure 4.11 Single and multiple debonding (10% by length half width debonding) for S-S beam

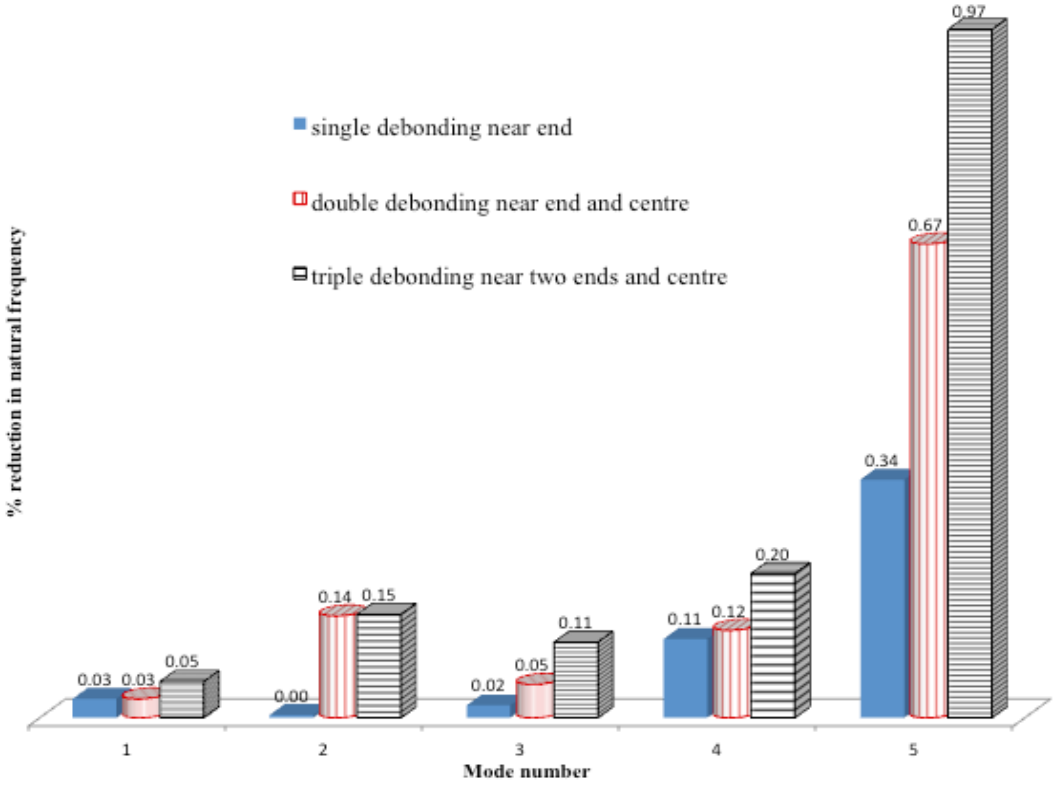

Figure 4.12 Comparison of single and multiple debonding for S-S beam with 10% half width debonds

It is revealed from Figure 4.12 comparison that the effect of multiple debonding on the extent of natural frequency variation for higher modes is generally larger than that for lower modes, yet this variation does not increase linearly as the mode number increases. This is the general trend seen in other boundary conditions as well, as

illustrated by Figure 4.13, which shows a similar scenario (10% by length half width debonding) for a beam having C-C boundary condition.

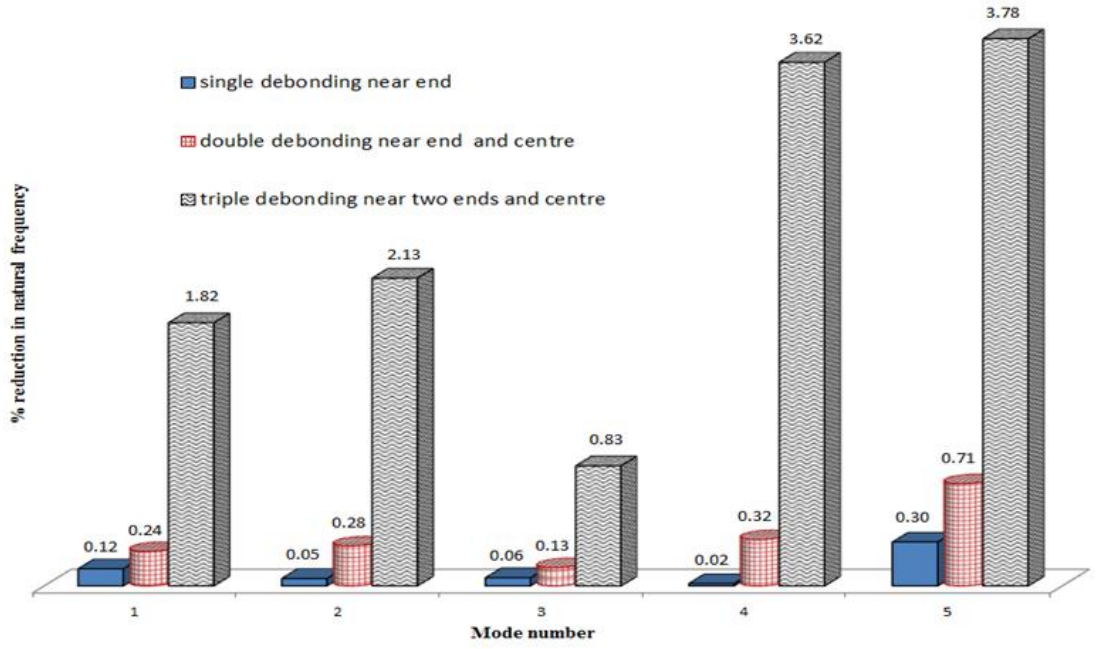

Figure 4.13 Comparison of single and multiple debonding for C-C beam with 10% half width debonds

Comparison of Figures 4.12 and 4.13 reveals that multiple debonding has a much higher effect on C-C boundary condition compared to S-S boundary condition, especially for higher modes. It is interesting to observe from Figure 4.13 that triple debonding (having three times the debonding area compared to single debonding) causes more than ten times the reduction in natural frequency compared to single debonding, even for the first natural frequency). Thus it is confirmed that the effect of multiple debonding on the free vibration behaviour considerably depends on the boundary conditions of the beam. For similar extents and locations of debonding, the effects of debonding on natural frequencies become much more pronounced when the panel is more restrained.

4.6.1.4 Influence of degree of contact in the debonding region

In models with spring elements assigned in place of master slave link elements, it was observed that, the frequency results give similar values as expected for similar debonding with master slave links, when the axial stiffness is increased to 1000

N/mm. Thus it is revealed that spring elements can successfully be accommodated to model the required degree of contact in debonding region, by assigning the appropriate stiffness for the spring element. Assigning zero stiffness to spring elements used in place of master slave links similarly simulates free models.

Figure 4.14 shows the comparison of natural frequencies for constrained (contact) and free models (developed using spring elements) for the test beam for 30 mm debonding length with half width and full width debonding for C-C case.

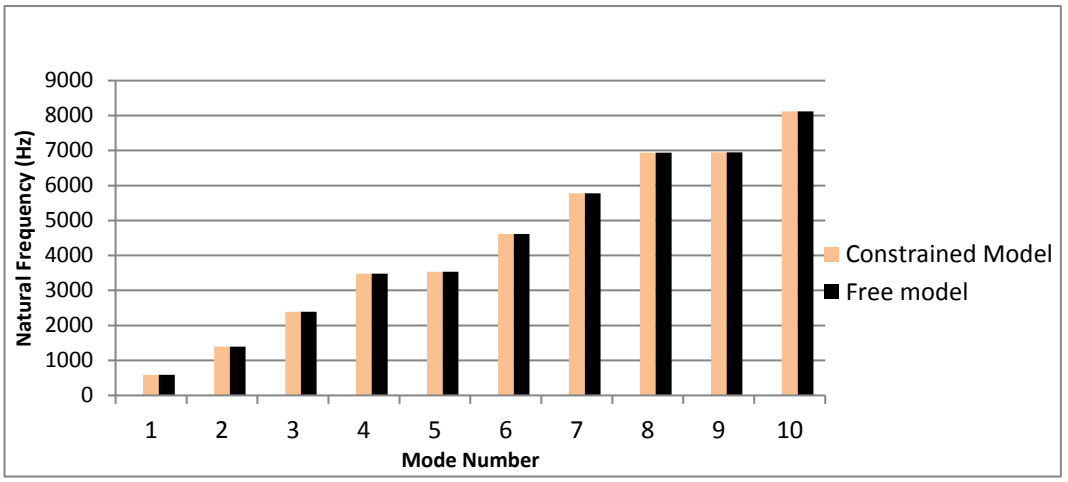

(a) 30 mm half width debonding for C-C case

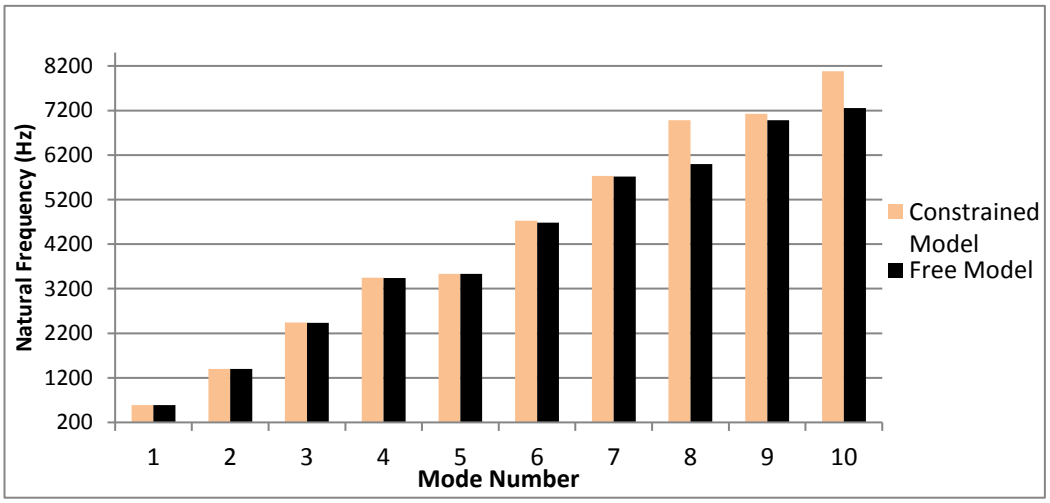

(b) 30 mm full width debonding for C-C case

Figure 4.14 Comparison of natural frequencies for constrained and free models for test beam

It is clearly observed that the variation in natural frequency for contact and free models are much more significant for full width debonding than half width debonding. Further it is revealed that this variation is negligible for lower mode numbers and becomes significant for higher mode numbers, but not necessarily in the increasing order of the mode numbers. For example, Figure 4.14 (b) reveals that the frequency variation is more significant for mode 8 than for mode 9. The same trend is seen for other cases and other debonding lengths as well.

Figure 4.15 demonstrates the comparison of natural frequencies for constrained (contact) and free models for the test beam for 270 mm debonding length with half width and full width debonding for C-C case.

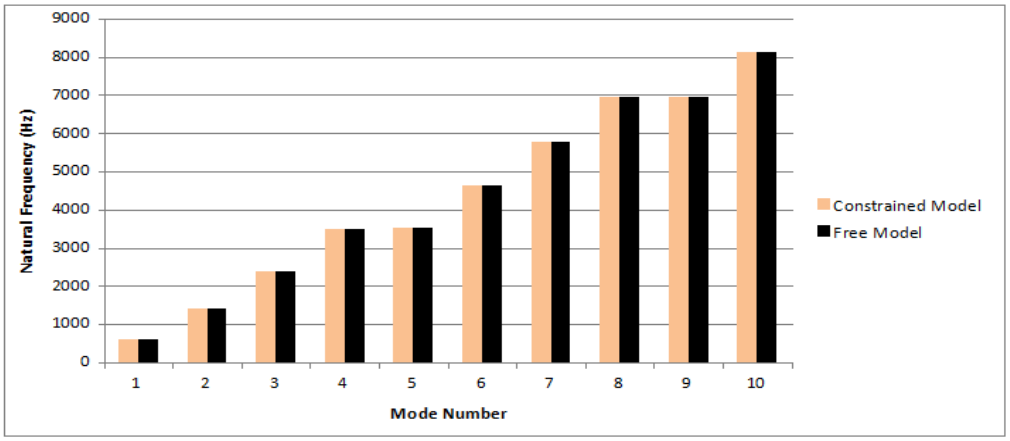

(a) 270 mm half width debonding for C-C case

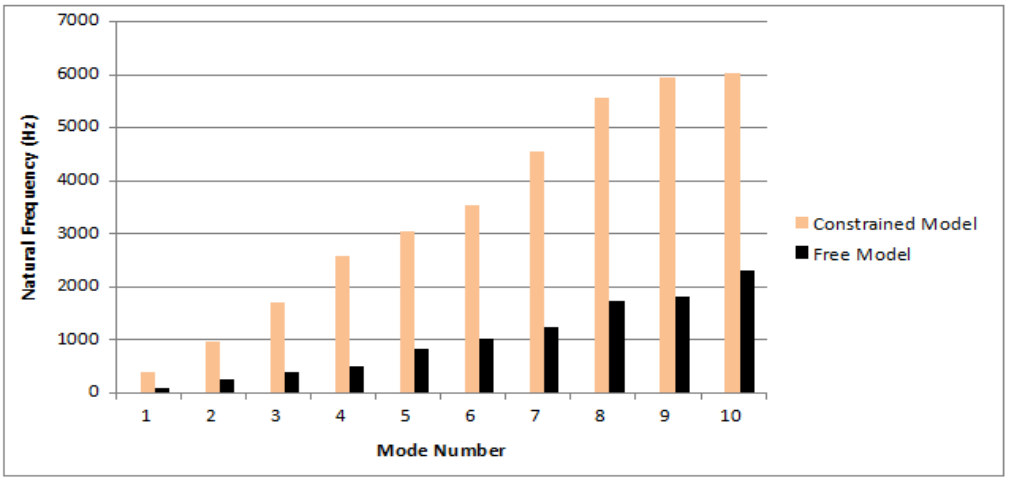

(b) 270 mm full width debonding for C-C case

Figure 4.15 Comparison of natural frequencies for constrained and free models for test beam

It is interesting to observe that there is a significant variation of natural frequency for contact and free models in 270 mm full width debonding, compared to 30 mm full width debonding. It can, therefore, be concluded that both width and length of debonding will greatly influence the extent of natural frequency variation between contact and free models. In addition it is also clear that full width debonding has much more pronounced effect on this variation than half width debonding, revealed by the vast discrepancy in frequency seen in contact and free models in 270 mm long full width debonding case illustrated in Figure 4.15. It is revealed that, free model shows unrealistically higher natural frequency reductions compared to contact model, (evidently due to physically unreal overlapping occurring at the debonded interface) for similar debonding scenarios. Furthermore it is evident that this influence becomes more pronounced when debonding areas are large. Thus it is confirmed from the results that the contact model represents the debonding behaviour more realistically, hence justifying the use of contact model for the present analysis. This in fact is a stimulating observation revealing the importance of choosing the proper degree of contact in debonding region in the analysis of debonded composite beams used in practice.

4.6.2 Results for the 3 m beam

4.6.2.1 Influence of extent of debonding and end conditions of the beam

Natural frequency results for case 1(full width debonding) for the 3 m beam are listed in Table 4.10, 4.11 and 4.12 for C-C, S-S and C-F respectively. Likewise, Tables 4.13, 4.14 and 4.15 illustrate case 2 results for half width debonding for the three end conditions stated above.

Table 4.10 First five frequencies (in Hz) of a clamped (C-C) novel sandwich beam with full-width debonding

Debond length, a/L	Mode 1	Mode 2	Mode 3	Mode 4	Mode 5
0	59.228	142.121	244.031	353.590	355.982
0.1	59.225	140.174	243.894	344.476	353.724
0.2	59.171	132.098	241.364	313.873	353.709
0.3	58.871	120.355	230.144	297.430	353.340
0.4	57.916	111.095	209.759	295.438	350.187
0.5	55.767	106.527	191.646	262.099	339.582
0.6	52.133	105.528	182.633	277.632	328.857
0.7	47.315	105.172	181.052	262.906	322.769
0.8	42.010	101.848	179.504	258.658	315.276
0.9	36.858	94.271	170.680	256.378	304.452

Table 4.11 First five frequencies (in Hz) of a simply supported (S-S) novel sandwich beam with full-width debonding

Debond length, a/L	Mode 1	Mode 2	Mode 3	Mode 4	Mode 5
0	28.978	101.526	158.087	210.339	315.296
0.1	28.978	100.414	157.727	210.216	306.859
0.2	28.972	95.404	156.191	208.511	281.874
0.3	28.943	86.498	153.775	201.143	266.067
0.4	28.848	76.890	150.578	186.639	263.619
0.5	28.615	68.994	144.213	173.726	261.009
0.6	28.156	63.354	134.737	168.634	247.764
0.7	27.387	59.735	127.042	167.593	228.838
0.8	26.272	57.746	123.009	166.679	213.718
0.9	24.791	56.999	121.840	162.904	206.235

Table 4.12 First five frequencies (in Hz) of a cantilever (C-F) novel sandwich beam with full-width debonding

Debond length, a/L	Mode 1	Mode 2	Mode 3	Mode 4	Mode 5
0	10.669	60.916	151.753	177.236	260.995
0.1	10.657	60.909	149.206	177.206	260.327
0.2	10.595	60.836	138.667	177.112	255.326
0.3	10.448	60.498	123.481	177.003	240.751
0.4	10.195	59.515	111.089	176.860	217.450
0.5	9.831	57.455	103.825	176.515	197.293
0.6	9.373	54.174	100.744	175.518	187.065
0.7	8.851	50.008	99.921	173.534	184.844
0.8	8.297	45.531	99.119	170.366	184.011
0.9	7.742	41.231	96.571	165.941	179.404

It is observed from the comparison of fully bonded frequencies (when debonding length a/L is zero) of Tables 4.10, 4.11 and 4.12 that C-C end condition has the highest frequency values indicating the highest stiffness whereas C-F beam shows the least stiffness. It is also revealed that full width debonding causes drastic changes to natural frequencies compared to fully bonded beams due to immense loss of stiffness due to full width debonding.

Table 4.13 First five frequencies (in Hz) of a clamped (C-C) novel sandwich beam with half-width debonding

Debond length, a/L	Mode 1	Mode 2	Mode 3	Mode 4	Mode 5
0	59.228	142.121	244.031	353.590	355.982
0.1	59.227	141.873	243.996	353.449	354.690
0.2	59.219	141.588	243.647	352.926	354.122
0.3	59.195	141.432	242.836	352.788	354.082
0.4	59.147	141.394	241.892	352.655	353.615
0.5	59.072	141.385	241.284	341.443	353.235
0.6	58.971	141.284	241.136	349.977	353.180
0.7	58.846	140.990	241.075	349.508	353.159
0.8	58.707	140.468	240.530	349.357	353.138
0.9	58.557	139.765	239.218	347.943	353.126

Table 4.14 First five frequencies (in Hz) of a simply supported (S-S) novel sandwich beam with half-width debonding

Debond length, a/L	Mode 1	Mode 2	Mode 3	Mode 4	Mode 5
0	28.978	101.526	158.087	210.339	315.296
0.1	28.978	101.384	158.040	210.313	314.235
0.2	28.977	101.207	157.971	210.098	313.375
0.3	28.975	101.081	157.896	209.576	313.253
0.4	28.970	101.016	157.814	208.893	313.009
0.5	28.962	100.997	157.727	208.335	311.968
0.6	28.951	100.994	157.638	208.078	310.548
0.7	28.937	100.970	157.551	208.043	309.671
0.8	28.920	100.895	157.464	207.941	309.527
0.9	28.898	100.732	157.377	207.404	309.162

Table 4.15 First five frequencies (in Hz) of a cantilever (C-F) novel sandwich beam with half-width debonding

Debond length, a/L	Mode 1	Mode 2	Mode 3	Mode 4	Mode 5
0	10.669	60.916	151.753	177.236	260.995
0.1	10.668	60.915	151.429	177.232	260.890
0.2	10.665	60.907	151.053	177.226	260.395
0.3	10.663	60.885	150.841	177.220	259.381
0.4	10.661	60.842	150.780	177.215	258.262
0.5	10.659	60.778	150.772	177.209	257.568
0.6	10.657	60.696	150.690	177.203	257.393
0.7	10.655	60.600	150.448	177.196	257.319
0.8	10.653	60.499	150.043	177.190	256.832
0.9	10.651	60.398	149.548	177.184	255.835

Comparison of full width and half width debonding as indicated by frequency values in the above tables reveals that half width debonding has much lesser effects on natural frequency compared to full width debonding. A closer look at the vibration modes and their corresponding mode shapes divulges that debonding causes changes in modes of vibration in some modes and these changes are more pronounced in full width debonding than half width debonding. More participation of twisting modes are perceived in full width debonding as demonstrated in Figures 4.16, 4.17 and 4.18 where notable changes observed in C-C, S-S and C-F end conditions respectively are exemplified. Figure 4.16 illustrates the mode shape comparison for 4^{th} mode of vibration for the C-C beam. It is stimulating to see that the sway mode for fully bonded beam is changed to a bending mode in half width debonding while full width debonding causes it to change to a mixed bending and twisting mode.

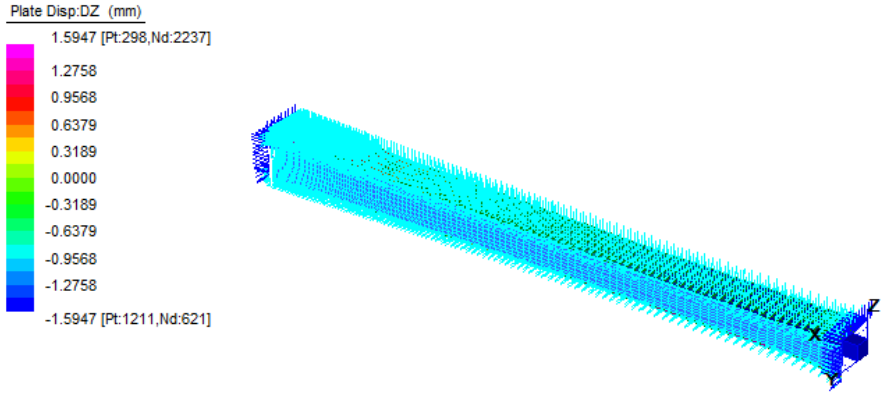

(a) C-C fully bonded beam (sway mode)

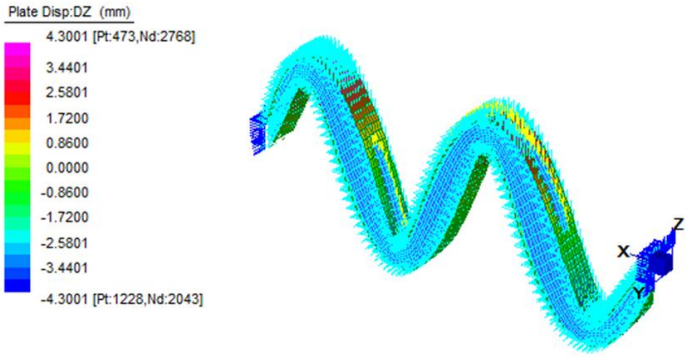

(b) C-C 150 cm long half width debonding (bending mode)

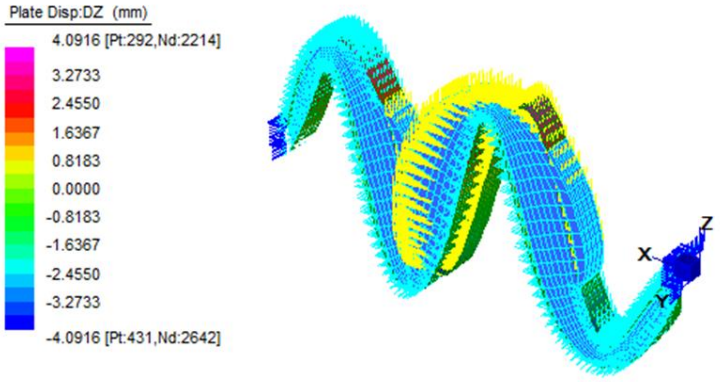

(c) C-C 150 cm long full width debonding (mixed mode; bending and twisting)

Figure 4.16 Comparison of mode shapes for mode 4 in C-C beam

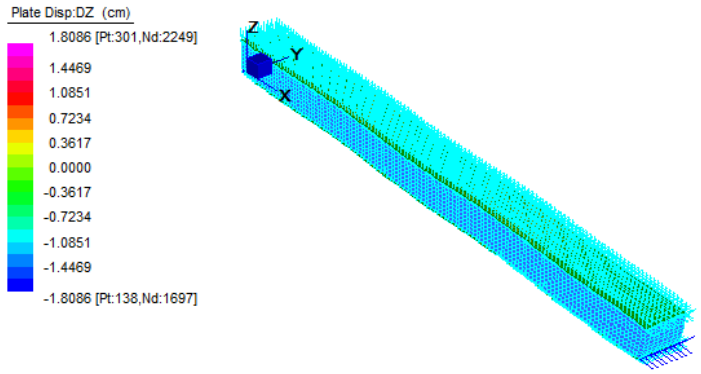

(a) S-S fully bonded beam (longitudinal mode)

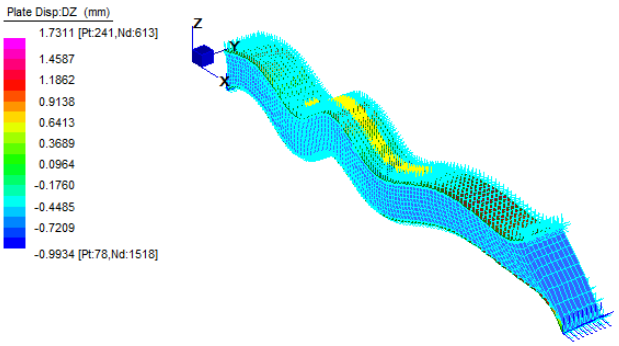

(b) S-S half width 150 cm long debonding (bending mode)

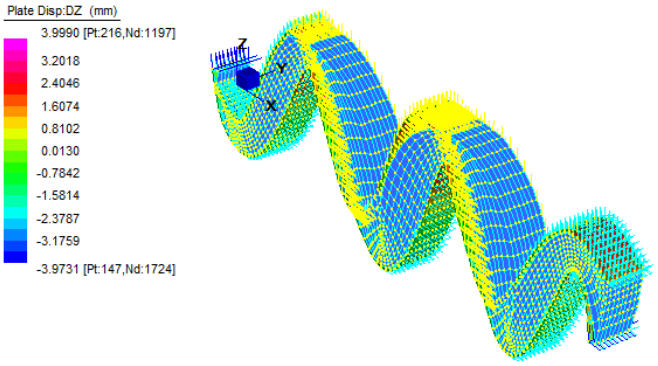

(c) S-S full width 150 cm long debonding (bending mode)

Figure 4.17 Comparison of mode shapes for mode 7 in S-S beam

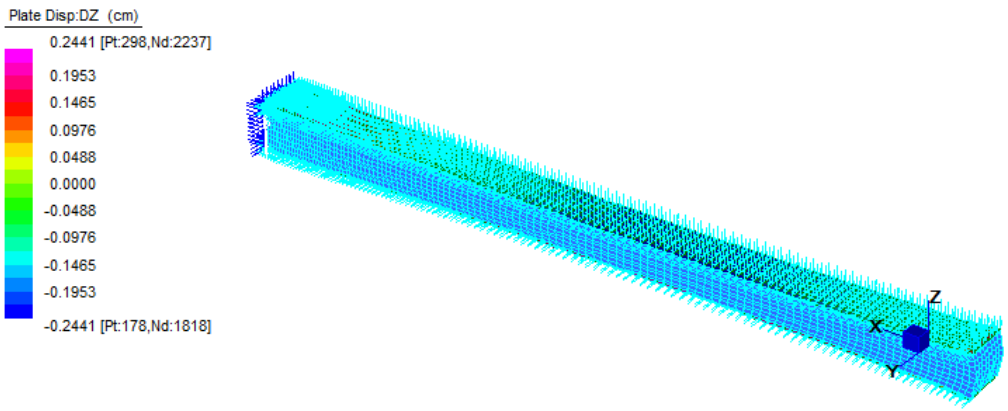

(a) Fully bonded beam (sway mode)

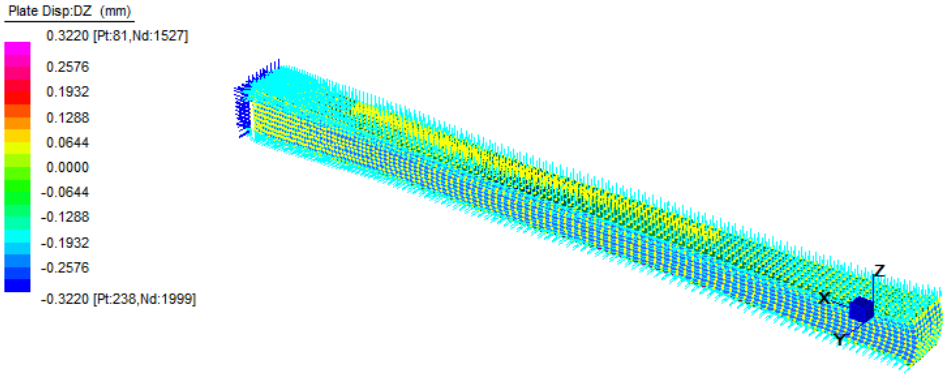

(b) Half width 150 cm long debonding (sway mode)

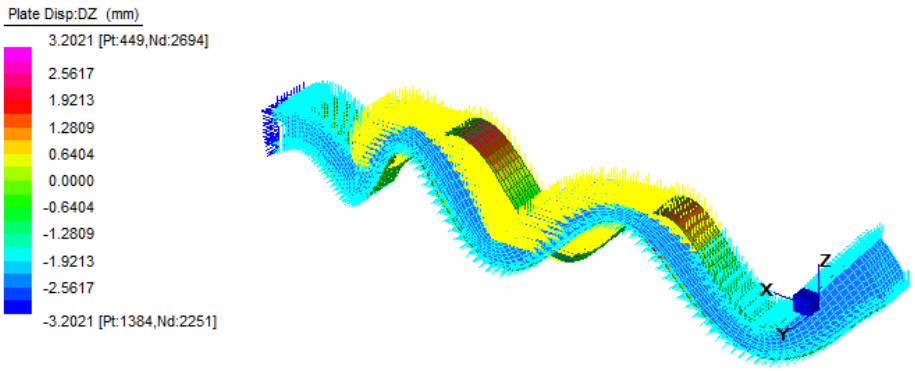

(c) Full width 150 cm long debonding (mixed mode; bending and twisting)

Figure 4.18 Comparison of mode shapes for mode 8 in C-F beam

Figure 4.17 shows the mode shapes for mode 7 in S-S beam where fully bonded beam is compared with half width and full width debonding cases. There the longitudinal mode for fully bonded beam changes to a bending mode in half width

and full width debonding. Somewhat similar scenario to C-C beam occurs in C-F beam mode 8 comparison as revealed from Figure 4.18. In that situation, half width debonding does not cause any change in vibration mode, yet full width debonding sources dramatic modifications giving very high lateral displacements compared to fully bonded and half width debonded cases, producing combined bending and twisting vibration mode.

A stimulating observation through mode shape comparison is that these mode changes seem to have a relationship with the extent of natural frequency reduction caused due to debonding in the particular mode of interest. For example, for the C-C beam, in the case of 150 cm long debonding scenario, mode 4 gives the maximum extent of reduction in natural frequency for both full width and half width debonding, as described in Table 4.16. Debonding length 0.5L refers to 150 cm long debonding. As anticipated, mode 4 shows dramatic changes in vibration modes as illustrated in Figure 4.16 for C-C beam. Similar results are seen in mode 7 for S-S beam in Table 4.17 and mode 8 for C-F beam in Table 4.18.

Another important observation from Tables 4.16, 4.17 and 4.18 is that full width debonding causes extreme changes in extents of natural frequency reductions compared to half width debonding.

Table 4.16 Percentage reduction in natural frequency comparison for half width and full width debonding for C-C beam

Debond length, a/L	Mode Number	% Reduction in natural frequency (Hz)	
		Half width debonding	Full width debonding
0.1	1	0.001	0.005
	2	0.174	1.370
	3	0.014	0.056
	4	0.040	2.578
	5	0.363	0.634
	6	0.057	0.224
	7	0.456	3.608
	8	0.001	0.007
	9	0.122	0.497
	10	0.470	3.695
0.5	1	0.263	5.843
	2	0.518	25.045
	3	1.125	21.467
	4	3.435	25.875
	5	0.772	4.607
	6	1.357	15.430
	7	1.768	17.541
	8	0.260	12.682
	9	1.938	4.996
	10	1.805	12.438
0.9	1	1.133	37.770
	2	1.658	33.669
	3	1.972	30.058
	4	1.597	27.493
	5	0.802	14.475
	6	2.543	25.419
	7	2.809	23.643
	8	0.575	20.642
	9	2.969	17.168
	10	3.209	28.457

Table 4.17 Percentage reduction in natural frequency comparison for half width and full width debonding for S-S beam

Debond length, a/L	Mode Number	% Reduction in natural frequency (Hz)	
		Half width debonding	Full width debonding
0.1	1	0.000	0.001
	2	0.140	1.095
	3	0.030	0.227
	4	0.012	0.058
	5	0.336	2.676
	6	0.043	0.169
	7	0.001	0.004
	8	0.419	3.363
	9	0.094	0.379
	10	0.492	3.831
0.5	1	0.055	1.251
	2	0.521	32.043
	3	0.228	8.776
	4	0.953	17.407
	5	1.056	17.218
	6	1.262	16.409
	7	2.180	19.040
	8	1.658	11.632
	9	1.690	13.351
	10	1.487	15.841
	1	0.276	14.447
	2	0.782	43.858
	3	0.449	22.929
	4	1.395	22.552
	5	1.946	34.590
	6	2.238	27.645
	7	0.311	19.322
	8	2.517	21.779
	9	2.768	25.609
	10	2.891	33.685

Table 4.18 Percentage reduction in natural frequency comparison for half width and full width debonding for C-F beam

Debond length, a/L	Mode Number	% Reduction in natural frequency (Hz)	
		Half width debonding	Full width debonding
0.1	1	0.015	0.116
	2	0.002	0.011
	3	0.214	1.678
	4	0.002	0.017
	5	0.040	0.256
	6	0.367	2.923
	7	0.115	0.719
	8	0.021	0.169
	9	0.415	3.216
	10	0.202	1.188
0.5	1	0.097	7.852
	2	0.227	5.682
	3	0.647	11.814
	4	0.015	0.406
	5	1.313	12.913
	6	1.486	18.337
	7	1.504	16.031
	8	2.030	18.540
	9	1.742	14.452
	10	1.928	14.373
0.9	1	0.165	27.435
	2	0.850	32.315
	3	1.454	36.363
	4	0.029	6.373
	5	1.977	31.261
	6	2.402	32.059
	7	2.748	29.645
	8	0.257	21.963
	9	3.008	25.302
	10	3.195	28.932

4.6.2.2 Influence of multiple debonding

In this section, influence of double (two equally sized debonding zones positioned near two ends as illustrated in Figure 4.2) debonding on natural frequency reduction is examined for full width and half width debonding cases. Secondly, comparisons are made between multiple debonding and equally sized single debonding.

Figure 4.19 illustrates the comparison of natural frequency variation for full width and half width debonding for 30 cm double debonding (two 30 cm long debonding zones near the two ends) in the C-C beam, whereas Figure 4.20 shows the same variation for S-S beam.

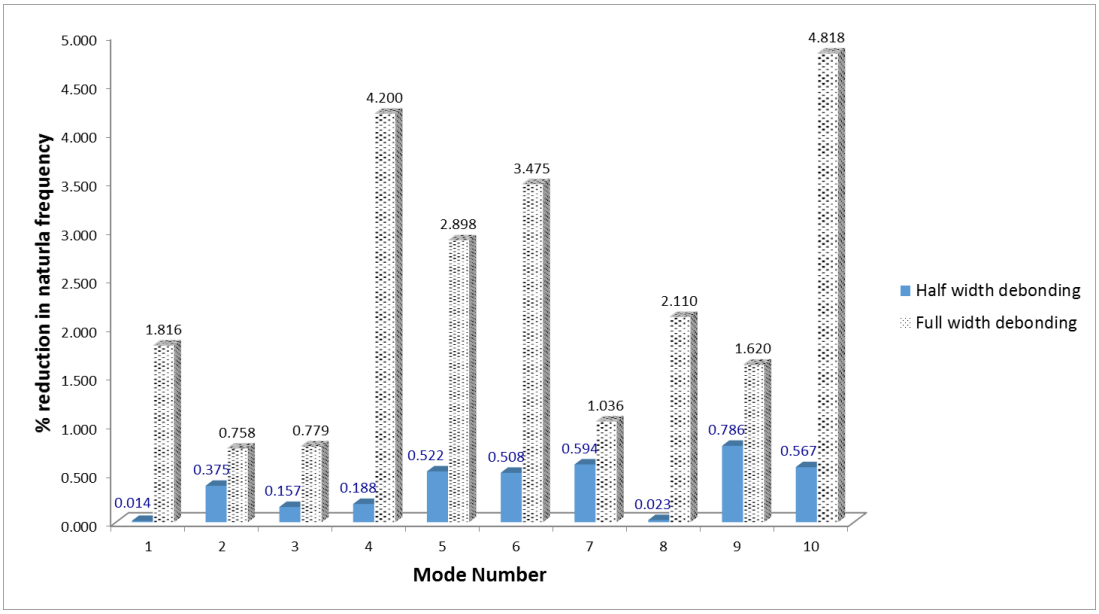

Figure 4.19 Comparison of full width and half width debonding for C-C beam with 30 cm double debonding

It is evident from both Figures 4.19 and 4.20 that full width debonding causes enormous changes in natural frequency compared to half width debonding for similar scenarios. These variations do not follow a monotonically increasing pattern with the mode number, as demonstrated by Figures 4.19 and 4.20.

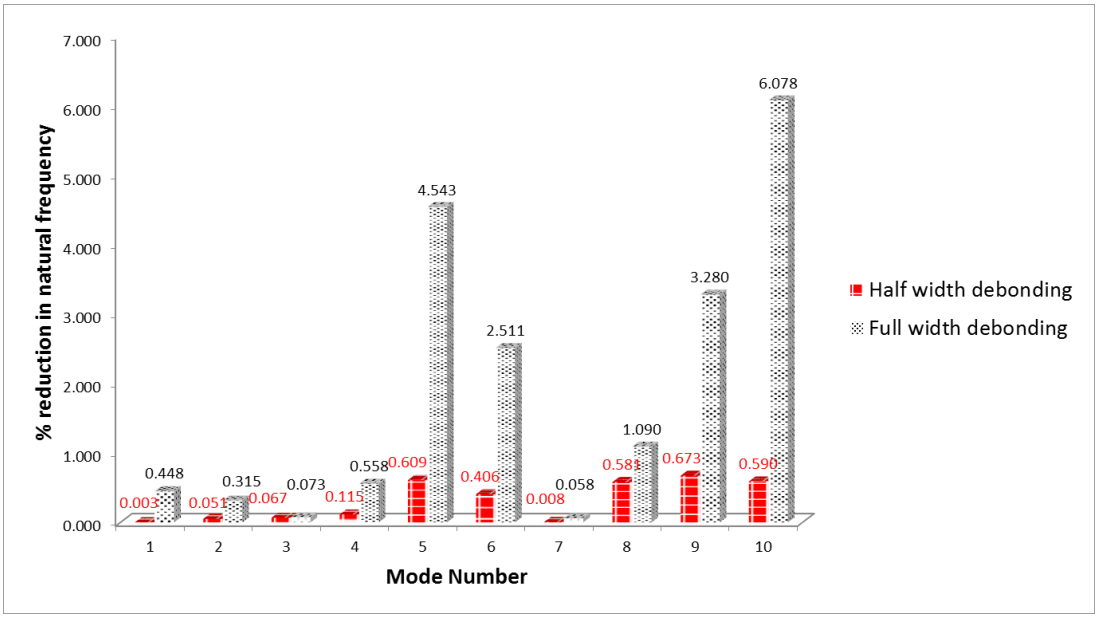

Figure 4.20 Comparison of full width and half width debonding for S-S beam with 30 cm double debonding

Comparison for Figures 4.19 and 4.20 also reveals that for the first four modes, the variations for full width compared to half width debonding is more significant for C-C case, and on contrary, higher modes shows more variations for S-S case than C-C case.

Figure 4.22 compares effects of two equally sized (30 cm long full width debonding regions each) symmetrically located debonding zones and equivalent single debonding (full width) for S-S beam. Figure 4.21 displays the FE models created for the two scenarios demonstrated in Figure 4.22.

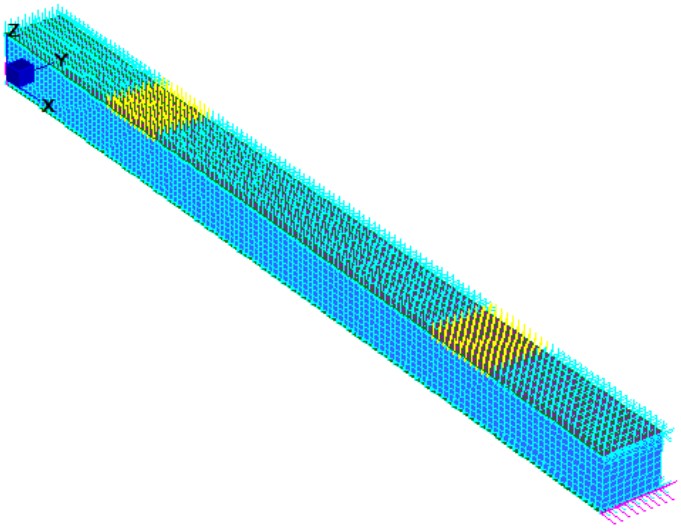

(a) S-S beam with two equally sized (each 30 cm long full width) debonding regions

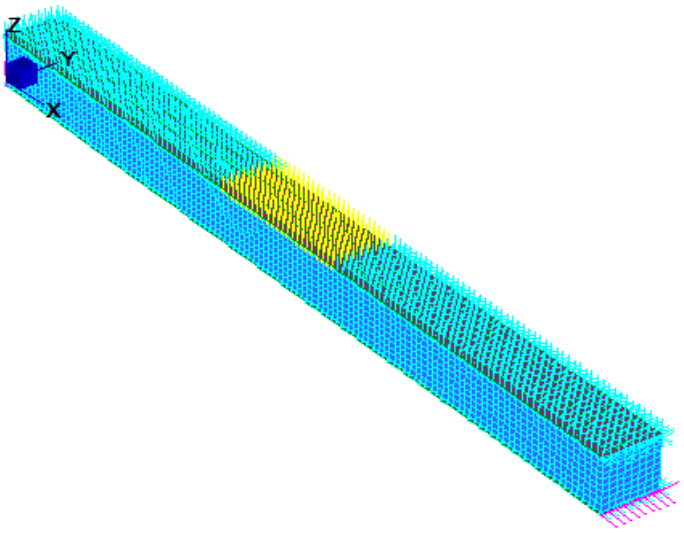

(b) S-S beam with equivalent single debonding region (60 cm long full width debonding)

Figure 4.21 FE models generated for S-S beam for Figure 4.20 comparison

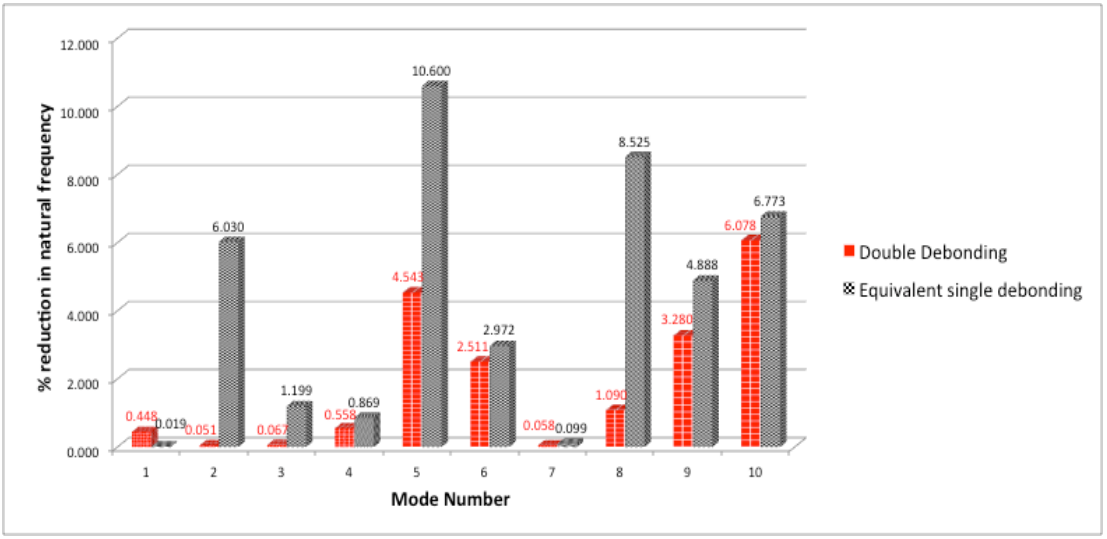

Figure 4.22 Comparison for double debonding and equivalent single debonding for S-S beam

It is evident from Figure 4.22 that single debonding of 60 cm length generally gives higher extent of reduction in natural frequency than two equally sized 30 cm long debonding regions. These percentage reductions do not seem to increase monotonically with the increase of the mode number. This is evident from the similar comparison for C-C beam as well, as illustrated in Figure 4.23.

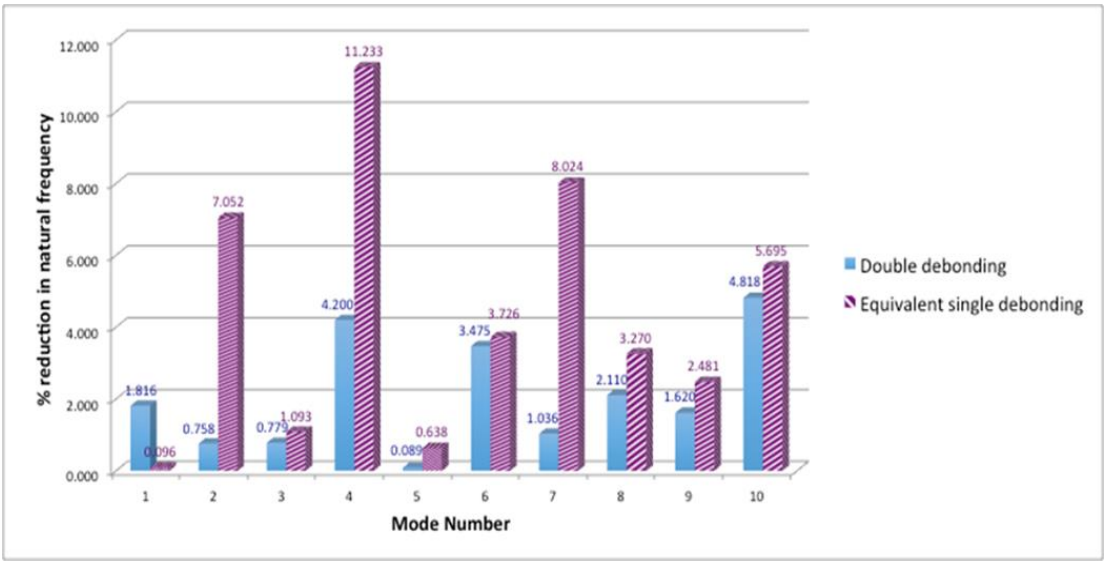

Figure 4.23 Comparison for double debonding and equivalent single debonding for S-S beam

The comparison of triple debonding, 30 cm long each, symmetrically located along the length (as illustrated in Figure 4.24) with equivalent single debonding of 90 cm for C-C beam is displayed in Figure 4.25. Figure 4.24 (a) and (b) illustrates the FE models generated for the two scenarios.

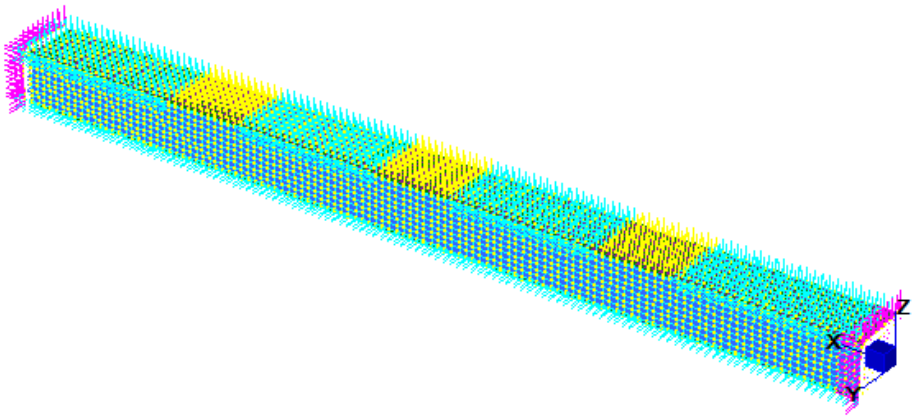

(a) Triple debonding 30 cm each (full width debonding)

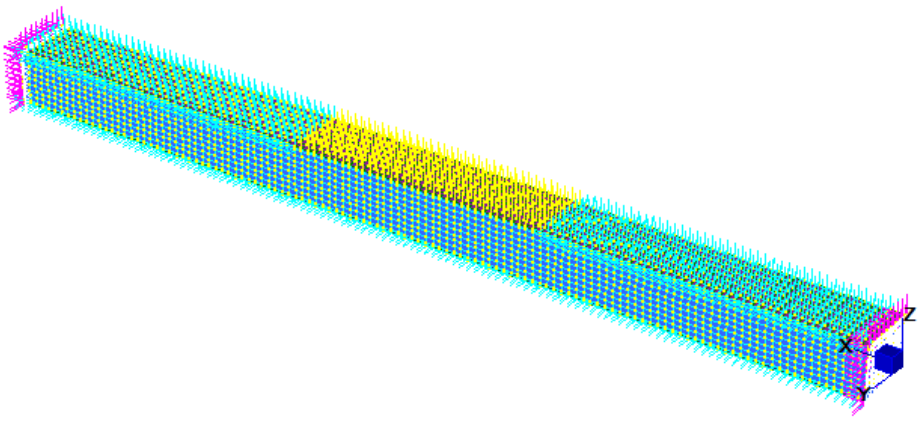

(b) Equivalent single debonding 90 cm long (full width debonding)

Figure 4.24 FE models generated for C-C beam for triple debonding and equivalent single debonding

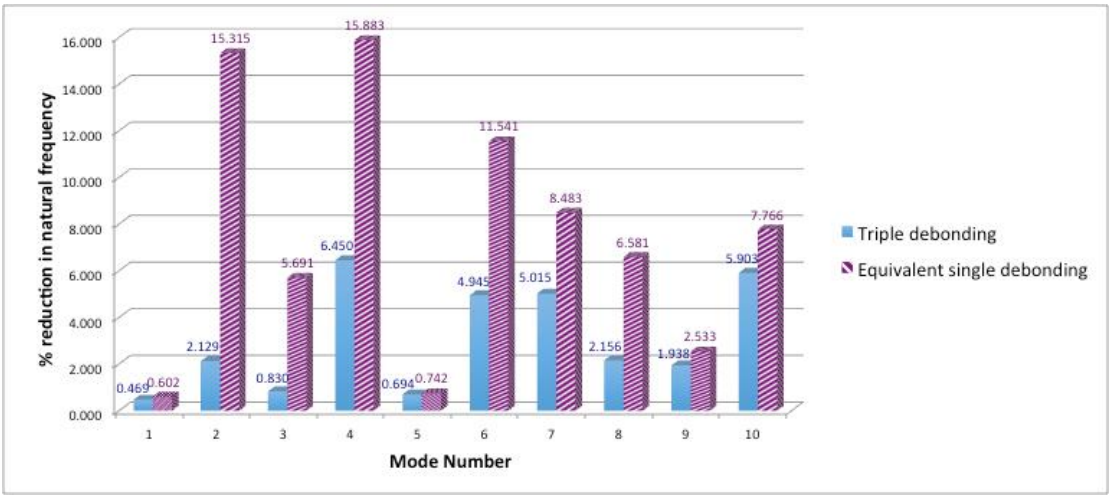

Figure 4.25 Comparison of triple debonding and equivalent single debonding for C-C beam

It is evident from Figure 4.25 that equivalent single debonding affects the free vibration frequencies much more that the isolated triple debonding of the same area, generally in the order of more than two times in most of the modes under consideration.

Generally it is observed that the reduction in natural frequency is more affected by single debonding than the equally sized multiple debonding regions located symmetrical to the single debonding position. Thus it is revealed that large single debonding area leads to more damage (in terms of natural frequency reduction) than isolated small debonding zones of equivalent area, appearing in a GFRP beam. Furthermore the extents of natural frequency shifts seem mode dependent, and do not seem to have a monotonous trend of increasing with the mode number.

4.7 Chapter conclusions

This chapter presented a numerical investigation about the changes in free vibration behaviour due to various amounts of debonding along the length and width of a composite sandwich beam for simply supported, clamped-clamped and clamped-free boundary conditions for a 300 mm test beam and a 3 m full scale beam. Findings of the present numerical investigations can be summarized as follows.

- Generally, debonding causes reduction in natural frequency when compared with fully bonded composite beams.
- In general, natural frequency decreases more rapidly as the mode number increases giving the least variation for the first natural frequency.
- Although there is a general tendency that the extent of natural frequency variation with respect to debonding increases with the mode number, this does not always exhibit an increasing trend as the mode number increases, but follows different trends depending on the boundary condition, extent of debonding and location of the debond.
- The decrease in natural frequency with the increase in the extent of debonding is more dependent on the width of debonding across the beam than the length along the beam for the novel composite beam considered in the analysis.
- It is perceived that if the working frequency of the beam is kept away from the range 50% to 100% of the fully bonded beam, there is no possibility of resonance happening due to debonding for the novel composite test beam considered.
- A debonding located near the end of the beam significantly worsens the free vibration characteristics compared to a debonding located near the centre of the beam. This becomes more pronounced when the beam is more restrained.
- For similar extents and locations of debonding, the effect of debonding on natural frequencies seems significantly dependent on the end conditions of the beam, giving higher reduction in natural frequency when the beam is more restrained. Hence it is revealed that the stronger the supports are restrained, the bigger the influence on free vibration characteristics.
- It is observed that full width debonding attributes to extremely severe reduction in natural frequency compared to half width debonding for all three support conditions considered. Full width debonding also attributes to drastic changes in modes of vibration and mode shapes.
- The effect of multiple debonding on the free vibration behaviour of a debonded beam is highly dependent of the boundary conditions, giving greater reductions in natural frequencies when the beam is more restrained. Moreover there is a general trend that the extent of reduction increases with the mode number.

- Generally it is observed that the reduction in natural frequency is more affected by single debonding than the equally sized multiple debonding regions located symmetrical to the single debonding position.
- The natural frequency reduction due to debonding is higher for the free model compared to the constrained model for similar conditions of debonding. This discrepancy becomes more pronounced for full width debonding compared to half width debonding. This is the case for both test beam and full scale beam scenarios.

CHAPTER 5 FREE VIBRATION BEHAVIOUR OF DEBONDED AND DELAMINATED COMPOSITE PLATES

5.1 Introduction

The versatility of the finite element method (FEM) for resolving complex topological and multi-physical problems has made it a popular technique in investigations of debonded sandwich panels (Burlayenko & Sadowski 2014). Dynamic analysis of three-dimensional models of structures enables more realistic assessment of their free vibration as well as forced vibration behaviour. While the dynamic behaviour of undamaged sandwich panels is the subject of extensive studies, papers reported on the dynamic behaviour of sandwich panels with debonding are less presented in the literature (Burlayanko & Sadowski 2014).

The natural frequencies of a debonded or delaminated composite plate will reduce because of the loss in stiffness caused by the presence of delamination (Ju et al. 1995). Since the natural frequencies and vibration modes change considerably with respect to the undamaged material, they can indeed be used to develop methods for damage detection and evaluation (Gallego et al. 2013). Hence it is vital to predict the changes in natural frequencies and mode shapes due to debonding and delamination with respect to developing damage detecting techniques.

This chapter describes the relative dynamic performance of fully bonded and debonded single layer GFRP slab panels in the onset and then investigate the influence of interlayer delamination in multilayer GFRP slab panels.

5.2 Research approach

The research approach is finite element modelling and analysis using three-dimensional modelling of the composite plates to simulate the real behaviour. Model development for fully bonded and debonded plates has been carried out as described in Chapter 3. After developing the model, verification for fully bonded and debonded models is realized using published experimental and numerical results as described in this Chapter. Once the model is verified, the dynamic parametric analyses are carried

out using STRAND7 FE Package with different configurations of debonding and boundary conditions of interest. As the intention is to assess the influence of the presence of debonding on the dynamic characteristics, free vibration analyses for the same fully bonded (intact) plates as well were conducted for comparison for each debonding scenario.

5.3 Assumptions and modelling

In the present study, debonding damage is assumed to be pre-existing before the vibrations start and to be constant during the free vibration period. The finite elements such as plate elements and 3D brick elements are used to discretise the skins and the core, respectively. In order to connect the skin elements to the core elements in the fully bonded region of the sandwich plate, rigid links have been utilised. The lack of adhesion between the elements in the debonded region has been modelled by removing of those rigid links and replacing them with master-slave links with the suitable degrees of freedom. A convergence study was carried out to obtain natural frequencies as accurately as possible at the minimum number of elements required in view of optimizing the computational time.

5.4 Model verification for plate model

5.4.1 Validation of the model for the fully bonded plate

For the verification of the accuracy of the results for the finite element model used in this study, the natural frequencies from the proposed model for fully bonded novel composite single layer sandwich slabs are computed and compared with experimental and FEA results reported by Awad et al (2012c). Awad et al. (2012c) conducted experimental work and 3D finite element (FE) simulation with ABAQUS to investigate the free vibration behaviour of the novel GFRP sandwich panels with different sizes and support conditions. The typical novel composite sandwich panel has a 12 mm core thickness and 3 mm GFRP skin thickness in the top and bottom faces, as shown in Figure 2.3 in Chapter 2. The total thickness of the panel is 18 mm. Four different sizes were used for the verification, namely 400, 600, 800 and 1000 mm one way square slab panels. The end condition considered here was fixed (glue) restraints for both ends of the slabs.

Table 5.1 illustrates the effective mechanical properties used by Awad et al (2012c) for the fibre composite skin and the phenolic core, and hence have been used for the verification for fully bonded slab model.

Table 5.1 Effective mechanical properties used for model verification (Awad et al. 2012c)

Property	Skin	Core
Young's modulus along long direction (MPa)	12360	1350
Young's modulus in transverse direction (MPa)	10920	1350
Poisson's ratio	0.3	0.2
Density (kg/m^3)	1425	950

5.4.2 Validation of the model for the debonded plate

Model verification for debonded plate was carried out using the numerical results by Burlayenko and Sadowsky (2014). They did nonlinear dynamic analyses for a rectangular simply supported sandwich plate (of length 270 mm and a width of 180 mm) with a central penny shaped debond of radius R (as shown in Figure 5.1) using the finite element analysis with the ABAQUS code. The size of the debond is 10% by area of the plate.

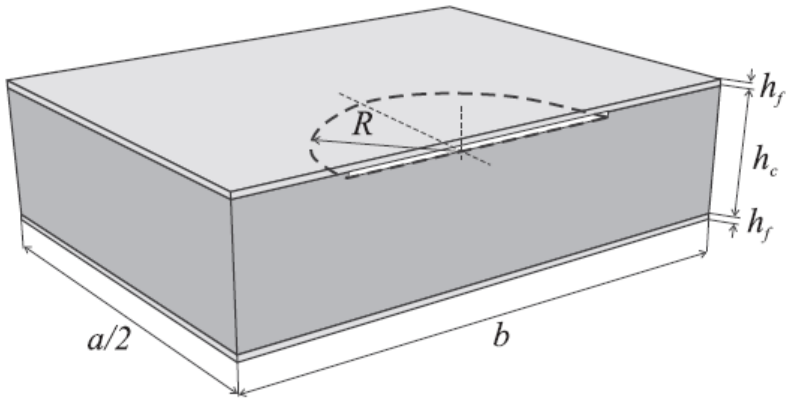

Figure 5.1 Half of sandwich plate with penny-shaped debonded zone (Burlayenko and Sadowsky 2014)

In Figure 5.1, h_f denotes the face sheet thickness while h_c is the core thickness.

The material properties of the foam-cored sandwich plate material used for the verification, extracted from Burlayenko and Sadowsky (2014) are listed below.

Foam core

E_c = 85 MPa, G_c= 30 MPa, ρ_c = 52 kgm^{-3}

Face sheet

$E_{xx} = E_{zz}$ = 19.3 GPa, E_{yy} = 3.48 GPa,

G_{zx} = 7.7 GPa, $G_{xy} = G_{yz}$ = 1.65 GPa,

ρ = 1650 kgm^{-3}

5.5 Model verification results

5.5.1 Results for the model validation for the fully bonded plate

The results of the verification study for fully bonded plate are presented in Table 5.2 where experimental and numerical results reported by Awad et al. (2012c) for the novel GFRP fully bonded sandwich plates are compared with the simulation results based on the model developed with STRAND7 (2010).

Table 5.2 Results for the model validation for fully bonded plate

Slab size (mm×mm)	Mode number	Experimental results (Awad et al. 2012c) Frequency in Hz	FEA with ABAQUS (Awad et al. 2012c) Frequency in Hz	Present analysis with STRAND7 Frequency in Hz
400×400	1	193	194	195
400×400	2	230	226	234
600×600	1	95	96	90
600×600	2	123	114	121
800×800	1	49	51	52
800×800	2	70	64	70
1000×1000	1	28	29	34
1000×1000	2	41	37	45

As illustrated in Table 5.2, the results provided by the present numerical model are in consonance with experimental and analytical results reported in the literature, and hence validate the developed model for accuracy.

5.5.2 Results for the model validation for the debonded plate

Model validation results for the debonded plate are displayed in Table 5.3, where numerical results published by Burliyenko and Sadowsky (2014) are compared with the results obtained using present model with STRAND7.

Table 5.3 Results for the model validation for debonded plate

Mode number	Analytical results Natural frequency (Hz) Burliyenko and Sadowsky (2014)	Results from present analysis with STRAND7 Natural frequency (Hz)
1	957	994
2	1309	1331
3	1406	1362
4	1621	1604

The reasonable agreement of the results validates the accuracy of the FE model developed for debonded plate.

5.6 Influence of skin-core debonding on dynamic behaviour

5.6.1 Introduction

Investigation of the free vibration behaviour of the fully bonded novel GFRP sandwich by experimental and numerical methods was carried out by Awad et al. (2012c), as reported in section 5.4.1. Although experimental and numerical research has been conducted on the examination of the free vibration behaviour of the fully bonded GFRP sandwich floor panels, there has been only a limited investigations on the free vibration behaviour of the debonded GFRP panels. With the aim of fulfilling this gap, an extensive parametric investigation has been carried out to examine the various parameters of concern with respect to change in dynamic behaviour due to pre-existing debonds.

5.6.2 Selection of parameters for the dynamic analyses

Firstly, the vibration analysis for the novel composite sandwich panels of 800 mm square section having skin and core thicknesses as in Figure 2.3 has been carried out. Secondly, a single layer sandwich panel of 3000 mm square section was selected for

the analyses and the skin core thicknesses were increased accordingly to satisfy the serviceability limits. The thickness used for top as well as bottom skin is 24 mm and the core is of thickness 96 mm giving the overall thickness of the slab 144 mm. Lastly, 1000 mm square multi-layer sandwich plate consisting of two layers of the sandwich plate given in Figure 2.3 glued together to form a double layer plate have been used to compare the influence of single layer and multilayer debonding on natural frequency characteristics. The total thickness of the double layer sandwich plate is 36 mm. Four boundary conditions, namely, all four ends clamped (two way clamped denoted by C-C-C-C), two opposite ends clamped and the other two ends free (one way clamped denoted by C-C-F-F), all four ends simply supported (Two way simply supported denoted by S-S-S-S) and two opposite ends simply supported and the other two ends free (one way simply supported denoted by S-S-F-F) have been selected for the parametric investigation. Typical S-S-F-F and S-S-S-S slab panels are shown in Figure 5.2 (a) and (b) respectively.

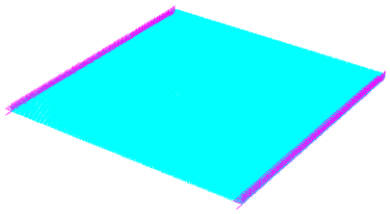

(a) S-S-F-F (one way simply supported) slab panel

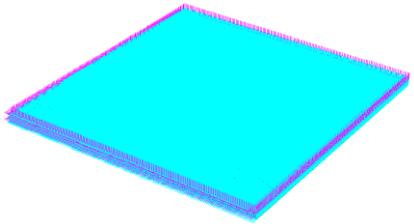

(b) S-S-S-S (two way simply supported) slab panel

Figure 5.2 Typical S-S-F-F and S-S-S-S slab panels

Different sizes (0.5%, 1%, 5% and 10% of plate area) and locations (position 1, 2 and 3 as explained in Section 3.6.2 with Figure 3.9 and also shown in Figure 5.3) of debonding are considered. Note that the debondings are located in the middle of the regions marked in Figure 3.9.

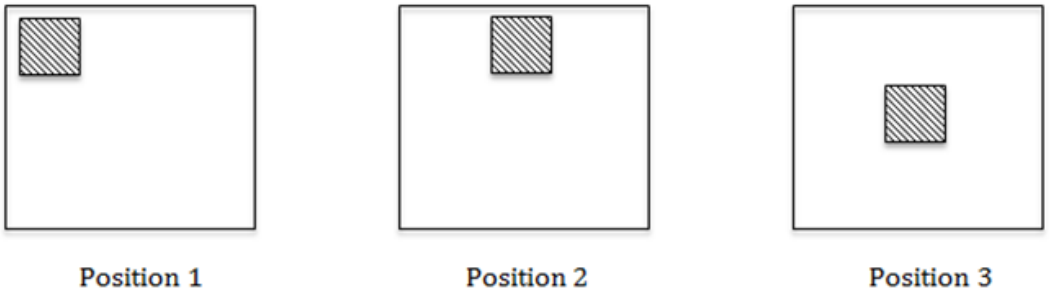

Figure 5.3 Debonding positions used for the present analysis

5.6.3 Mechanical properties used for the GFRP sandwich plates

The effective mechanical properties used for the glass fibre composite skin and the phenolic core of the sandwich plate for the present analysis were extracted from Manalo et al. (2010b), and have been listed in Table 2.1 in Chapter 2.

5.7 Influence of interlayer delamination on dynamic behaviour of multilayer GFRP plates

5.7.1 Introduction

Multi-layered structures are increasingly used in aerospace, automotive and ship vehicles, the most common and best-known examples being composite sandwich panels (Carrera 2002). Delamination occurs in a multilayer laminated sandwich material, leading to split-up of the sandwich layers, which in turn can severely affect the structural integrity of the laminated multilayer composite panel. Delaminations cause reductions in natural frequency, which may result in resonance if the reduced frequency is close to the working frequency of the structure. It is vital that we should be able to predict the variation in natural frequency and the mode shape due to delamination, in a dynamic environment (Della & Shu 2005).

5.7.2 Selection of position of delamination, extents of delamination and end conditions

The slab size selected for modelling and analysis is 1000 mm square slab with two composite sandwich layers as shown in Figure 5.4. Each sandwich plate or layer consists of top and bottom skins and a middle core (dimensions as shown in Figure 2.3). Hence the overall thickness of the multilayer slab is 36 mm.

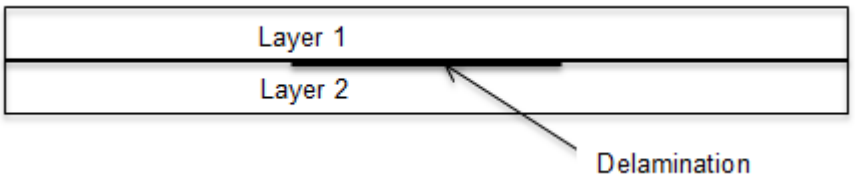

Figure 5.4 Two layer composite sandwich used for the present analysis

The interlayer delamination between the two attached composite sandwiches in the 1000 mm two layer square plate has been considered in the present analysis (see Figure 5.4). Three different positions (as shown in Figure 5.3 under debonding) of delamination and four different percentages of delamination (0.5%, 1%, 5% and 10% by area of the plate) have been selected for modelling and analysis. Only for position 3, in addition to the above-mentioned percentages, 20% delamination also was selected and analysed.

Four different types of end conditions for the slab panel are considered, namely, one way simply supported (S-S-F-F), two way simply supported (S-S-S-S), one way clamped (C-C-F-F) and two way clamped (C-C-C-C). The effective mechanical properties of the skin and core of the novel composite multilayer slab panel used for the present analysis have been given in Table 2.1.

5.7.3 Fastening the delaminated regions as a remedial measure

Mechanical fasteners (like bolts, rivets, pin-connectors) are commonly used in structural applications for transferring loads between the structural components. Such fasteners are extensively used, mainly, because they are easy to assemble or disassemble (Ju et al. 1995). According to Chutima and Blackie (1996), mechanical fasteners such as bolts and rivets are commonly utilized in composite structures to provide a convenient means of assembly or to enable disassembling of sections

where regular inspection and/or repair is required. As such, the possibility and effectiveness of using bolts to fasten the delaminated regions of the multilayer composite plates as a remedial measure to reduce the effects of delamination are considered. The fastening of the regions of delamination is simulated by converting master slave links in the delaminated region to rigid links at the intended locations of the bolts. The 1000 mm square double layer slab panel is considered for the analysis.

5.8 Results and discussion

5.8.1 Influence of skin-core debonding on dynamic behaviour

5.8.1.1 Results for 800 mm single layer square plate

Three different positions of debonding and four different percentages of debonding (0.5%, 1%, 5% and 10% by area of the plate) have been investigated and some typical 3D models developed are shown in Figure 5.5 to show the different scenarios used.

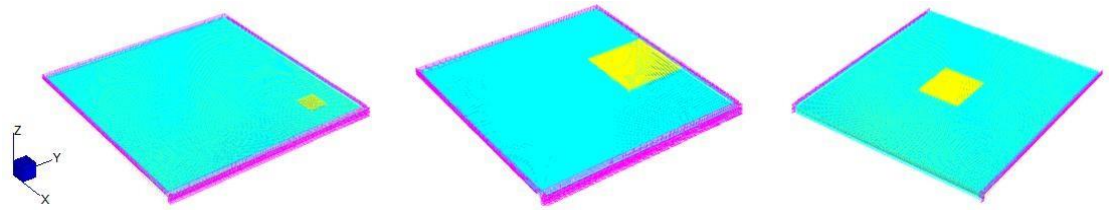

(a) Position 1(C-C-C-C) 1% debonding (b) Position 2 (C-C-C-C) 10% debonding (c) Position 3 (C-C-F- 5% debonding

Figure 5.5 Typical 3D models created using STRAND7 for the analyses

It is observed that the most adverse boundary condition giving highest drop in natural frequency due debonding in general is the C-C-C-C form and the least reduction in natural frequency is seen in S-S-F-F end condition in general. The most adverse location in terms of percentage of natural frequency shift seems to be dependent on the boundary condition of the slab. For C-C-C-C end condition this is position 3, whereas for C-C-F-F boundary condition the worst location is position 1. The results for these two scenarios are presented graphically in Figures 5.6 and 5.7, respectively.

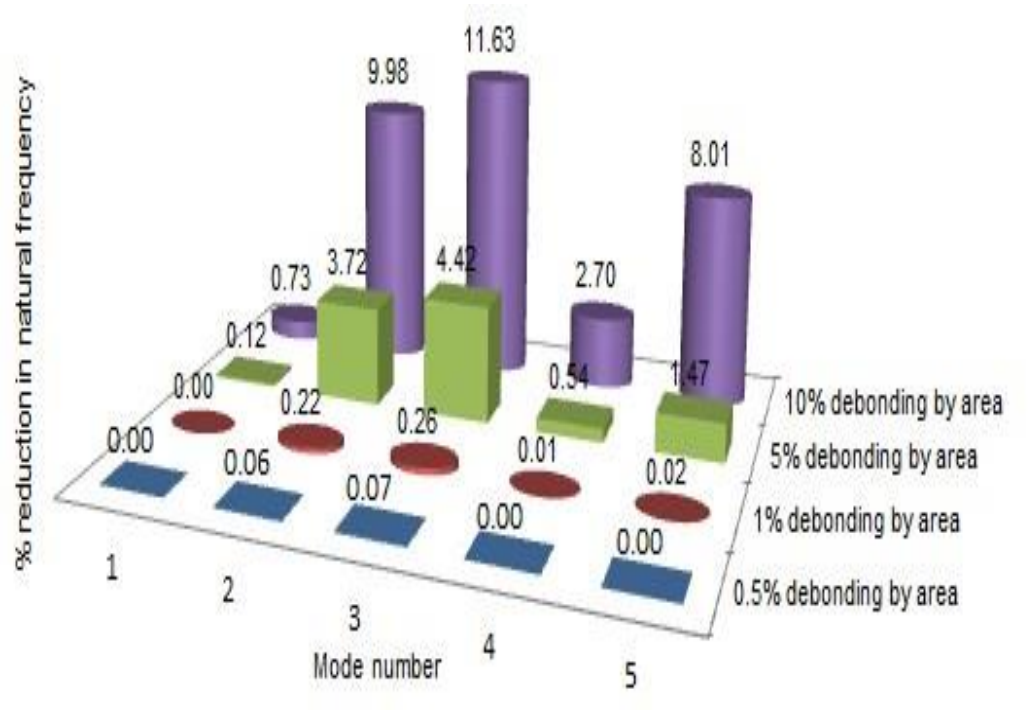

Figure 5.6 Comparison of percentage natural frequency reduction for different extents of debonding in 800 mm C-C-C-C plate for debonding position 3

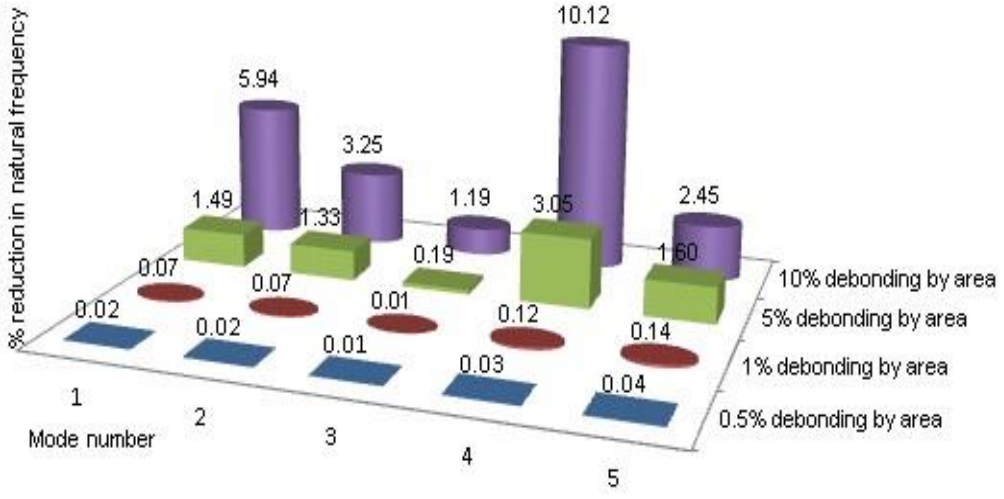

Figure 5.7 Comparison of percentage natural frequency reduction for different extents of debonding in 800 mm C-C-F-F plate for debonding position 1

It is observed from Figures 5.6 and 5.7 that some modes are more sensitive to debonding, and it seems that this sensitivity is related to vibration mode shapes as illustrated in Figure 5.8.

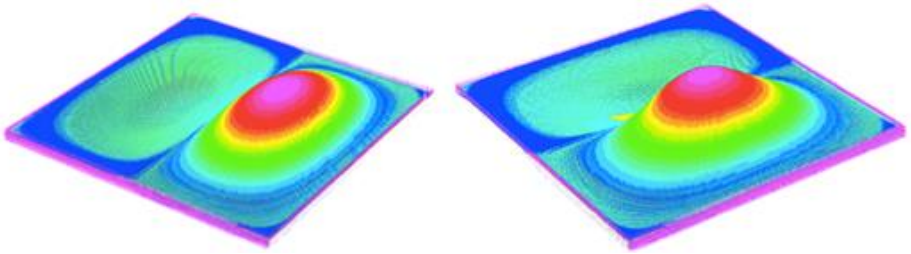

Fully bonded slab 10% debonding by area of slab

(a) Comparison of mode shapes for mode 2

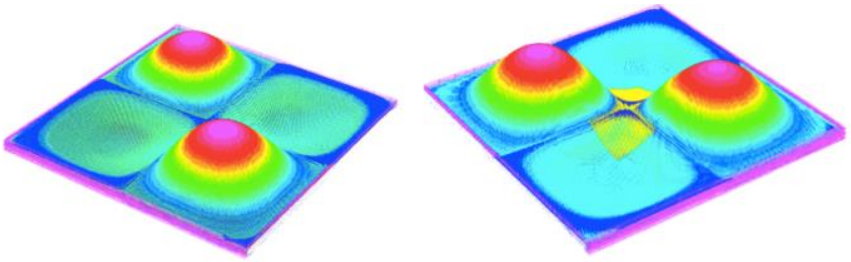

Fully bonded slab 10% debonding by area of slab

(b) Comparison of mode shapes for mode 4

Figure 5.8 Comparison of mode shapes for C-C-C-C fully bonded and 10% debonded for position 3

Figure 5.8 shows the comparison of mode shapes for C-C-C-C case for the fully bonded plate and 10% debonding by area (for position 3 debonding). Here, the mode shapes for the second and fourth modes of vibration are compared where (a) and (b) correspond to mode 2 and mode 4 comparisons, respectively. Careful observation of mode shape comparisons for fully bonded and debonded slabs in Figure 5.8 reveals that vibration mode 2 is more triggered by the position 3 debonding than the vibration mode 4 due to the vibration mode shape of the debonded panel with respect to the debonding location. This clarifies the greater sensitivity to debonding shown in mode 2 frequency shift (9.98%) compared to percentage variation for mode 4 (2.7%), as illustrated in Figure 5.6. Similar variations were observed for other boundary conditions as well.

It is interesting to observe that when the extent of debonding is not greater than 1% of the surface area of the panel, the percentage reduction in natural frequency is less than 0.3% even for the worst case. This indicates that small debonding extents cause insignificant changes in natural frequency. On contrary, large extents of debonding result in rapid reductions natural frequency. It can also be pointed out that the fundamental mode is generally very poorly sensitive to debonding even when the debonding extent is 10%. Furthermore, these reductions in natural frequencies not only depend on the extent of debonding but also on boundary conditions, position of the debond and the mode number. It is revealed that C-C-C-C end condition has the most significant effect on free vibration behaviour when compared with the other three end conditions. It is of special interest to observe that the effect on debonding does not always exhibit an increasing trend as the mode number increases, and follows different trends depending on the boundary condition, extent of debonding, vibration mode shape and location of the debond.

Figure 5.9 compares multiple debonding against single debonding of equivalent area. Comparisons are made with regards to the most adverse end condition (C-C-C-C), and three different scenarios with similar debonding areas are considered. Here equally sized double debonding occurred at two distinct locations (at positions 1 and 2 simultaneously), each 5% of plate area is compared with 10% single debonding at position 1 as well as at position 2. It is interesting to observe that multiple debonding is less sensitive to natural frequency variation when compared with single debonding of equivalent area. This is the case with comparisons of other boundary conditions as well. Thus it is revealed that debonding occurred in a single large area is more sensitive to natural frequency reduction than small extents of multiple debonding of equivalent area arose a distance apart in the slab.

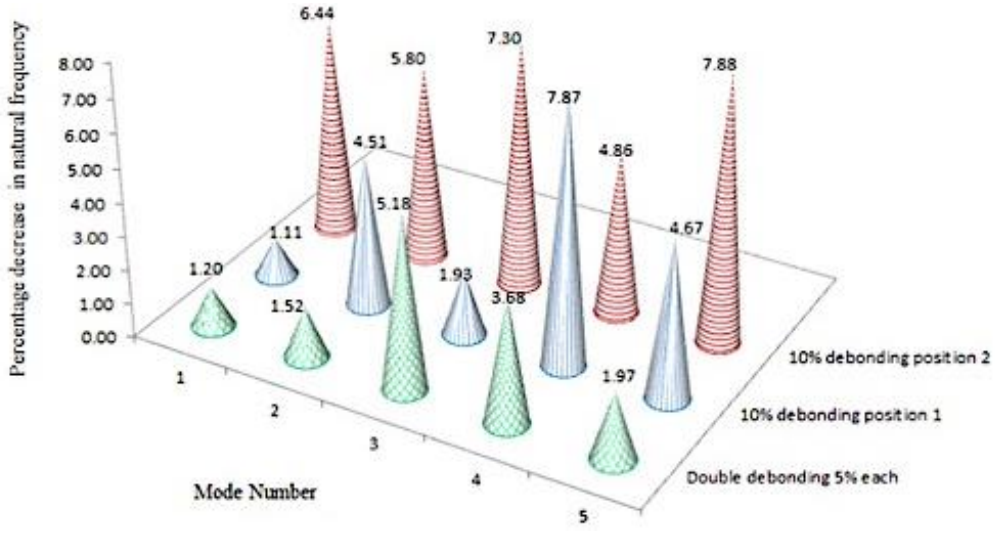

Figure 5.9 Comparison of multiple debonding with equivalent area of single debonding

Figure 5.11 reports the natural frequency variation in 800 mm slab with triple debonding (three equally sized debonding zones) of each 10% of slab area at positions 1, 2, 1 (as illustrated in Figure 5.10) for boundary conditions C-C-C-C and C-C-F-F. Noticeably there are two distinct cases of for C-C-F-F boundary condition, one along free edge and the other case along clamped edge (as illustrated in Figure 5.10). It is of special interest to observe here that multiple debonding along free end is more sensitive to natural frequency variation than the same along clamped end in C-C-F-F panel in general. Interestingly, C-C-C-C boundary condition generally gives the highest variation in natural frequency for multiple debonding as well, as was the case with single debonding.

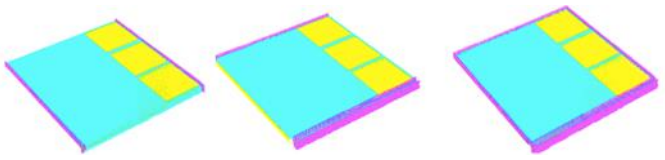

(a) C-C-F-F along fixed end (b) C-C-F-F along free end (c) C-C-C-C

Figure 5.10 End conditions and locations of debonding used for triple debonding comparison

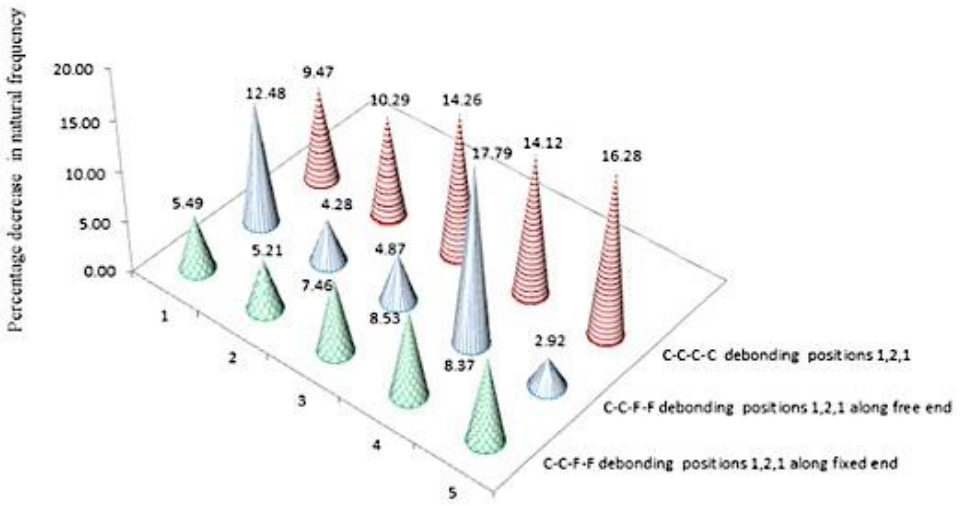

Figure 5.11 Comparison of natural frequency variation for triple debonding for the three scenarios shown in Figure 5.9

5.8.1.2 Results for the 3000 mm single layer square plate

From all the numerical analyses carried out it was observed that C-C-C-C boundary condition was generally the most critical end condition in terms of variation of dynamic characteristics due to debonding. The least influenced boundary condition is S-S-F-F, which represents least restrained plate. It is witnessed that for C-C-C-C end condition, position 3 debonding gives highest reduction in natural frequency. Figure 5.12 below demonstrates the comparison of percentage reduction in natural frequency for position 3 and 10% debonding for all four end conditions. It is evident from Figure 5.12 that the highest effect on natural frequency occurs in C-C-C-C case, second highest being S-S-S-S situation while the least variation occurs in S-S-F-F case.

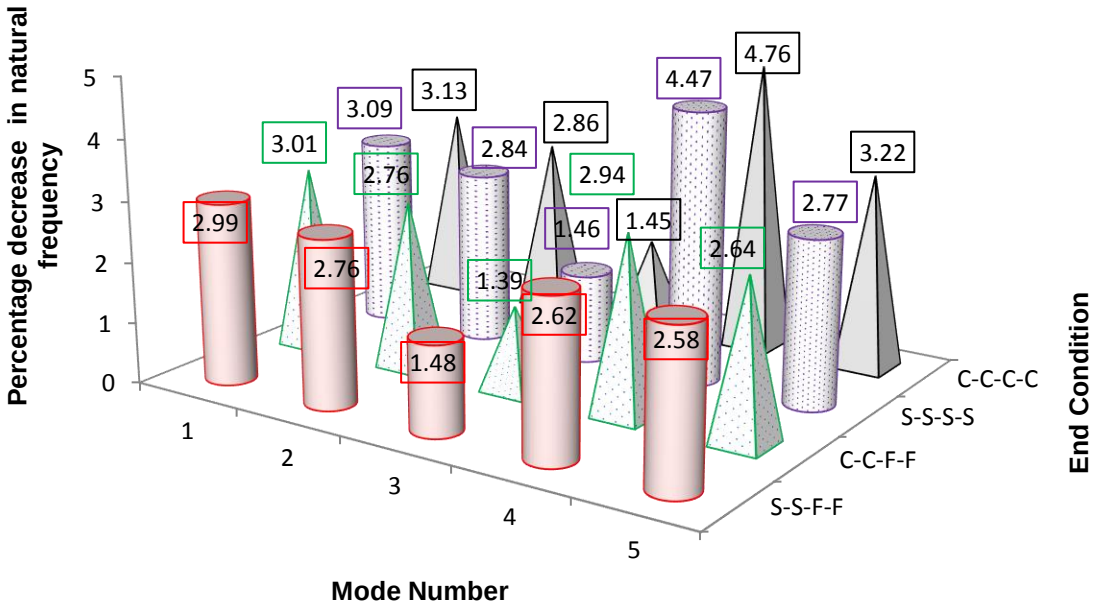

Figure 5.12 Comparison of percentage natural frequency reduction for different end conditions (10% debonding for position 3)

Table 5.4 gives the natural frequency values corresponding to first 5 modes for different extents of debonding for all four boundary conditions considered. Note here that the Table 5.4 values correspond position 3 debonding. Table 5.5 gives the same for position 1 debonding. Natural frequency values for corresponding fully bonded (intact) plates as well are tabulated for easy comparison. It is interesting to observe that C-C-C-C end condition, which has the highest stiffness out of the four boundary conditions, has the highest natural frequency values for fully bonded plate as well as similar debonding conditions. Accordingly S-S-F-F exhibits the lowest natural frequency values, due to its least restraint conditions.

Table 5.4 Comparison of first five natural frequencies in Hz for the four end conditions due to position 3 debonding

Percentage debonding by total area of plate	Mode number	C-C-C-C end condition	S-S-S-S end condition	C-C-F-F end condition	S-S-F-F end condition
0% (Fully bonded)	1	51.652	49.228	29.864	27.984
	2	102.802	98.308	35.741	33.964
	3	107.927	103.153	74.091	73.007
	4	154.385	148.979	84.799	80.389
	5	191.071	185.49	94.398	90.403
0.5% of plate area	1	51.652	49.228	29.864	27.984
	2	102.648	98.17	35.739	33.962
	3	107.737	102.982	74.091	73.007
	4	154.38	148.974	84.745	80.339
	5	191.058	185.478	94.397	90.402
1% of plate area	1	51.651	49.227	29.864	27.984
	2	102.374	97.922	35.736	33.958
	3	107.397	102.675	74.089	73.005
	4	154.358	148.955	84.648	80.25
	5	191.001	185.428	94.396	90.401
5% of plate area	1	51.628	49.208	29.86	27.981
	2	99.835	95.61	35.698	33.923
	3	104.263	99.824	74.031	72.95
	4	153.83	148.487	83.683	79.365
	5	189.484	184.083	94.355	90.363
10% of plate area	1	51.47	49.076	29.833	27.959
	2	93.836	90.048	35.585	33.817
	3	97.002	93.086	73.654	72.59
	4	151.04	145.988	80.939	76.835
	5	180.46	176.006	94.112	90.139

Table 5.5 Comparison of first five natural frequencies in Hz for the four end conditions due to position 1 debonding

Percentage debonding by total area of plate	Mode number	C-C-C-C end condition	S-S-S-S end condition	C-C-F-F end condition	S-S-F-F end condition
0% (Fully bonded)	1	51.652	49.228	29.864	27.984
	2	102.802	98.308	35.741	33.964
	3	107.927	103.153	74.091	73.007
	4	154.385	148.979	84.799	80.389
	5	191.071	185.49	94.398	90.403
0.5% of plate area	1	51.644	49.220	29.855	27.977
	2	102.774	98.284	35.731	33.956
	3	107.9	103.130	74.084	73.000
	4	154.294	148.904	84.778	80.374
	5	191.039	185.461	94.368	90.381
1% of plate area	1	51.629	49.206	29.838	27.963
	2	102.722	98.239	35.713	33.941
	3	107.851	103.088	74.071	72.986
	4	154.127	148.765	84.739	80.347
	5	190.075	185.403	94.314	90.341
5% of plate area	1	51.463	49.054	29.652	27.813
	2	102.129	97.740	35.51	33.777
	3	107.385	102.689	73.918	72.827
	4	152.428	147.353	84.28	80.029
	5	190.13	184.627	93.728	89.896
10% of plate area	1	50.034	47.708	28.964	27.148
	2	99.867	95.520	34.754	33.026
	3	106.359	101.645	73.063	71.926
	4	147.035	142.316	82.309	78.285
	5	184.927	180.348	91.902	88.069

Figure 5.13 displays the comparison of percentage reduction in natural frequency for position 1 and 10 % debonding for the four boundary conditions under consideration. Similar to position 3 comparison, here also the maximum reduction generally occurs in C-C-C-C condition, which is the fully restrained situation. Least reduction occurs in S-S-F-F scenario, where the plate is least restrained.

It is interesting to observe that the extent of reduction natural frequencies due to debonding is not the same for different modes. In all the cases considered in the analyses, the debonding-induced reduction in natural frequencies can hardly be seen

in the first mode. Furthermore, the results show that the presence of relatively small debonding has an insignificant effect on the natural frequencies.

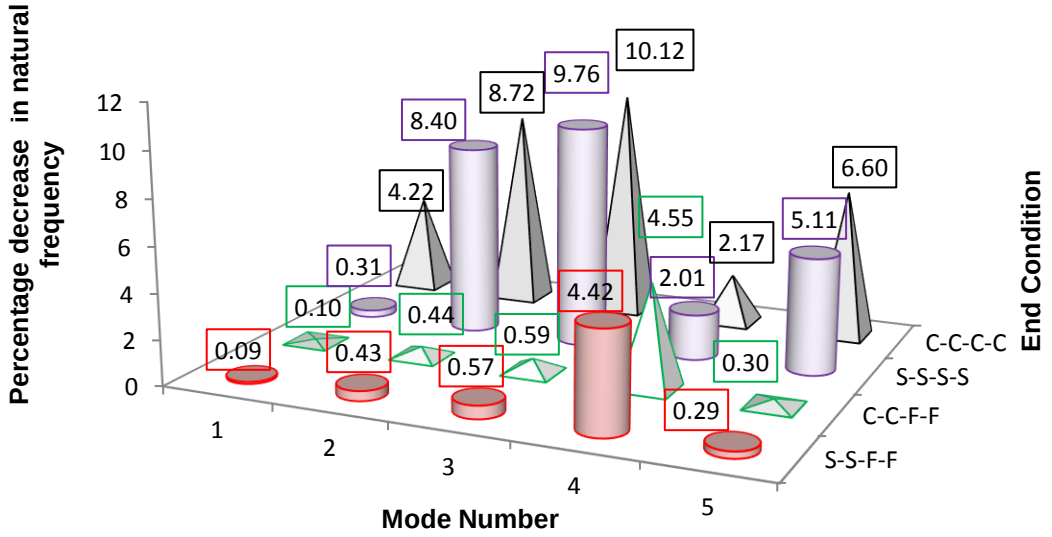

Figure 5.13 Comparison of percentage natural frequency reduction for different end conditions (10% debonding for position 1)

The first 10 mode shapes of the C-C-F-F fully bonded plate and the plate with 10% debonding in location 3 are depicted in Figures 5.14 and 5.15, respectively.

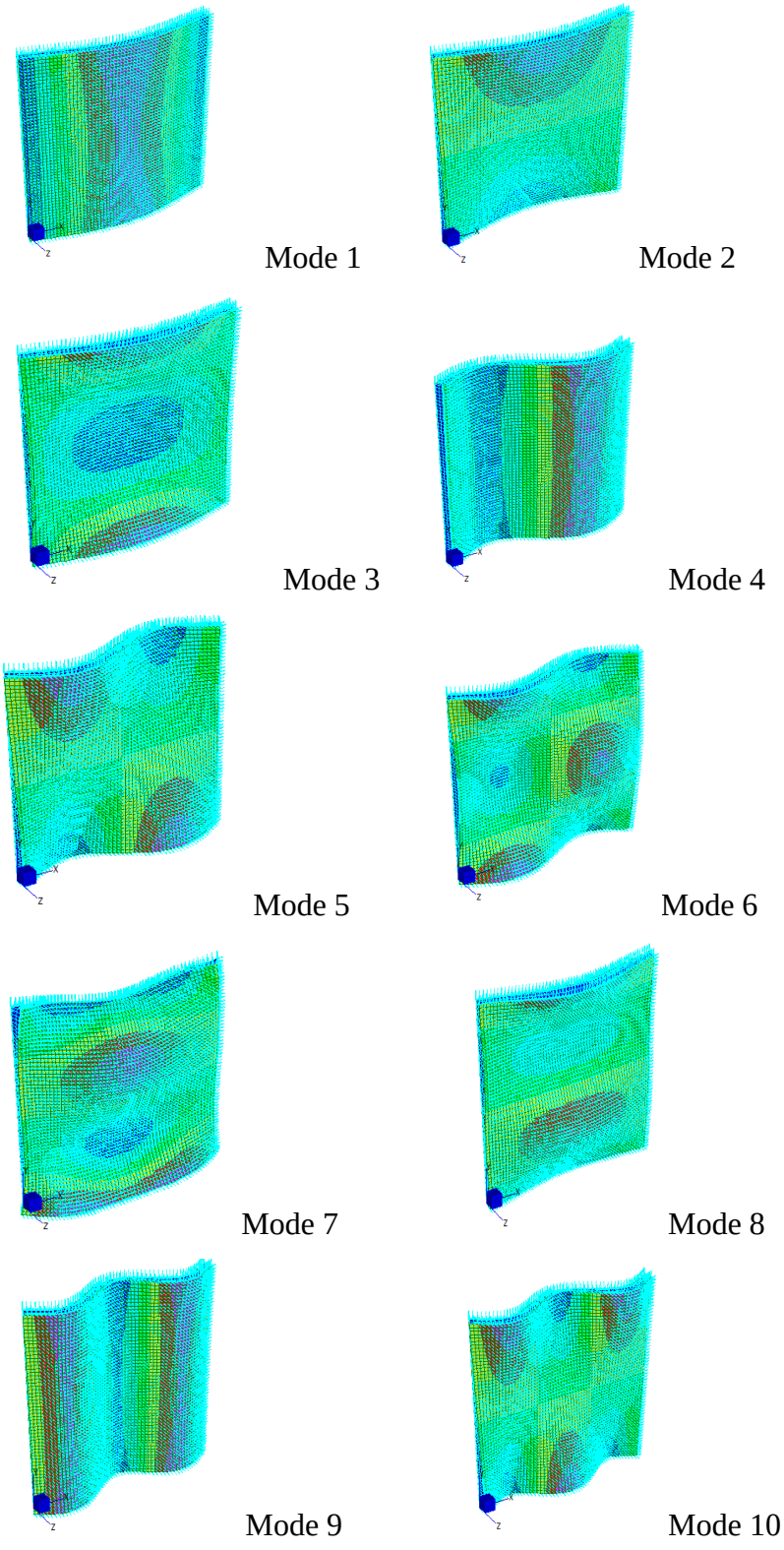

Figure 5.14 First ten eigenmodes for C-C-F-F fully bonded plate

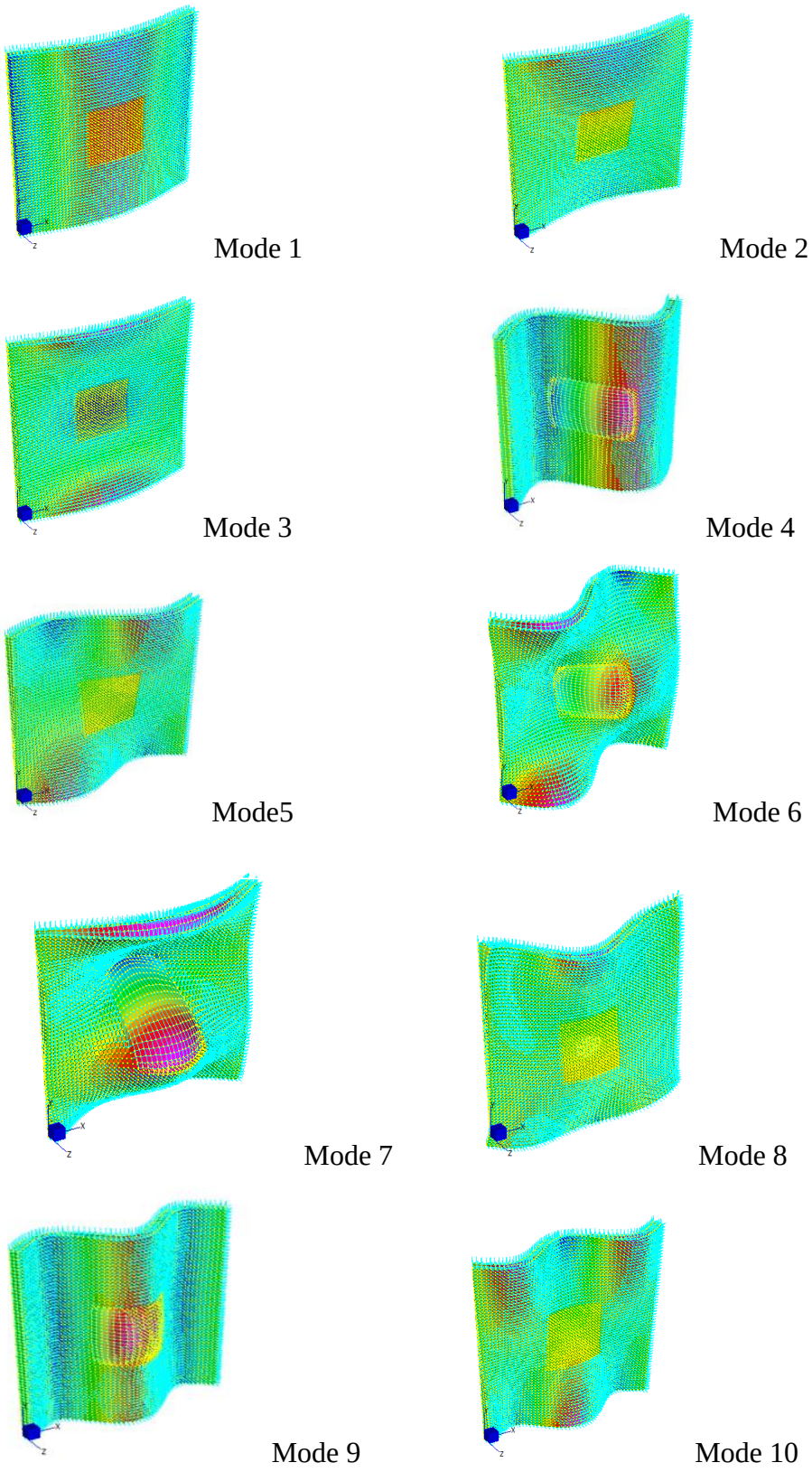

Figure 5.15 First ten eigenmodes for C-C-F-F position 3 and 10% debonding

The differences in vibration modes for fully bonded and debonded plates are clearly visible on the contour plots given above. The vibration modes 4, 6 and 7 markedly show that the vibration modes of the debonded plate contain local deformation within its damaged region (middle region). This is attributed to the loss of structural stiffness of the plate. Generally, this effect is more significant for higher vibration modes. The Figures 5.14 and 5.15 also illustrate that the mode shapes are changed due to debonding and it seems that local deformation takes place at the debonded region rather than global deformation.

As seen from Figures 5.11 and 5.12, there is no significant change in natural frequency and mode shape for vibration mode 1 for fully bonded and debonded plate whereas mode 7 comparisons give a significant change in natural frequency and mode shape. This occurrence is more visible in Figure 5.13 where mode shapes for the mode 7 are directly compared for fully bonded and debonded plates. It was observed from animations of the two vibration modes that there is a dramatic change in the mode of vibration exhibiting transition from bending mode to a torsional mode due to debonding thus exhibiting modifications to the mode shape as clear from Figure 5.16. As illustrated in Figure 5.17 there is no significant variation seen in mode 1 comparison for fully bonded and debonded plate.

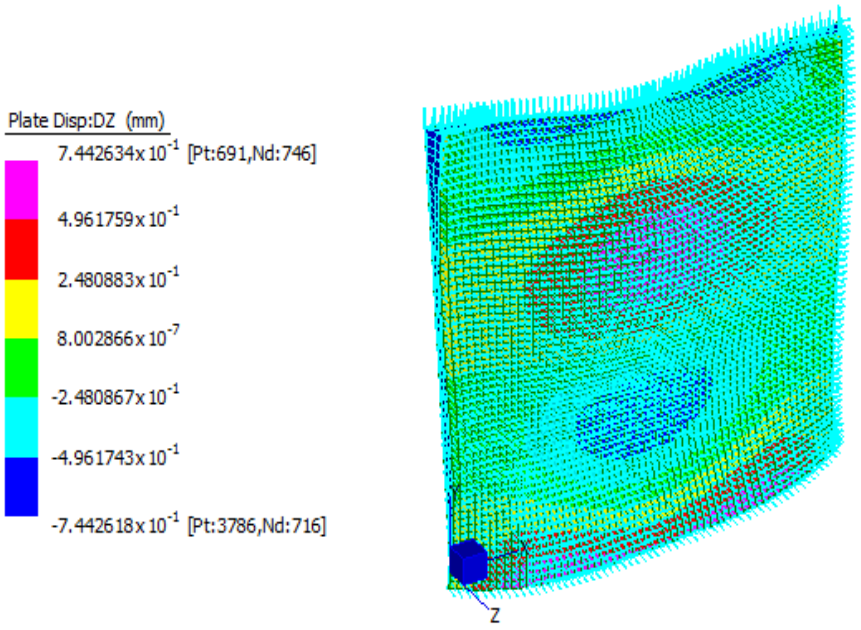

(a) Mode 7 for fully bonded plate

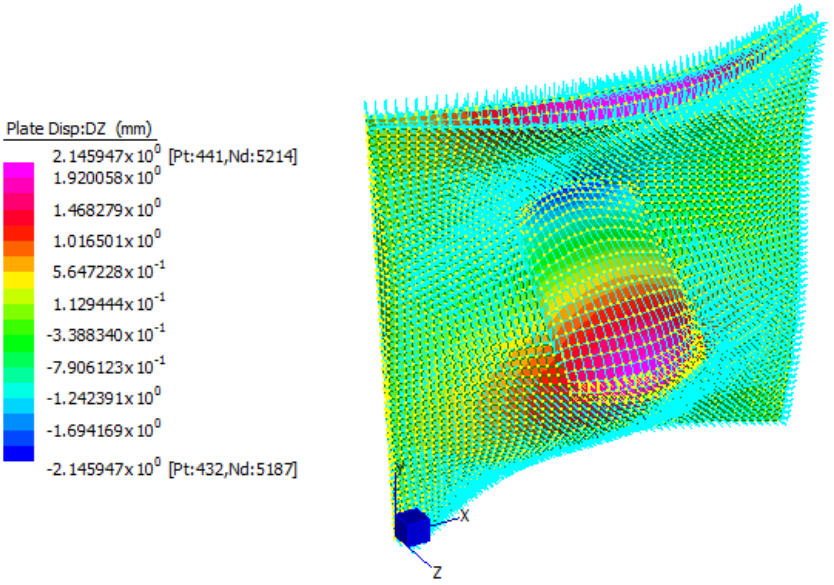

(b) Mode 7 for debonded plate

Figure 5.16 Comparison of mode 7 for fully bonded and debonded plates (C-C-F-F plate with 10% debonding in position 3)

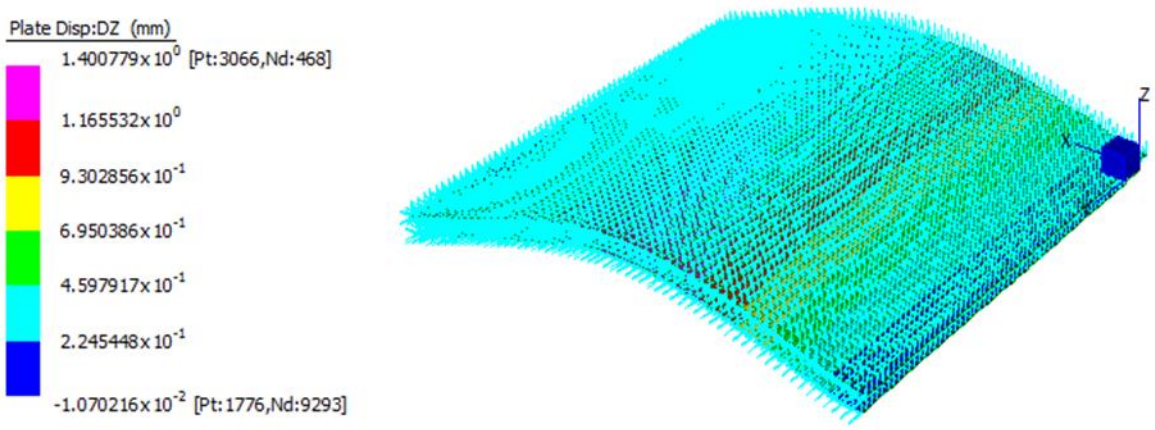

(a) Mode 1 for fully bonded plate

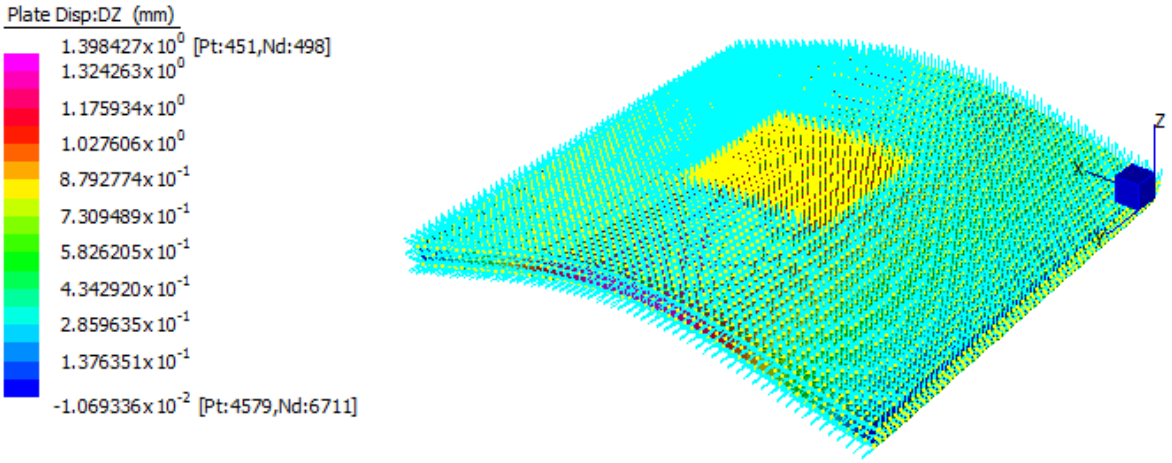

(b) Mode 1 for debonded plate

Figure 5.17 Comparison of mode 1 for fully bonded and debonded plates (C-C-F-F plate with 10% debonding in position 3)

For C-C-C-C plate, out of the first ten modes of vibration, the lowest extent of reduction (2.17% reduction) in natural frequency occurs in mode 4 whereas the highest (10.67%) occurs in mode 10. The mode shapes for these two modes are given in Figures 5.18 and 5.19.

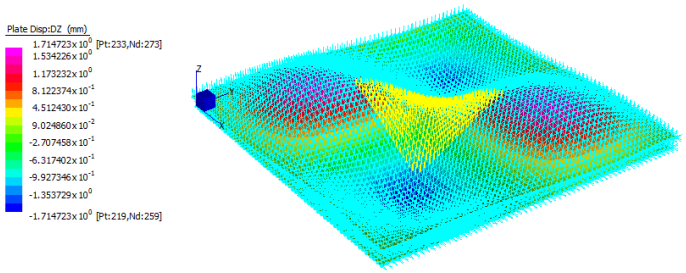

(a) Mode 4: X-Y view

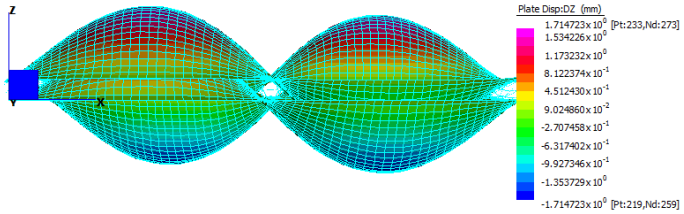

(b) Mode 4: X-Z view

Figure 5.18 Mode 4 for the C-C-C-C plate with 10% debonding in position 3

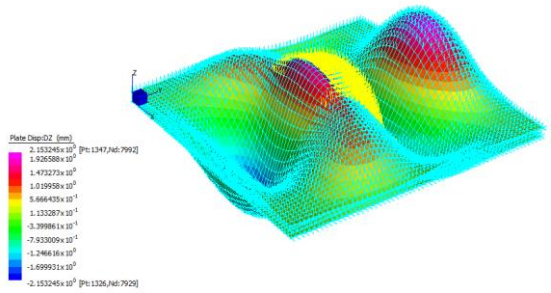

(a) Mode 10 X-Y view

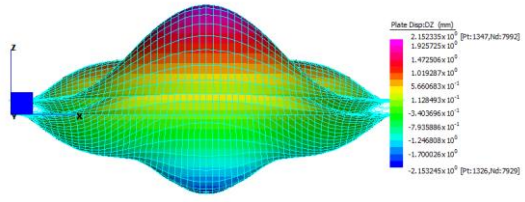

(b) Mode 10 X-Z axis view

Figure 5.19 Mode 10 for C-C-C-C plate with 10% debonding in position 3

The transverse displacement of mid-region (where the debond is located for position 3 debonding) is particularly high for mode 10 as clearly seen form X-Z view of the mode shape of Figure 5.19 while it is much less for mode 4 in accordance with Figure 5.18. Figures 5.18(b) and 5.19(b) that show the X-Z view of the plate are particularly provided for a better visualization of the mode shape, with respect to the debonding location. Comparison of the Figures 5.18 (b) and 5.19 (b) make it clear that debonding location 3 severely affects mode 10 vibration whereas it is much less affected by mode 4 vibration, which is seen by the comparison of extents of natural frequency reduction for the two cases. These patterns are observed in all the debonding positions and boundary conditions specifically for large extents of debonding, depending on how severely the modes are affected. Thus it is clear that the mode shapes well explicate the inconsistencies in extent of natural frequency reductions seen in different vibration modes.

For one-way simply supported plate (S-S-F-F), for 10% debonding in position 3 scenario, the maximum natural frequency reduction occurs in mode 7 (12.9% reduction). The specific mode shape is shown in Figure 5.20 where corresponding mode shape for fully bonded plate is also given for comparison. Another distinctive feature evident through a close look at the animation of the vibration modes is that debonding causes more participation of torsional modes of vibration. For example, for fully bonded plate under consideration (S-S-F-F plate 10% debonding in position 3), mode 7 is a sway mode whereas this changes to a torsional mode for the debonded case as shown in Figure 5.20. This demonstrates that debonding causes significant changes to vibration modes particularly when the extent of debonding is large. Generally, these variations in vibration modes increase with the mode number, yet this effect does not exhibit a monotonic variation, as exemplified in Figures 5.14 and 5.15 mode shapes.

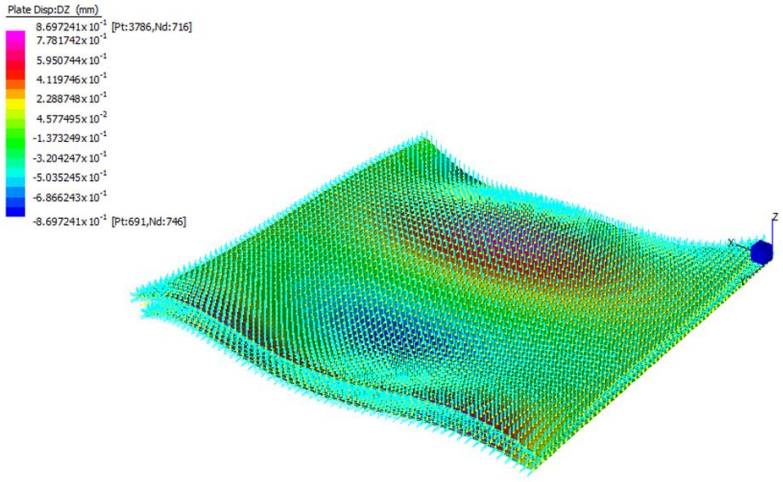

(a) Mode 7 fully bonded plate

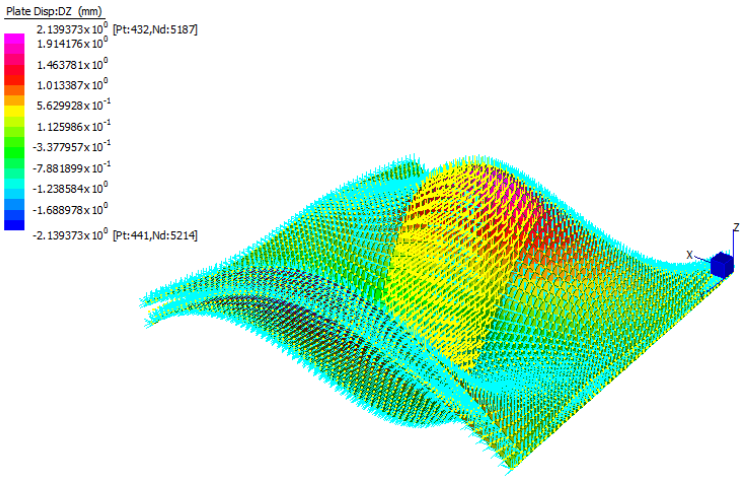

(b) Mode 7 for debonded plate

Figure 5.20 Comparison of mode 7 for S-S-F-F position 3 and 10% debonding

In case of S-S-F-F and C-C-F-F boundary conditions, there are two scenarios for position 2 debonding, first case being when debonding occurs near the supported end and the latter is near free end of the plate, as shown by 5.21 (a) and (b).

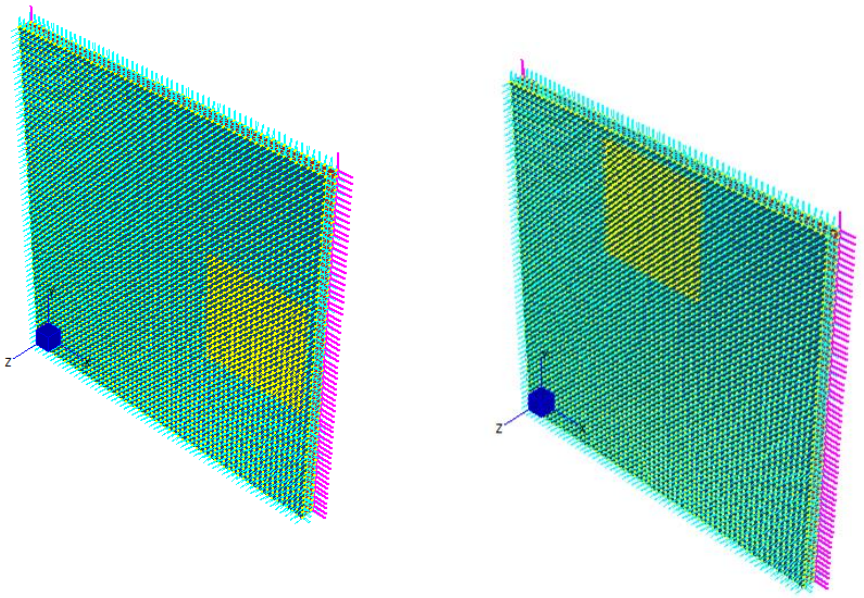

(a) Debonding near supported end (b) Debonding near free end

Figure 5.21 two scenarios of debonding for the S-S-F-F plate with position 2 and 10% debonding

Table 5.6 presents the comparison of percentage reduction in natural frequency for two scenarios (as illustrated in Figure 5.21) in S-S-F-F plate in the case of position 2 debonding. It is interesting to observe here that for this particular boundary condition, generally, debonding near free end of the plate setup displays higher percentage reductions than the other case where debonding occurs near the simply supported end of the plate. Another important observation is that for minor extents of debonding, the extents of natural frequency reductions are negligible.

The comparison for the two scenarios in the case of C-C-F-F boundary condition (for position 2) is presented in Table 5.7.

Table 5.6 Comparison of percentage reduction in natural frequency due to debonding near clamped end and free end for position 2 debonding for S-S-F-F plate

Percentage debonding by total area of plate	Mode number	Debonding near supported end % reduction	Debonding near free end % reduction
0.5% of plate area	1	0.03	0.00
	2	0.00	0.00
	3	0.02	0.05
	4	0.01	0.07
	5	0.01	0.08
	6	0.03	0.00
	7	0.01	0.02
	8	0.05	0.11
	9	0.00	0.00
	10	0.01	0.00
1% of plate area	1	0.07	0.00
	2	0.00	0.00
	3	0.07	0.14
	4	0.04	0.20
	5	0.02	0.22
	6	0.10	0.02
	7	0.04	0.05
	8	0.15	0.30
	9	0.02	0.02
	10	0.02	0.02
5% of plate area	1	0.53	0.01
	2	0.02	0.03
	3	0.53	1.03
	4	0.33	1.66
	5	0.13	1.46
	6	0.77	0.26
	7	0.53	0.89
	8	0.98	1.39
	9	0.36	0.46
	10	0.20	0.47
10% of plate area	1	1.96	0.12
	2	0.20	0.20
	3	2.17	3.58
	4	1.36	8.02
	5	0.54	4.03
	6	3.20	2.04
	7	4.13	4.84
	8	1.78	1.81
	9	3.20	5.08
	10	1.63	1.83

Table 5.7 Comparison of percentage reduction in natural frequency near clamped end and free end for position 2 debonding for C-C-F-F plate

Percentage delamination by total area of plate	Mode number	Debonding near supported end % reduction	Debonding near free end % reduction
0.5% of plate area	1	0.03	0.00
	2	0.00	0.00
	3	0.03	0.05
	4	0.02	0.07
	5	0.01	0.08
	6	0.04	0.01
	7	0.01	0.01
	8	0.05	0.12
	9	0.01	0.00
	10	0.01	0.01
1% of plate area	1	0.12	0.00
	2	0.00	0.00
	3	0.11	0.14
	4	0.08	0.21
	5	0.03	0.23
	6	0.16	0.02
	7	0.05	0.03
	8	0.25	0.32
	9	0.03	0.02
	10	0.03	0.03
5% of plate area	1	0.61	0.02
	2	0.02	0.03
	3	0.60	1.04
	4	0.45	1.74
	5	0.12	1.49
	6	0.93	0.28
	7	0.38	0.74
	8	1.04	1.57
	9	0.42	0.50
	10	0.24	0.50
10% of plate area	1	2.00	0.13
	2	0.19	0.22
	3	2.23	3.63
	4	1.54	8.36
	5	0.52	3.90
	6	3.36	2.10
	7	3.58	4.71
	8	1.96	1.97
	9	3.19	5.54
	10	2.36	1.83

Here it is noted that there is no definite pattern for the two cases (namely, debonding near supported end and free end) on contrary to the S-S-F-F situation. A unique feature common to both boundary conditions is that, for all the percentages of debonding considered, natural frequency reduction for the first mode of vibration is always higher when debonding occurs near the supported end than free end. In fact for debonding happening near free end, natural frequency does not vary at all, till the percentage of debonding is 5%.

5.8.1.3 Results for 1000 mm two layer square plate

In this section the results for the skin-core debonding in the two-layer 1000 mm square panel are presented. The 10% debonding area scenario, which numerical experiments show as giving the highest reduction in natural frequency, is presented for comparison of single layer and multilayer debonding. Here, debonding between the top skin and core (single debonding) is compared with debonding in both top and bottom skins and the core (double debonding) of the top layer of two layer slab panel (as illustrated in Figure 5.22) are considered. The debonding location selected for the analysis is position 3.

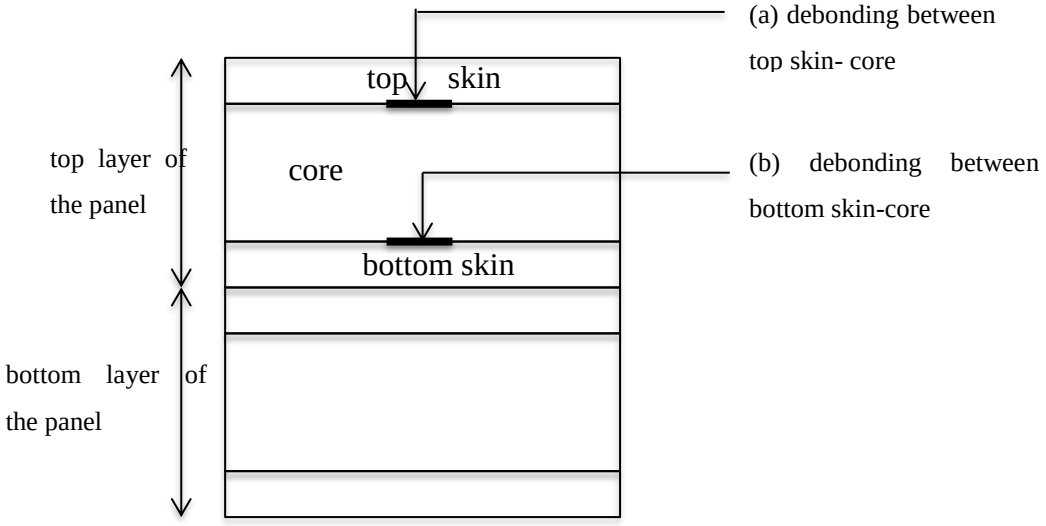

Figure 5.22 Debonding locations considered for 1000 mm square two layer composite sandwich panel

Figure 5.23 shows the comparison of percentage reduction in natural frequency with regard to the position 3 debonding location for both single and double layer debonding as illustrated in Figure 5.22.

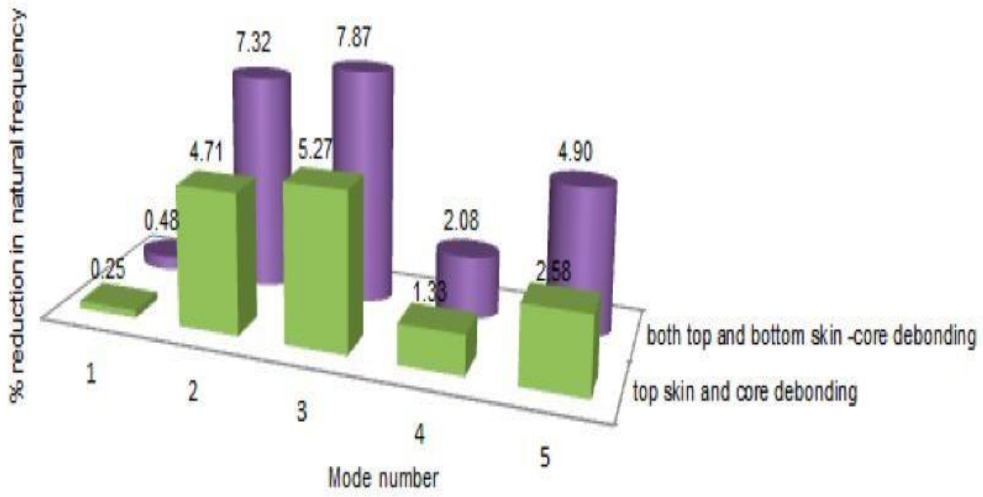

Figure 5.23 Comparison of single debonding double debonding in the top sandwich layer of the two layer 1000 mm slab panel

It is of special interest to observe here that the double layer debonding gives nearly double the extent of reduction in natural frequency when compared to single layer debonding. The extent of reduction is mode dependent as was the case with the 800 mm and 3000 mm panels.

5.8.2 Influence of interlayer delamination on dynamic behaviour

This section presents some notable comparisons and related observations with regards to the broad parametric analysis done on 1000 mm double layer composite sandwich plates with interlayer delaminations (as shown in Figure 5.4). First, it was observed from the comparison that, the end condition, which gives highest reduction in natural frequency due to delamination, is the two way clamped (C-C-C-C) end condition. Moreover, the least reduction is seen in one-way simply supported (S-S-F-F) end condition. Furthermore, it was revealed that position 3 is the most critical delamination position for the end conditions (C-C-C-C) and (S-S-S-S) in general. Interestingly the critical position of delamination is observed to be greatly dependent of the end conditions of the panel.

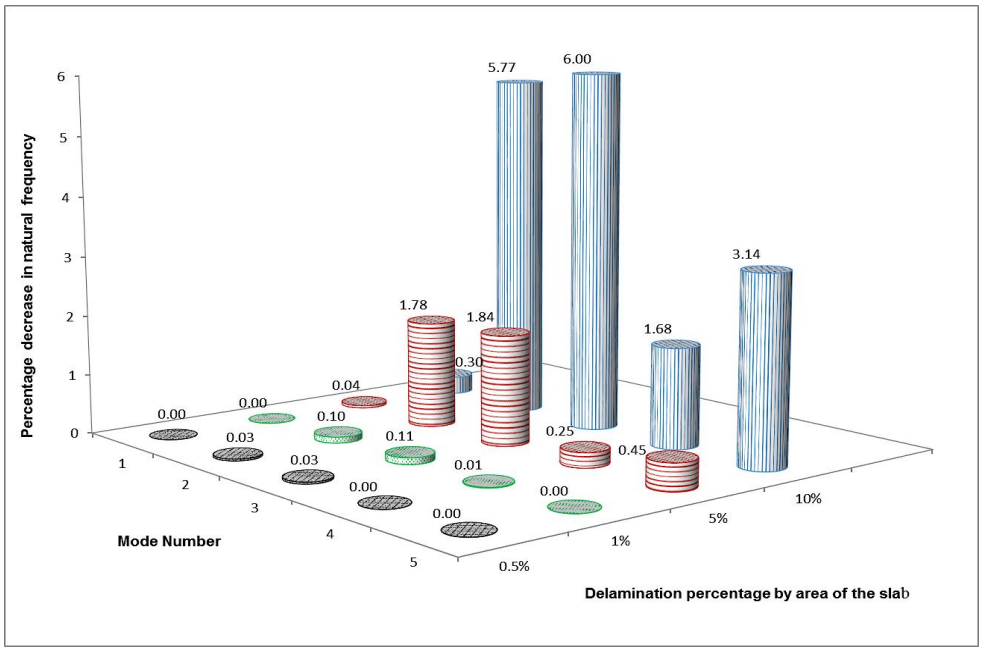

Figure 5.24 Shift in natural frequency for the C-C-C-C slab panel: delamination position 3

Figure 5.24 above displays the variation of percentage reduction in natural frequency due to various percentages of interlayer delamination's in 1000 mm square slab panel with C-C-C-C end condition for delamination position 3, which is the most adverse position for this particular end condition. It is of importance to observe here that when the percentage of delamination is not higher than 1% of the surface area of the plate, the percentage decrease in natural frequency is negligibly small, even for the most critical delamination position illustrated in Figure 5.24. Additionally, it is observed that even though there is a general trend that the extent of natural frequency variation with respect to delamination increases with the order of the natural frequency (specifically for the first three natural frequencies), there are inconsistencies depending on the degree of delamination and mode number. Furthermore, it is revealed that these variations are attributed to the vibration mode shapes of the modes of interest.

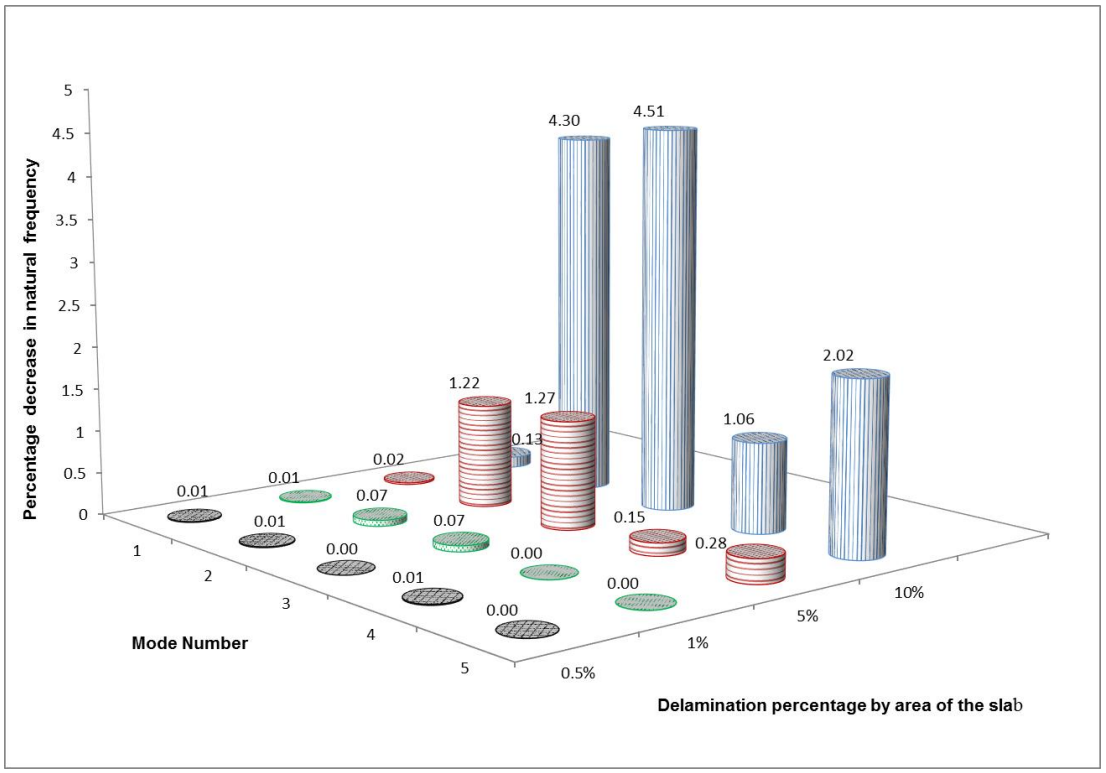

Figure 5.25 Shift in natural frequency for S-S-S-S slab panel: delamination position 3

The most critical position for SS two way case (S-S-S-S) is also position 3, as was the worst position for FF two way case (C-C-C-C) as described above. The extent of natural frequency reduction for different extents of delamination in the case of (S-S-S-S) end condition for position 3 is illustrated in Figure 5.25. It is interesting to observe from Figures 5.21 and 5.22 that the percentage reduction in natural frequency is less for S-S-S-S case when compared to C-C-C-C case for all the delamination percentages in general. This is confirmed true in the comparisons for other two positions as well. Thus it is revealed that when the panel is more restrained the influence on natural frequency reduction is more.

Comparison of percentage reduction in natural frequency for one way fixed case for the three positions of delamination reveals that the most critical position for this particular case is position 1. Figure 5.26 shows the variation of percentage reduction in natural frequency due to various percentages of interlayer delaminations in 1000 mm square slab panel with C-C-F-F end condition for delamination position 1, which is the worst location for this end condition. Furthermore it is of special interest to observe from all the

comparisons explained above that delamination size plays a major role in reducing natural frequency thus leading to significant stiffness reduction for larger delamination size.

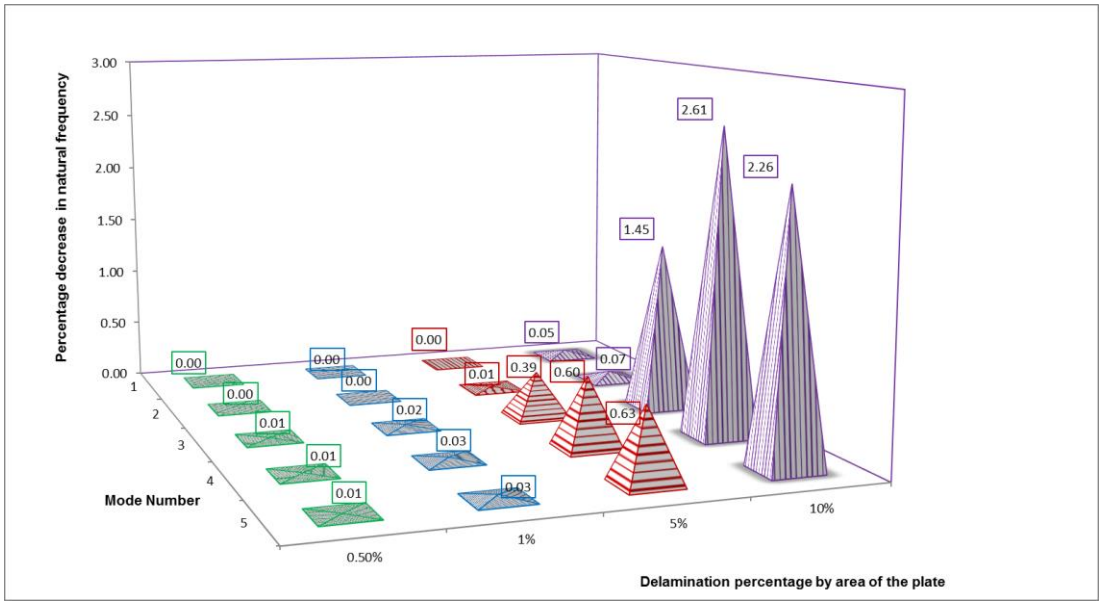

Figure 5.26 Shift in natural frequency for C-C-F-F panel: delamination position 1

Careful observation of Figures 5.24, 5.25 and 5.26 confirms that the percentage of natural frequency decrease with respect to delamination follows different trends depending on the boundary condition, extent of delamination and location of the delamination.

Table 5.8 reports the natural frequency values in Hz for the first five modes of vibration for the four end conditions in the case of fully bonded plate as well as delaminated plates. Note here that the position considered is delamination position 3.

Table 5.8 Natural frequency values in Hz for the position 3 delamination

Percentage delamination by total area of plate	Mode Number	C-C-C-C end condition	S-S-S-S end condition	C-C-F-F end condition	S-S-F-F end condition
0% (Fully bonded)	1	142.02	102.21	88.73	57.91
	2	274.00	198.46	98.34	69.72
	3	288.11	207.83	160.61	143.17
	4	392.65	311.21	235.67	154.84
	5	473.98	390.52	248.51	181.40
0.5% of plate area	1	142.02	102.21	88.73	57.91
	2	273.93	198.45	98.34	69.72
	3	288.03	207.82	160.61	143.17
	4	392.64	311.17	235.64	154.80
	5	473.98	390.51	248.51	181.40
1% of plate area	1	142.02	102.21	88.73	57.91
	2	273.72	198.32	98.33	69.72
	3	287.80	207.68	160.61	143.17
	4	392.63	311.20	235.58	154.80
	5	473.96	390.51	248.51	181.40
5% of plate area	1	141.97	102.19	88.72	57.91
	2	269.13	196.04	98.28	69.68
	3	282.80	205.19	160.56	143.14
	4	391.66	310.74	234.05	154.32
	5	471.84	389.44	248.45	181.37
10% of plate area	1	141.60	102.08	88.65	57.89
	2	258.18	189.92	98.11	69.57
	3	270.82	198.45	160.23	142.91
	4	386.07	307.90	229.57	154.25
	5	459.11	382.62	248.05	181.14

It is obvious from Table 5.8 that the plate with C-C-C-C end condition, which has the highest end fixity, gives highest natural frequency variation. A close examination of Table 5.9 reveals that the fundamental natural frequencies remain the same when the percentage of delamination is not greater than 1%, for all four end conditions considered in the analysis. This leads to a major reflection that variations of free vibration characteristics are negligible for small delaminations, in the order of 1% of the plate area.

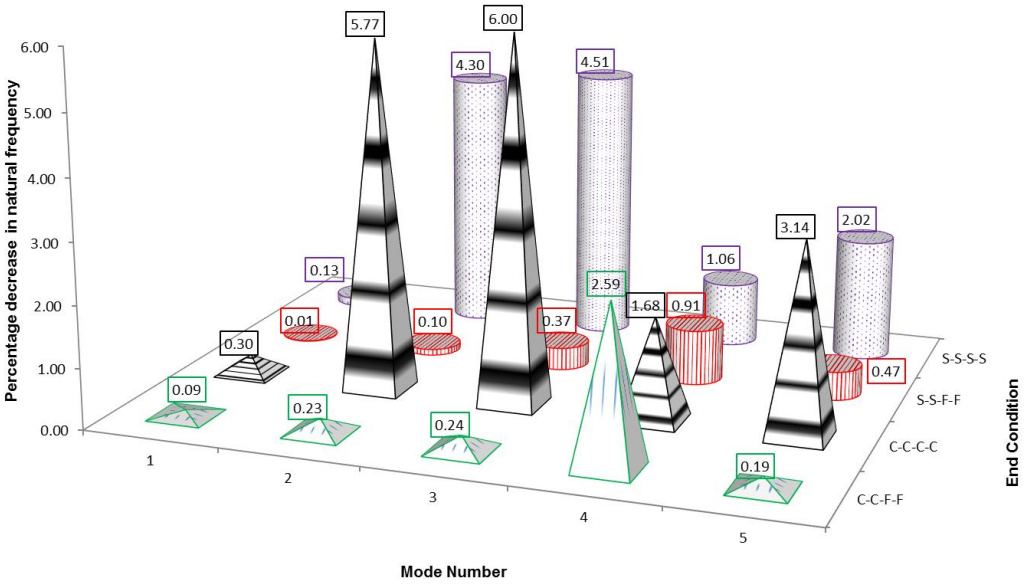

Figure 5.27 Comparison of the shift in natural frequency for the four end conditions

Figure 5.27 illustrates the comparison of the variation in natural frequency with regard to the four end conditions used in the analysis for similar conditions of location and extent of delamination. Here the location of interest is position 3 and the percentage of delamination considered is 10% by area of the plate. It is interesting to reveal that C-C-C-C end condition, which has the highest end fixity, exhibits the highest variation out of the four conditions considered in the simulation. Comparison between the percentage natural frequency decrease for end conditions C-C-F-F and C-C-C-C (see Figure 5.27) reveals that higher end fixity attributes to significant variations in natural frequency for identical sizes and locations of delamination.

5.8.3 Results for simulations with fastening the delaminated regions as a corrective measure

Here the 1000 mm double layer GFRP plate with most adverse end condition and the corresponding delamination position have been selected to predict the efficiency of fastening (or some other form of joining) to improve the dynamic performance of a delaminated double layer 1000 mm square panel. As such, the end condition considered here is two way clamped (C-C-C-C) with position 3 and 20% delamination by area of the panel. Three cases of bolting are considered. The delaminated region is bolted using a single bolt line along the middle line of the delaminated region at first. Second case is the

use of three bolt lines and thirdly using seven bolt lines equally spaced in the delaminated region (see Figure 5.28). For all three cases, the distance between bolts in a bolt line is 30 mm. Figure 5.28 shows the arrangement for the case 2 with three bolt lines.

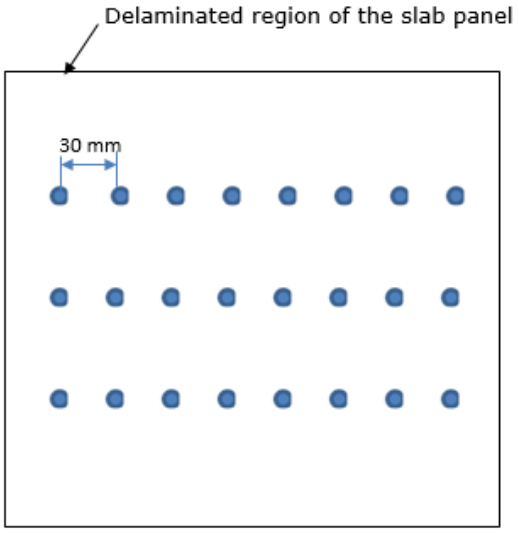

Figure 5.28 Bolt arrangement for case 2 with three bolt lines in the delaminated region

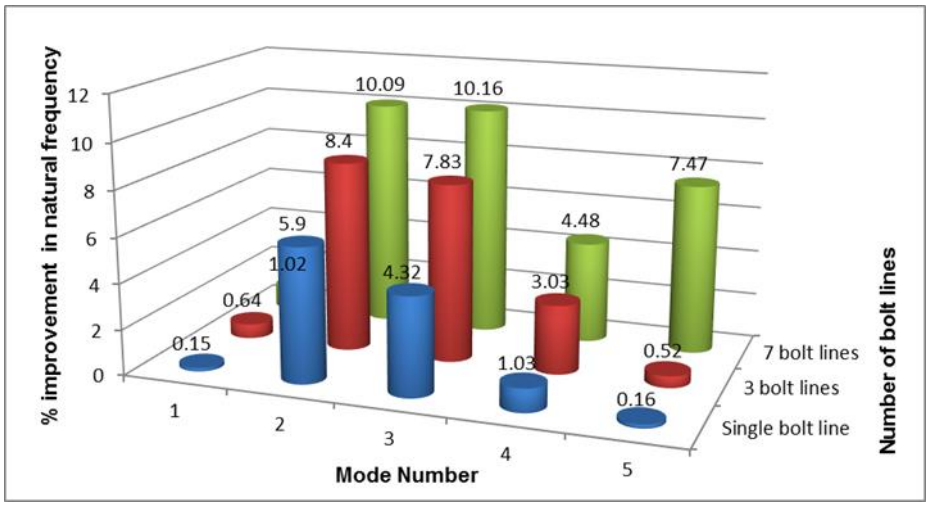

Figure 5.29 Improvement in natural frequency due to fastening delaminated region in C-C-C-C panel

Figure 5.29 shows the percentage improvement in natural frequency (when compared with delaminated plate frequency) for the above mentioned panel with single bolt line, three bolt lines and seven bolt lines connected through the delamination region.

It is observed that, effectively, bolting the delaminated region gives significant improvement of natural frequency when compared to the initially delaminated panel.

5.9 Chapter conclusions

- Generally, it was evident from all the analyses that debonding and interlayer delamination cause reduction in magnitudes of natural frequency. Moreover, some vibration modes and accordingly the mode shapes are also noticeably changed. Vibration mode denotes here whether it is translational, bending or rotational as can be captured from the animation facility in STRAND7 results file.
- Abrupt changes of the vibration modes (comparing the vibration modes of the debonded plate with the fully bonded one) lead to substantial drops in corresponding natural frequencies.
- Furthermore, the results show that the presence of relatively small debonding or delamination has an insignificant effect on the natural frequencies and associated mode shapes of the GFRP plates considered in the present analysis. Additionally, it was observed that equivalent single debonding affects the free vibration frequencies much more than equally sized isolated two debonding zones.
- The findings of the dynamic analyses with plates suggest that the debonding or delamination size and the end fixity of the plate are the most important factors in stiffness reduction due to debonding and delamination damage in composite laminates.
- The results also suggest that fastening the delamination region is an effective corrective measure in decreasing the natural frequency variation, hence improving its dynamic performance compared to the delaminated panel.
- It is discovered that the more the supports are restrained, the more the influence on free vibration behaviour due to debonding and interlayer delamination, especially in terms of natural frequency reduction and influence on modes of vibration.

- It is generally observed that higher natural frequencies and mode shapes are more influenced by the presence of debonding. Yet there are inconsistencies in this trend depending on how severely the local modes are affected by debonding. It is established that the associated mode shapes explain the causes of these inconsistencies.
- It also follows from the results of the analyses that percentage increase in the debonding size results in the appearance of local modes even for the lower mode numbers. Hence, by the observation of such sudden variations in the modes, the severity of debonding may be appraised. This demonstrates the feasibility of non-destructive methods to detect debonding and delamination damage in practical composite slabs.

CHPATER 6 DYNAMIC BEHAVIOUR OF DEBONDED COMPOSITE PLATES SUBJECTED TO SEISMIC LOADING

6.1 Introduction

The Australian continent lies entirely within the Indo-Australian Plate and hence Australian earthquakes are shallow and occur within the crust. The Newcastle mainshock of 28 December 1989 is a typical example of how an intra-plate earthquake with moderate magnitude can cause loss of life and extensive damage if it occurs close to a population centre (Sinadinovski et al. 2000).

According to Ronagh and Eslami (2013), amongst different methods recommended for upgrading of RC buildings, the use of fibre-reinforced polymers has increased significantly in recent years. Earthquake simulation using finite element modelling is important for understanding their behaviour and for comparative performance studies. Response-spectrum analysis (RSA) is a linear-dynamic statistical analysis technique, which measures the contribution from each natural mode of vibration to specify the probable maximum seismic response of an elastic structure. It gives insight into the dynamic behaviour of structures and hence is useful for design decision making.

The main objective of this chapter is to quantify the differences in the earthquake response of mid-rise R/C buildings with fully bonded and debonded GFRP slab panels. The building selected for the earthquake analysis has been extracted from STRAND7 Web notes (2015). The method used in this study is to use the response spectrum approach to predict the comparative responses. In this research, the seismic action has been modelled by means of the acceleration response spectrum. Assumptions are made where the necessary data are not available or when the situation is outside the scope of this study.

6.2 Selection of building for the seismic analysis

The building selected for the investigation of seismic performance comparison is a six-storey reinforced concrete framed structure, representing typical mid-rise office buildings. The example building in STRAND7 Web notes ST7-1.40.35.22 (2015) is selected and appropriate alterations made within the scope of the study. This is a typical office building with a single lift core and a fixed base.

The building has a constant floor-to-floor height of 3.5 m and the total height of 21 m. The dimensions of floor panels are 6 m x 6 m, whereas the lift core size is 3 m x 3 m. The building structural elements have the same dimensions for all six floors. The building has two bays in the North–South (N-S) direction and three bays in the East–West (E-W) direction as illustrated in Figure 6.1 with Y and X directions respectively. The typical floor plan (generated by STRAND7) of the buildings is shown in Figure 6.1 and the dimensions of the concrete structural members are given in Table 6.1.

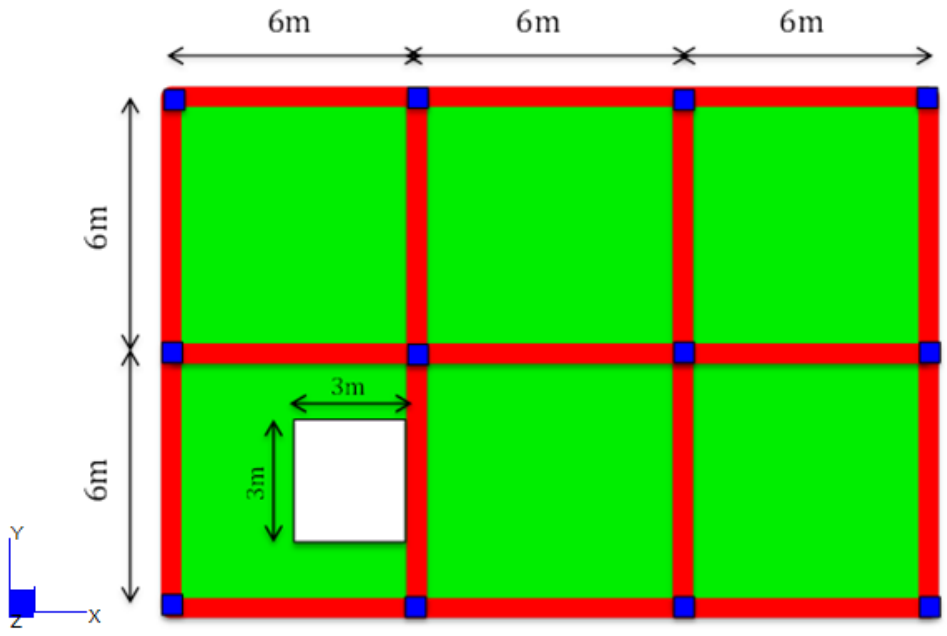

Figure 6.1 Typical floor plan of the building

Table 6.1 Dimensions of structural members in mm

Member Type	Details
Column (Cross section)	500×500
Beam (Cross section)	500×500
Slab thickness	200
Lift core (Cross section)	3000×3000

The material properties assigned to R/C members are given below.

Density of concrete = 24 kN/m^3

Young's modulus of concrete = 30.96 kN/mm^2

Poisson's ratio = 0.2

Compressive strength of concrete = 32 N/mm^2

The live load used is 3 kN/m^2, which is typical for an office building according to AS1170.1 (2002). This pressure has been converted to an equivalent mass and applied to floor slab elements of the building using 'plate non-structural mass attributes' option in STRAND7.

It is to be noted that the detailed design of the building is out of the scope of the current study, since only comparative seismic performance results are assessed. For simplicity, the torsional effects attributed to seismic loading have been neglected in the present study. The selection of a simplified model is in compliance with the aim of the study, which was to make a comparative parametric presentation of the seismic response of the building under consideration.

6.3 Parameter selection to investigate the influence of debonding

The original R/C six storey building extracted from STRAND7 Web notes (2015) have been modified to replace some of R/C slabs with GFRP single layer sandwich slab panels having a total thickness of 144 mm. Preliminary studies with the original building with all R/C slabs and building with some R/C slabs replaced by GFRP panels revealed that the total weight of the building is reduced when GFRP panels are substituted, due to the lightweight property of GFRP composite material. In order

to compare the seismic performance with and without debonding, initially a preliminary seismic study was carried out to determine the most effective floor level to be considered for replacement of R/C slabs with GFRP panels. Preliminary parametric seismic analyses where the GFRP panels were placed in different floors of the building revealed that the influence of debonding is negligible when panels are located in lower floors, and becomes more pronounced when located in higher floors. Although the influence was highest when the GFRP panels are placed in the top floor (roof slab), fifth floor was selected for the detailed analysis for the parametric investigation, the reason being to avoid any design and practical complications due to environmental effects on the GFRP slabs when functioning as the roof slab of the building.

Hence for the detailed comparative analysis, fifth floor R/C slab panels of the selected original building have been replaced by 144 mm thick single layer novel GFRP slab panels described in Chapters 3 and 5. Mid beams are placed as illustrated (parallel to X direction in Figure 6.2) in each bay of the 5^{th} floor level to keep the span of the GFRP slab panels as 3 m. The R/C slab panel in the lift core region was not replaced by GFRP panels, to reduce complexity of analyses. Generally the mass of the building being designed controls seismic design in addition to the building stiffness, because earthquake induces inertia forces that are proportional to the building mass. Hence the resulting building can be assumed of as an R/C structure upgraded with lightweight GPRP slab panels to improve seismic performance.

According to STRAND7 (2010), plate element edges can have the rotational stiffness released (‘plate edge release’) along one or more edges by releasing one common edge, thus simulating a hinged edge connection. The GFRP panels in the fifth floor are assumed to be precast, and hence to accurately model the simple support condition prevailing between GFRP slab panels and the supporting R/C beams, ‘plate edge release’ attribute in STRAND7 has been utilised for all the necessary plate edges. Accordingly, plate edge release condition is applied to all beam slab connections on the fifth floor GFRP slab panels as illustrated in Figure 6.2. In order to determine the appropriate mesh density for the slab panels, a mesh refinement process was conducted. Figure 6.2 explicates the 3D finite element model created accordingly as described above by replacing R/C panels with GFRP panels in the

fifth floor. The top floor (6th floor) of the building is not shown in the Figure 6.2 in order to clearly show the GFRP slab arrangement with plate edge releases applied. Fixed supports are provided to the columns at the base of the building as demonstrated.

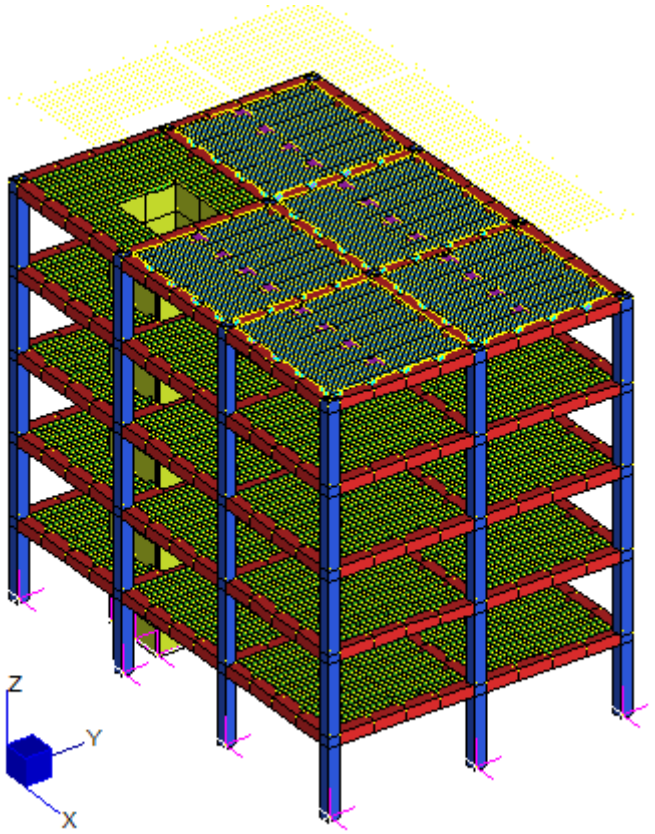

Figure 6.2 FE model of the R/C building with GFRP panels on 5th floor

Initially, the seismic analysis has been carried out for the reference building with fully bonded GFRP slabs in the fifth floor. Three different debonding positions of the slab have been considered for parametric investigation, as shown in Figure 3.8 in Chapter 3. Four percentages of debonding on each slab panel, namely, 5%, 10%, 25% and 50% were analysed for each debonding location. Figure 6.3 exemplifies the FE model with 50% debonding in location 3 of the GFRP panels. In Figure 6.4, the top floor (6th floor) of the building is not shown in order to clearly show the GFRP slab panels with debonding.

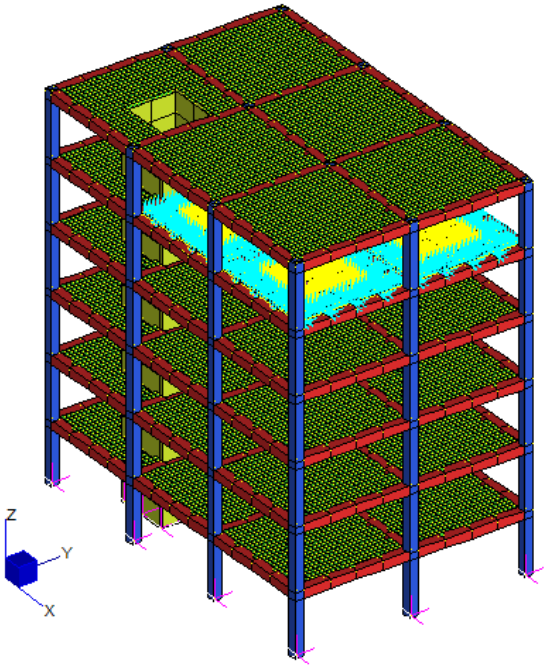

Figure 6.3 FE model for the building configuration with 50% debonding in position 3

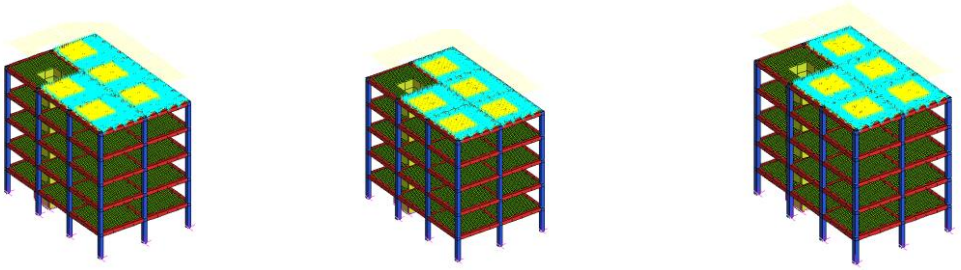

(a) position 1 (b) position 2 (c) Position 3

Figure 6.4 FE models for the building configurations with 50% debonding in positions 1,2 and 3 (6^{th} floor not shown for clarity)

6.4 Dynamic earthquake analysis procedure according to AS1170.4 (2007)

AS 1170.4 (2007) gives three types of analysis procedures under dynamic analysis.

(a) Horizontal design response spectrum (HS): The complex and random nature of ground motion renders it necessary to work with a general characterisation of ground motion. This is accomplished by using horizontal design response spectra to hypothesise the intensity and vibration content of ground motion at a given site (Bangash 2011).

(b) Site-specific design response spectra (SS): SS is developed for specific site sub-soil classifications and replicates the soil profile and bed-rock ground motion. SS is the method commonly used, which is based on the sub-soil class of the area of interest, where modal responses are joined in a statistical approach to get the maximum value of the building response.

(c) Ground motion time histories: Time history method encompasses calculating the response of a structure at each time increment when the base is subjected to a specific ground motion time-history. This procedure is complex and requires the availability of ground motion time histories.

6.5 Outline of the response spectrum analysis procedure

Response-Spectrum Analysis (RSA) is carried out using structural vibration characteristics such as mode shapes and frequencies, and it encompasses estimating the maximum dynamic structural response rather than calculating the response at each point in time. RSA method includes modal or eigenvalue analysis of the equation of motion. With the aid of eigenvalue analysis results, multiple-degree-of-freedom (MDOF) structural system matrices, force vectors, and displacement vectors can be transformed into single-degree-of-freedom (SDOF) modal properties, forces, and displacements for each mode. After the model has been transformed into modal coordinates, an analysis of the modal equations of motion can be conducted.

RSA carried out can be summarized into the following steps:

- Suitable three dimensional finite element model is developed
- The number of modes to be used in the finite element analysis is decided
- Modal analysis of the building is carried out to get the mode shapes, frequencies and modal participation factors according to the code requirements
- Results are combined from two orthogonal directions according to code requirements
- Maximum modal responses are combined using CQC method to find the total maximum response

- After running the response spectrum analysis, seismic and gravity loads are combined according to the code requirements to obtain the design maximum responses for the buildings

6.6 Drift considerations

The important parameter that affords an estimate of the lateral stiffness of a building is the drift index or drift ratio, defined as the ratio of the maximum lateral deflection at the top of the building to the total height. In addition, the equivalent value for a single story height, the interstorey drift index (interstorey drift ratio), gives a measure of possible localized excessive deformation (Smith and Coull 1991). The inter-storey drift ratio is defined as the maximum relative displacement between two consecutive storeys (interstorey drift) normalized to the height of the storey of interest. This ratio is one of the most important parameters for the assessment of response of structural members subjected to seismic loading.

Design drift ratio limits that have been used in different countries range from 0.001 to 0.005. For conventional structures, the preferred acceptable range is 0.0015 to 0.003 (Smith & Coull 1991). Clause 5.4.4 of AS1170.4 (2007) requires that the inter-storey drift to be less than 1.5% of the storey height for each level. A structure with less drift will be a stiffer structure.

6.7 Seismic analysis procedure for the present study

The dynamic analysis method used for seismic analysis in the research is response spectrum analysis using site specific (SS) response spectra. SS is the common dynamic seismic analysis method based on sub-soil class of the region of interest. STRAND7 requires two solvers, namely natural frequency solver and response spectrum solver for the analysis. The base excitation spectrum is applied as a translational excitation at the base, equally at all fixed degrees of freedom. The excitation may act in any arbitrary direction in the global X-Y-Z system and can be defined in terms of acceleration, velocity or displacement. Typical input spectra include those based on a particular earthquake or an averaged design spectrum given in the design codes. The STRAND7 response spectrum database comprises acceleration response spectra for all five sub-soil classes (STRAND7 2010). In this

study, Australian Code Response Spectrum included in STRAND7 will be generated for seismic analysis taking the sub soil class of the area (Class C_e- Shallow soil) into account. Damping effects are in fact very important in seismic analysis. In STRAND7, damping can be modelled through two viscous damping models: Rayleigh damping and modal damping (STRAND7 2010). This option is available in response spectrum analysis, and will be used for seismic analyses.

The results of a response spectrum analysis are given as envelopes of maximum values of nodal displacements, element stresses and strains, recovered reactions at constrained nodes and elastic forces at unconstrained nodes. The maximum response values are calculated by combining the maximum response of all modes included in the analysis. Contributions from individual modes are available as well as the combined maximum values (STRAND7 2010). The maximum inter-storey drift ratios, maximum top displacements and accelerations are the critical indicators of the expected damage to the structure.

6.8 Seismic parameter selection for the selected building configurations

It has to be noted here that the parameter selection and analysis procedure are in accordance with AS1170.4 (2007) and assumptions are made where necessary within the scope of the study.

6.8.1 Earthquake design categories

AS 1170.4 (2007) categorizes buildings under Earthquake Design Category (EDC) in Section 2.2 and this classification is based on the probability factor (k_p), the hazard factor (Z), and the height of the building. For the 6-story building under consideration, the following conditions are applicable.

k_P = 1.25 (Section 3.1)

The hazard factor (Z) depends on the specific location under consideration, and the region selected for the present analysis is Newcastle, NSW. Accordingly from Table 3.2 of AS1170.4 (2007);

Z = 0.11 (for Newcastle)

Therefore; $k_pZ = 1.25 \times 0.11 = 0.1375$.

6.8.2 Selection of sub-soil class for building models

The city of Newcastle developed mainly along the Hunter River, and the soils in these areas consist mainly of alluvial deposits. The sub-soil classification most closely related to the region is assumed for sub-soil class. Hence Class C_e – Shallow soil given in section 4 of the Standard is selected for the present analysis.

6.8.3 Selection of earthquake design category for the building

Selection of earthquake design category is according to Table 2.1 of AS1170.4 (2007);

$k_pZ > 0.12$

Height of the building = 18 m (< 25 m).

From Table 2.1 (AS1170.4 2007), earthquake design category is II (EDC II).

According to Clause 5.4.2.2, for EDC II, the earthquake forces shall be calculated using equivalent static method, in accordance with Section 6, and it further says that dynamic analysis, in accordance with Section 7, may be used if required. Dynamic analysis captures dynamic response characteristics, which cannot be attained using static analysis. The response spectrum method enjoys wide acceptance as an accurate method for predicting the response of any structural model to any base excitation. The response spectrum technique is faster and easier than dynamic time history analysis and more accurate than the static procedure, and hence is selected for the present study. The site-specific response spectrum method, which is a commonly used dynamic analysis method, is implemented for the current seismic analysis.

6.8.4 Selection of number of natural frequencies to be included

For two-dimensional models, AS 1170.4 (2007) recommends 90% mass participation for the direction under consideration, and for three-dimensional models the requirement is quoted below;

In three-dimensional analysis, where structures are modelled so that modes that are not those of the seismic-force-resisting system are considered, then all modes not part of the seismic-force-resisting system shall be ignored. Further, all modes with periods less than 5% of the fundamental natural period of the structure (<0.05T_1) may be ignored.

Hence when performing natural frequency solver analysis, the solver setup has to include the adequate number of modes to satisfy the above mentioned code requirement.

The fundamental natural period of the reference model with fully bonded GFRP panels in the fifth floor (T1) was 0.6847 s.

0.05T1 = 0.05×0.6847 = 0.03424 s
Therefore modes below the natural period of 0.03424 s can be ignored. The corresponding natural frequency for the natural period of 0.03424 s is 29.2099 Hz.

From a few trial solver runs, it was found that there are 128 modes above T (5%) period limit (corresponding to natural frequency values up to 29.2099 Hz). Hence for the 3D analysis of this building configuration, natural frequency solution for 128 modes has been used. Accordingly, to find the adequate number of modes required, a few iterations were done for each building configuration under consideration.

6.8.5 Spectral Response Table used for the spectral analysis

Spectral response solver in STRAND7 can be used with normalised response spectrum in the analysis or as an acceleration response spectrum. The STRAND7 response spectrum table database contains both normalised and acceleration response spectra for all five sub-soil classes (STRAND7 2015).

For the present study, the response spectra given in AS 1170.4 (2007) are generated using STRAND7 equation editor. The proposed response spectra included in AS 1170.4 (2007) are piecewise continuous with different mathematical function description, and hence the appropriate curve was generated by using three

applications of the equation editor. The response spectrum generated by STRAND7 using equation editor for relevant soil class (Ce) for the present analysis is shown in Figure 6.5.

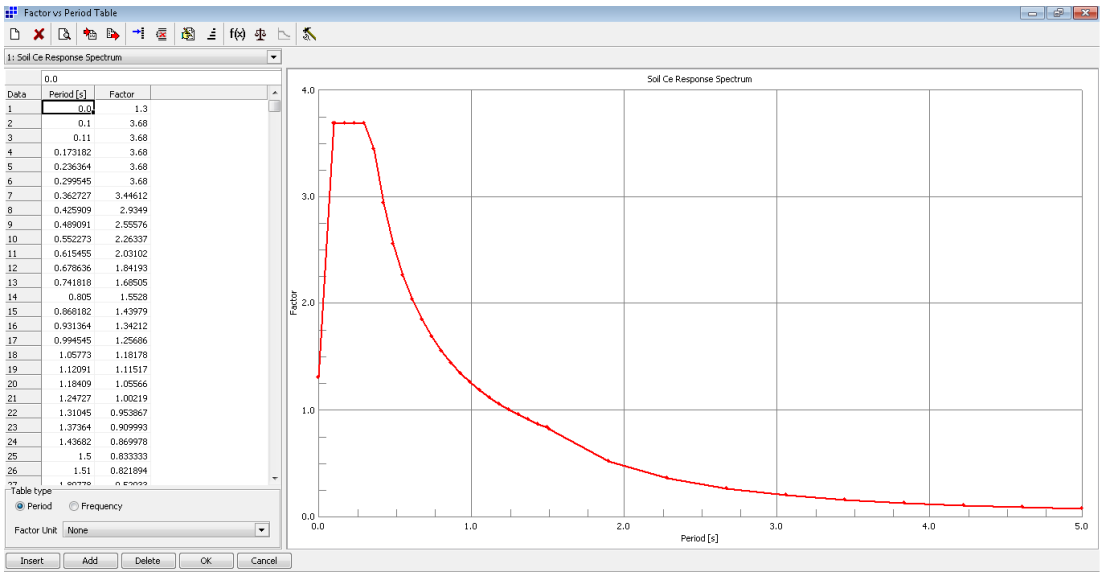

Figure 6.5 Response spectrum curve for soil subclass C_e

According to STRAND7 (2010) recommendations, after running a response spectrum analysis, it is necessary to confirm that the total mass participation factor is greater than 90% to ensure that the number of modes are sufficient. This too has been checked for all the building configurations of interest, by checking the 'spectral solver log file' for each case.

6.9 Directions of Earthquake application

According to Clause 5.4.2.1 of AS 1170.4(2007) the horizontal earthquake response is the sum of the responses to the excitation acting in two separate directions along the major axes of the structure, with 100% of the horizontal earthquake in one direction and 30% in the perpendicular direction.

According to STRAND7 Webnotes (2015) each result case in STRAND7 considers the full design load in a single direction that is applied along one major axis of the structure and then the total effect is combined using 'Results/Linear Load Case Combination' to determine the worst possible structural response.

To find out the worst possible loading, all the possible direction and factor combinations have to be considered. As such, for each design earthquake acting along the major axes, eight result case combinations were generated in STRAND7 model to obtain the worst structural response as detailed in Table 6.2.

Table 6.2 Seismic load combination cases with load factors for the two major directions

Combination Number	1	2	3	4	5	6	7	8
Direction 1	+1.0	+1.0	-1.0	-1.0	+0.3	-0.3	+0.3	-0.3
Direction 2	+0.3	-0.3	+0.3	-0.3	+1.0	+1.0	-1.0	-1.0

For the present analysis, the major earthquake axes are taken to be in the global Y direction (Direction 1) and global X direction (Direction 2) correspondingly (see Figure 6.6). The three dimensional FE model created by STRAND7 for the building configuration with fifth floor R/C slabs (excluding the slab panel connected to lift core) replaced by GFRP slab panels is shown in Figure 6.6. Note here that the Figure 6.6 corresponds to the reference model created with all five GFRP slab panels fully bonded.

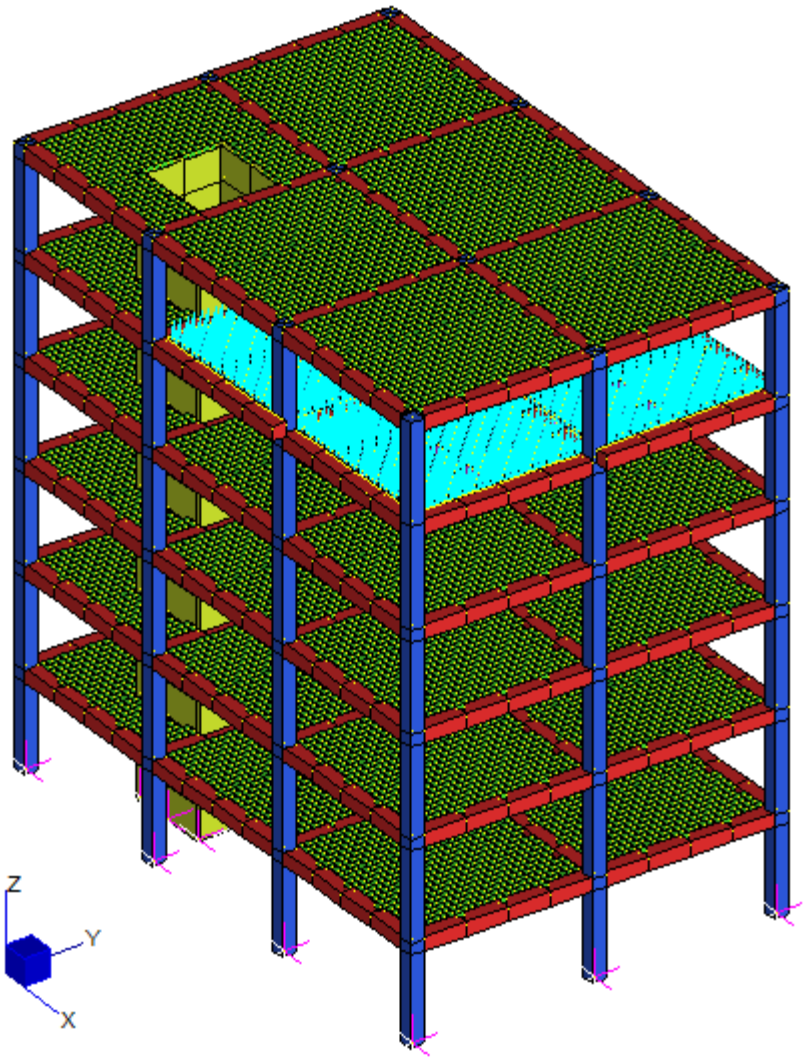

Figure 6.6 Typical three-dimensional FE model of the building

6.10 Superposition of modal results

In response spectrum analysis procedure, when the results for the single modes are calculated, they should be combined to get the estimated maximum forces and displacements during the earthquake excitation. There are two combination methods available in STRAND7, namely, SRSS (or Square Root of the Sum of the Squares) and CQC (Complete Quadratic Combination). According to Gupta (1992), it is well known that for structures with closely spaced modes, CQC results are much more accurate.

The method used for modal combination in the present analysis is CQC, due to the fact that the structural models of the building are three dimensional with the likelihood of closely spaced modes

6.11 Load combination for seismic analysis

As per Australian Standards, the following seismic and gravity load combination is used finally to analyse the seismic performance of the buildings under consideration.

G + 0.3Q + EQ

where;

G = Dead Load

Q = Live Load

EQ = Earthquake Load

This is the basic gravity plus seismic load combination to be considered. The two gravity (dead and live loads) loadings in combination with the eight seismic load combinations (as illustrated in Table 6.2) have been created using 'linear load case combinations' tab in STRAND7, with appropriate combination factors for each load case. Once the spectral response solver run is complete, all eight load combinations can be generated and examined to determine the worst structural response for each response parameter under consideration.

6.12 Results of structural analysis

One of the main objectives of the study was to make comparisons between the seismic response of building structures with GFRP panels with and without debonding. For the comparison of seismic response of the buildings with fully bonded and debonded GFRP slab panels, the building model with fully bonded GFRP slabs has been selected as the reference building, and comparisons are made with respect to its response.

For the reference building, 128 modes were needed to satisfy the code requirement for 3D analysis. 99.342% mass participation has been observed for the 128 modes included in the response spectrum analysis. Appendix A Table 1 stipulates the mass

participation factors for the 128 modes considered for the reference building model. Ux and Uy are the participation masses of each mode in the X and Y directions, respectively.

6.12.1 Influence of natural frequency and mode shapes due to debonding

The first two modes of vibration and modal shapes of the model with fully bonded GFRP slab panels (reference building) are illustrated in Figure 6.7.

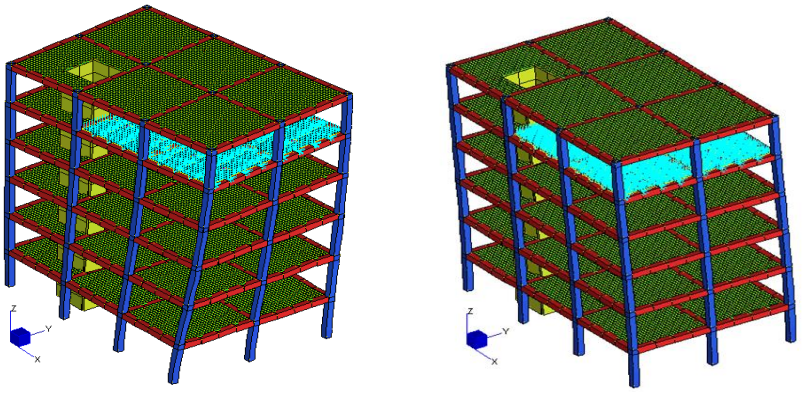

Mode 1 Mode 2

Figure 6.7 First two mode shapes for the reference building

Close examination of the mode of vibration in the model with fully bonded GFRP panels reveals that, the first mode involves translational mode of vibration in the weakest transversal direction, ie in Y direction. The mass participation factor indicated in Table 1: Appendix A for the fundamental mode (39.918 % participation) confirms that mode 1 is the dominant mode shape in Y direction (translational mode). The second mode of vibration is also a translational mode, and in the X direction, hence confirming that the building shows a greater stiffness in this direction compared to Y direction. Another interesting observation from natural frequency analysis results tabulated (see Table 1 Appendix A) is that the first 10 modes of frequency capture approximately 80% of the mass participation of the building under consideration.

Figures 6.8, 6.9, 6.10 and 6.11 show comparison of mode shapes for modes 1, 2, 3 and 4 respectively for the reference building and buildings with 50% debonding in locations 1,2 and 3. It is evident that for all the four configurations illustrated above,

first two modes are translational in Y and X directions, respectively, while the 3rd mode seems to be predominantly rotational and fourth mode is a mixed mode.

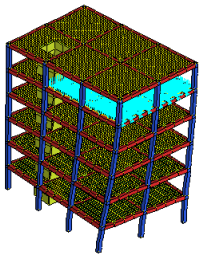

(a) Fully bonded

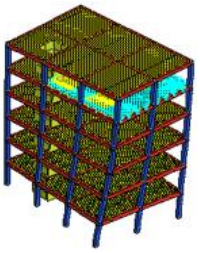

(b) Debonding position 1

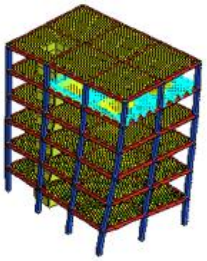

(c) Debonding position 2

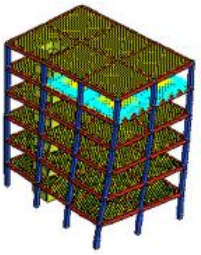

(d) Debonding position 3

Figure 6.8 Comparison of mode shapes for the first mode

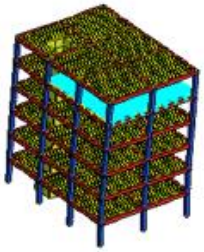

(a) Fully bonded

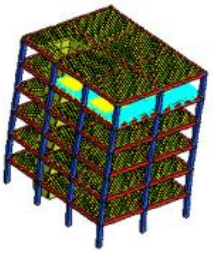

(b) Debonding position 1

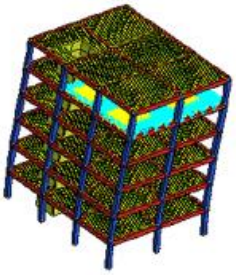

(c) Debonding position 2

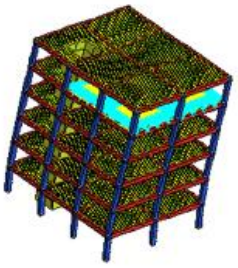

(d) Debonding position 3

Figure 6.9 Comparison of mode shapes for the second mode

(a) Fully bonded

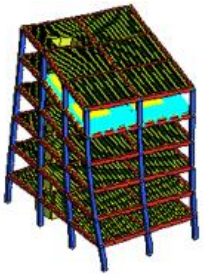

(b) Debonding position 1

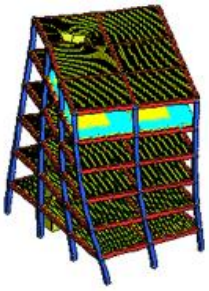

(c) Debonding position 2

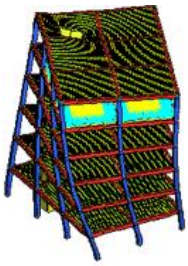

(d) Debonding position 3

Figure 6.10 Comparison of mode shapes for the third mode

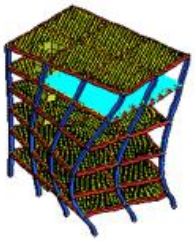

(a) Fully bonded

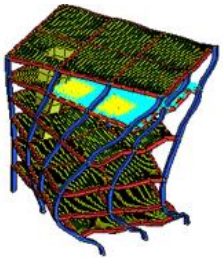

(b) Debonding position 1

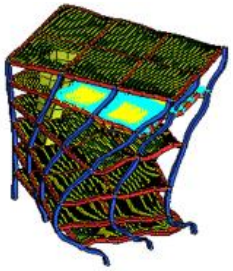

(c) Debonding position 2

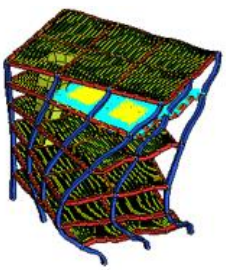

(d) Debonding position 3

Figure 6.11 Comparison of mode shapes for the fourth mode

Significant changes in mode shapes are not seen among buildings with fully bonded and debonded GFRP panels as exemplified. Reductions in corresponding natural frequencies are observed in buildings with debonded panels compared to the building with fully bonded panels. The natural frequency variations are insignificant for the first few modes and become more pronounced with the mode number. The reduction of the frequencies between buildings with fully bonded and debonded GFRP panels indicates the reduction of the global stiffness of the building due to debonding of GFRP panels.

Table 6.3 lists the first four natural frequencies for the reference building and the building configurations with 50% debonding. It is witnessed that the natural frequency reductions for the first few modes are negligibly small.

Table 6.3 Comparison of first four natural frequencies for the reference building against buildings with 50% debonding in positions 1, 2 and 3

Mode No.	Building with Fully bonded panels Natural frequency (Hz)	Building with 50% debonding (position 1) Natural frequency (Hz)	Building with 50% debonding (position 2) Natural frequency (Hz)	Building with 50% debonding (position 3) Natural frequency (Hz)
1	1.4604	1.4604	1.4604	1.4604
2	1.9519	1.9518	1.9518	1.9518
3	2.7735	2.7734	2.7734	2.7734
4	4.3790	4.3789	4.3789	4.3789

Table 6.4 shows the comparison of natural frequencies for modes 125,126,127 and 128 (which are the last four modes needed to satisfy the code requirement for the seismic analysis of the reference building) for the configurations exemplified above.

Table 6.4 Comparison of last four natural frequencies for the reference building against buildings with 50% debonding in positions 1, 2 and 3

Mode No.	Building with Fully bonded panels Natural frequency (Hz)	Building with 50% debonding (position 1) Natural frequency (Hz)	Building with 50% debonding (position 2) Natural frequency (Hz)	Building with 50% debonding (position 3) Natural frequency (Hz)
125	28.863	27.206	27.199	26.772
126	28.908	27.282	27.262	26.793
128	29.102	27.384	27.362	26.885
128	29.277	27.479	27.443	26.945

It is apparent from Table 6.3 that, out of the three debonding positions considered, natural frequency reduction is most effected by debonding position 3, while position 1 is least influenced. These reductions in natural frequencies are due to stiffness reduction happening as a result of debonding.

6.12.2 Influence of maximum top lateral displacement due to debonding

Table 6.5 lists the maximum lateral nodal displacements in X and Y directions for the building configuration with position 1 debonding for the four percentages of debonding considered.

Table 6.5 Maximum top lateral displacement comparison for debonding position 1

Percentage of debonding in each panel	Maximum top displacement In X direction (mm)	Maximum top displacement In Y direction (mm)
0% (fully bonded)	14.971	19.851
5%	14.971	19.851
10%	14.971	19.851
25%	14.971	19.852
50%	14.972	19.853

It is of special interest to observe here that displacement in Y direction is always considerably higher than the X direction, due to the fact that it is the weaker direction having less number of frames to resist lateral forces. It is evident from the

comparison that the increase in lateral displacement due to debonding of GFRP panels is insignificant, even when the percentage debonding is as high as 50%. Similar results were observed for the other two debonding positions as well, as presented in Tables 6.6 and 6.7. For small debonding percentages, absolutely no change in displacement values was seen as illustrated. Even when the percentage debonding is as high as 50%, the increase in displacement was insignificantly small. In light of these observations, it is revealed that the influence of debonding on lateral displacement of the buildings with GFRP panels considered in the present analysis is insignificant.

Table 6.6 Maximum top lateral displacement comparison for debonding position 2

Percentage of Debonding in each panel	Maximum top displacement In X direction (mm)	Maximum top displacement In Y direction (mm)
0% (fully bonded)	14.971	19.851
5%	14.971	19.851
10%	14.971	19.851
25%	14.971	19.852
50%	14.972	19.854

Table 6.7 Maximum top lateral displacement comparison for debonding position 3

Percentage of debonding in each panel	Maximum top displacement In X direction (mm)	Maximum top displacement In Y direction (mm)
0% (fully bonded)	14.971	19.851
5%	14.971	19.851
10%	14.971	19.851
25%	14.971	19.852
50%	14.972	19.853

6.12.3 Influence of maximum vertical displacement due to debonding

Figure 6.12 shows the percentage increase in vertical (downward) displacement for buildings with debonding (in positions 1, 2 and 3) compared with the reference building (with fully bonded slab panels).

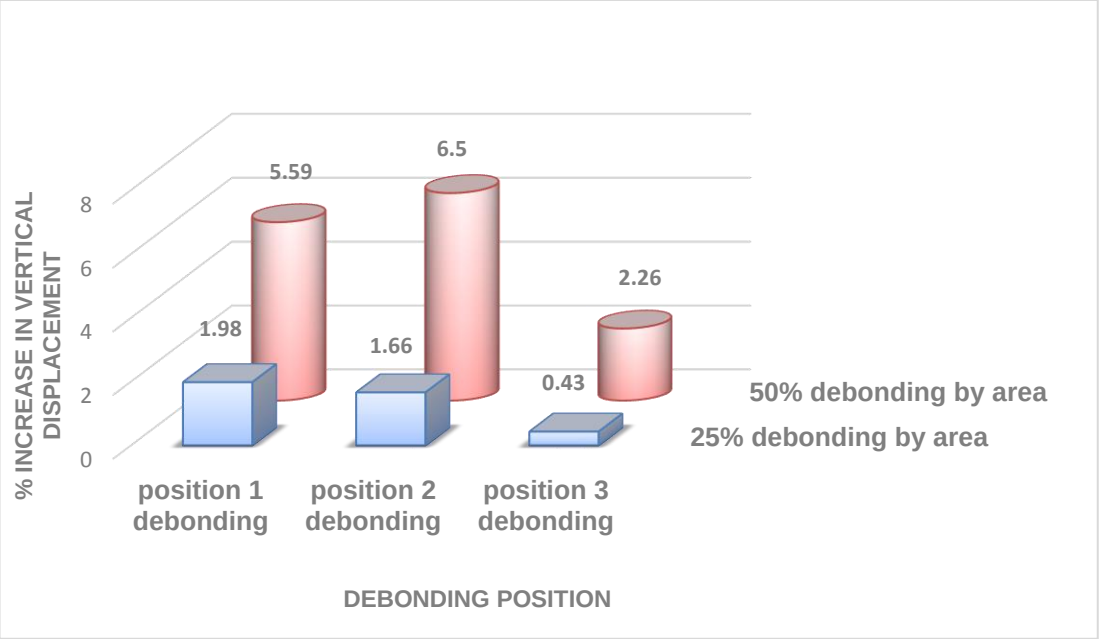

Figure 6.12 Percentage increase in vertical displacement for buildings with debonding in positions 1, 2 and 3 compared with the reference building

It is interesting to observe that debonding in GFRP slab panels causes increase in maximum vertical displacement. The percentage increase in vertical displacement seems to depend on the position of debonding of the slab panels in addition to the extent of debonding. Generally, increase in vertical displacement seems to be least sensitive to position 3 debonding whereas position 2 debonding shows highest sensitivity. Hence it is revealed that large debonding areas cause sensible increases in maximum vertical displacements under seismic loadings, for the building configurations considered.

6.12.4 Comparison of interstorey drift

This interstorey drift or the relative lateral displacement between two adjacent floors is one of the key parameters for the assessment of structural response under seismic loading. In STRAND7, this can be examined on a floor-to-floor basis using 'Relative to node' contour display mode. Figures 6.12, 6.13, 6.14 and 6.15 illustrate the comparison of fifth floor maximum interstorey drift relative to fourth floor for the

most critical cases (for the three locations with the highest percentage of debonding considered), compared to fully bonded case. Figure 6.12 depicts the fully bonded case while Figures 6.13, 6.14 and 6.15 represent the building configurations with 50% debonding in locations 1, 2 and 3 respectively. Comparison of these figures reveal that the building with fully bonded GFRP panels gives the same maximum interstorey drift compared to the configurations with 50% debonding. Thus it is revealed that debonding seems to have no significant effect on the maximum interstorey drift of the building configurations analysed.

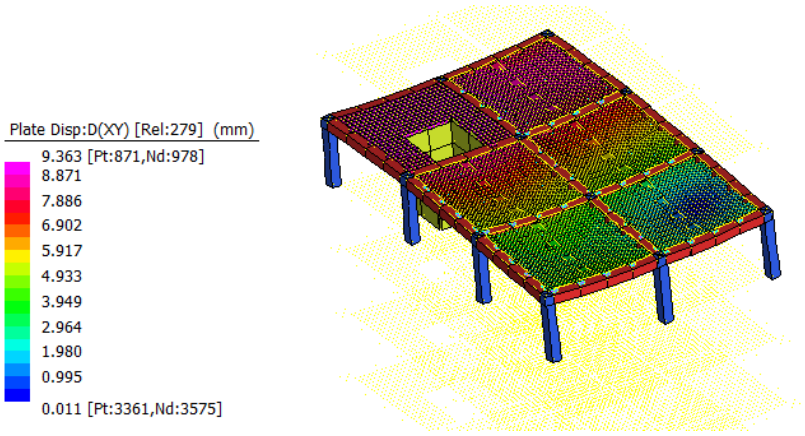

Figure 6.13 Maximum interstorey drift for the fifth floor for reference building

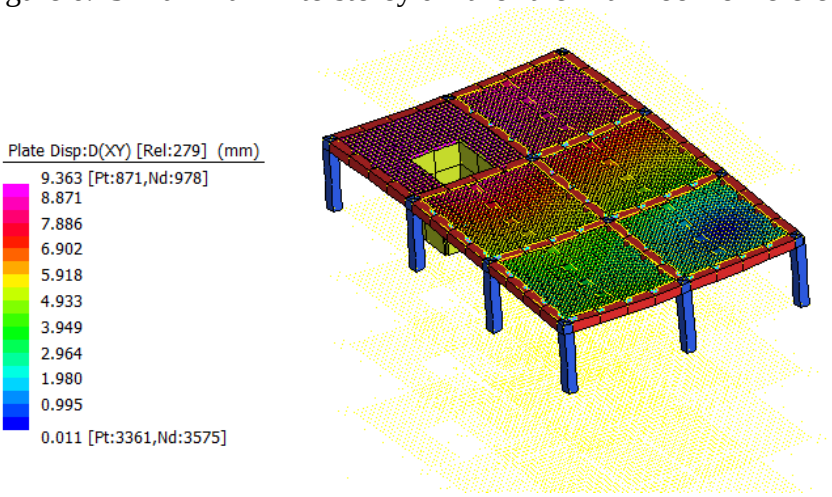

Figure 6.14 Maximum interstorey drift for the fifth floor (50% debonding: position 1)

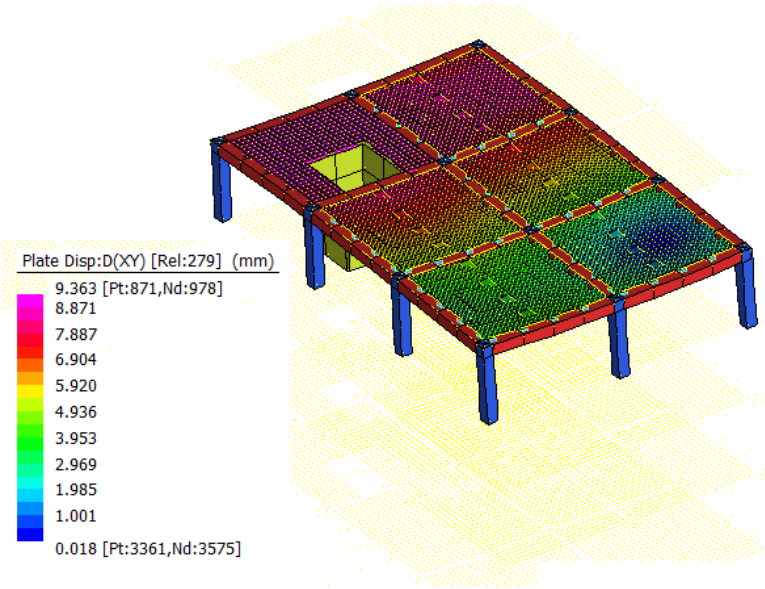

Figure 6.15 Maximum interstorey drift for the fifth floor (50% debonding: position 2)

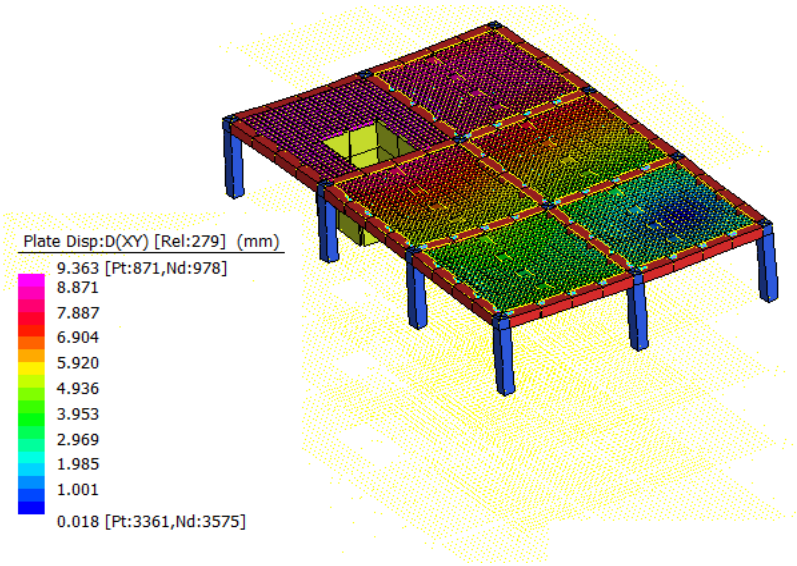

Figure 6.16 Maximum interstorey drift for the fifth floor (50% debonding: position 3)

Figures 6.17 to 6.20 represent the same comparisons for the 6th floor interstorey drift (relative to 5th floor) for the same building configurations as above.

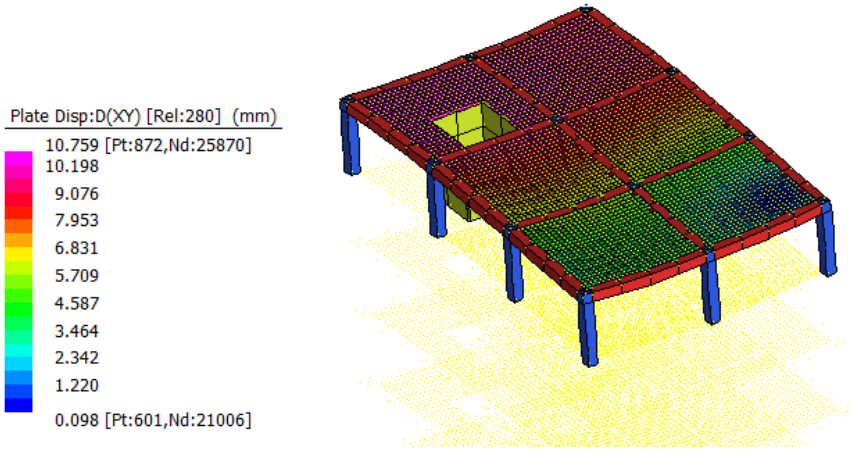

Figure 6.17 Maximum interstorey drift for the top floor for the reference building

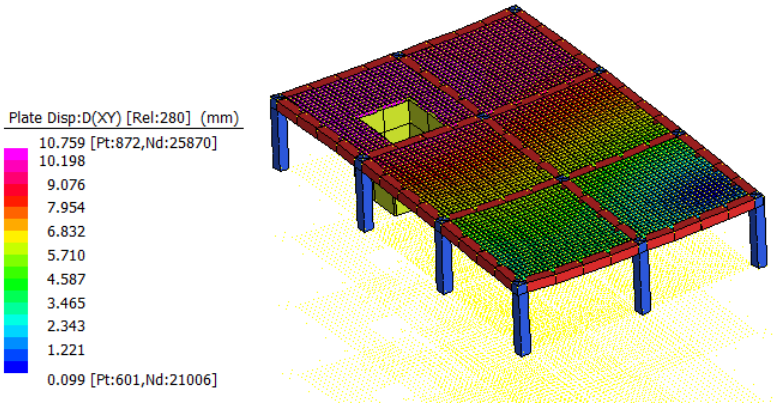

Figure 6.18 Maximum interstorey drift for the top floor (50% debonding position 1)

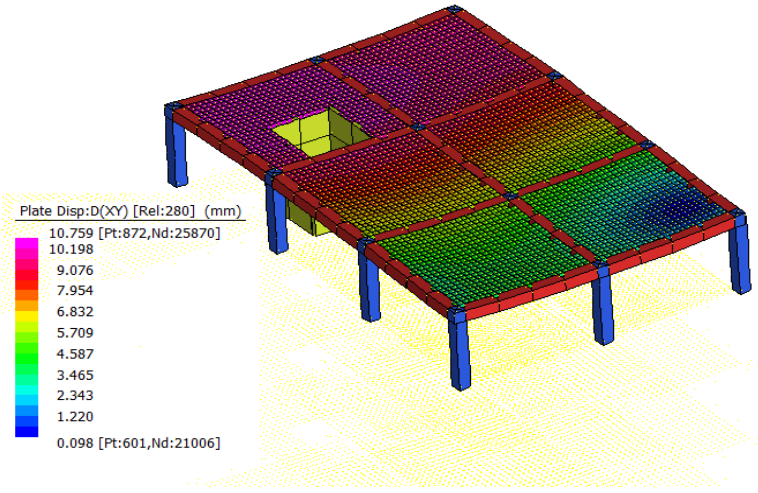

Figure 6.19 Maximum interstorey drift for the top floor (50% debonding position 2)

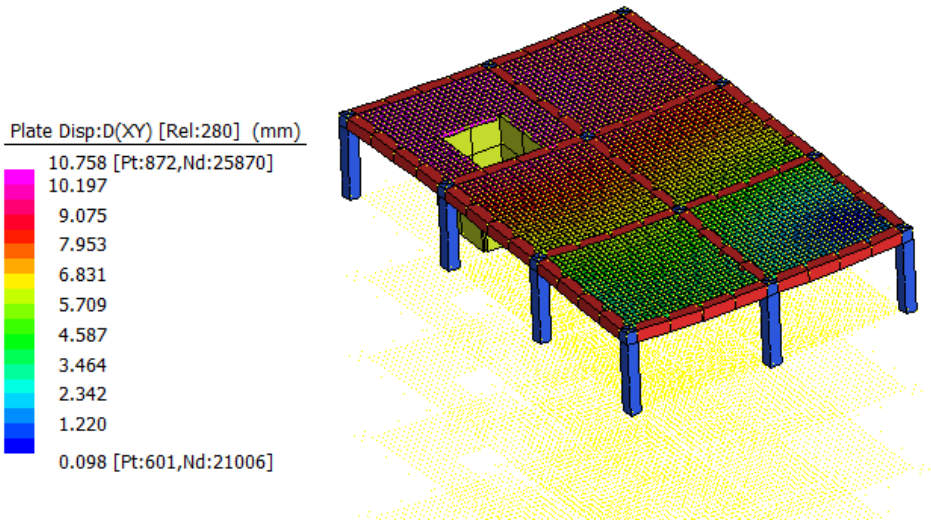

Figure 6.20 Maximum interstorey drift for the top floor (50% debonding position 3)

Table 6.8 lists the maximum interstorey drift values in mm for all six storeys for fully bonded and 50% debonded building configurations.

It is interesting to observe here as well, that fully bonded and debonded configurations have similar interstorey drift values, confirming that interstorey drift is not effected by even 50% debonding of the GFRP slab panels for the building configurations considered. The interstorey drifts for the debonded models are more or less the same for all three locations of debonding, implying that debonding location does not influence interstorey drift.

Table 6.8 Maximum interstorey drift values in mm for fully bonded and 50% debonded building configurations for the three positions of debonding

Floor	Fully bonded	Position 1	Position 2	Position 3
1	3.722	3.722	3.722	3.722
2	5.147	5.147	5.147	5.147
3	4.901	4.901	4.901	4.901
4	7.341	7.341	7.341	7.341
5	9.363	9.363	9.363	9.363
6	10.759	10.758	10.759	10.759

It should be noted that, careful examination of response figures for all the buildings under consideration reveals that the largest inter-storey drift is 10.759 mm, which occurs between 5^{th} and 6^{th} floors of fully bonded and debonded configurations. AS 1170.4 (2007) clause 5.4.4 states that the drift of each storey should not exceed 1.5% of the storey height. For the buildings used for the present study, the relevant value for the maximum interstorey drift is 52.5 mm (1.5×3500/100). Hence it is clear that all the buildings under consideration lie within the acceptable range for seismic analysis considered in the present study.

6.13 Chapter conclusions

- A reduction in natural frequencies occurs when GFRP panels are debonded, when compared to the reference building where the panels are fully bonded.
- The fall of natural frequencies with the increasing debonding damage is a direct result of the loss of stiffness of the buildings due to debonding.
- A sensible increase in downward deflection in upper floors is observed in building configurations with substantial debonding.
- Furthermore, it is observed that the top lateral displacements are not noticeably influenced by debonding for the building configurations considered for the present analysis.
- Generally, lighter buildings having less mass and hence less inertia suffer less damage under seismic loading. Hence the replacement of heavyweight R/C slabs with lightweight GFRP slab panels would be a viable option to improve seismic response of buildings. An existence of substantial percentage of debonding causes a sensible increase in the downward displacement due to debonding.
- Overall the work presented herein provides an insight regarding the effects of debonding on the seismic performance of RC buildings upgraded with GFRP slab panels.

CHAPTER 7 CONCLUSIONS AND RECOMMENDATIONS

7.1 Conclusions

This research appraised the relative dynamic performance of novel GFRP beams and slabs with and without debonding and delamination damage. Furthermore, it evaluated the comparative seismic performance of buildings upgraded with GFRP slab panels as well, with and without debonding. Free vibration analyses and dynamic response spectrum analyses were respectively carried out using STRAND7 finite element program by developing complete 3D models to investigate the realistic behaviour. The concluding remarks made here are limited to the findings based on the scope of the analysis covered in this research. Based on the results of the analyses, the following major conclusions were arrived at.

7.1.1 Common conclusions regarding dynamic behaviour of debonded beams and slabs

- Generally, debonding causes reduction in natural frequency when compared with fully bonded composites.

- In general, natural frequency decreases more rapidly as the mode number increases giving the least variation for the first natural frequency.

- Although there is a general tendency that the extent of natural frequency variation with respect to debonding increases with the mode number, this does not always exhibit an increasing trend as the mode number increases, but follows different trends depending on the boundary condition, extent of debonding and location of the debond.

- It is generally observed that higher natural frequencies and corresponding mode shapes are more influenced by the presence of debonding. Yet there are inconsistencies in this trend depending on how severely the local modes are affected by debonding. It is witnessed that the associated mode shapes explain the causes of these inconsistencies.

- Abrupt changes of the vibration modes (when comparing the vibration modes of the debonded beam or slab with the fully bonded one) lead to rapid drops in corresponding natural frequencies.

- Generally it is observed that the reduction in natural frequency is more affected by a large single debonding than small multiple debonding regions (of equivalent total area) located symmetrical to the single debonding position.

- For similar extents and locations of debonding, the effect of debonding on natural frequencies seems significantly dependent on the end conditions of the beam or slab, giving higher reduction in natural frequency when the structural element is more restrained. Hence it is revealed that the stronger the supports are restrained, the bigger the influence on free vibration characteristics. Therefore the presence of local debonding damage within the sandwich beams or slabs can be detected more easily by imposing fully restrained (clamped) boundary conditions.

- Finally it is evident that the finite element model developed and the analysis procedure described in this report can be useful for investigating features of debonding damage identification.

7.1.2 Conclusions with regard to dynamic behaviour of debonded beams

- The decrease in natural frequency with the increase in the extent of debonding is more sensitive to the width of debonding across the beam than the length along the beam for the novel composite beam considered in the analysis. It is established that full width debonding attributes to extremely severe reduction in natural frequency compared to half width debonding for all three support conditions considered for the GFRP beams.

- Full width debonding also attributes to significant changes in modes of vibration (for example, changing the modes of vibration from translational to rotational) and corresponding mode shapes.

- The end conditions of the beam are a governing factor dictating which modes are more affected.

- It is revealed that if the working frequency of the beam is kept away from the range 50% to 100% of the fully bonded beam, there is no possibility of resonance happening due to debonding considered for the novel composite test beam analysed.

- A debonding located near the end of the beam significantly worsens the free vibration characteristics compared to a debonding located near the centre of the beam. This becomes more pronounced when the beam is more restrained, thus indicating that the effects of local debonding on dynamic response become lesser as the debonding damage zone is moved away from the clamped edge/edges of the beam.

- The effect of multiple debonding on the free vibration behaviour of a debonded beam is highly dependent of the boundary conditions, giving greater reductions in natural frequencies when the beam is more restrained. Moreover there is a general trend that the extent of reduction increases with the mode number.

- The natural frequency reduction due to debonding is higher for the free model compared to the constrained model (contact model) for similar conditions of debonding. This discrepancy becomes more pronounced for full width debonding compared to half width debonding, and increases with the extent of debonding damage. This is the case for both test beam and full scale beam scenarios. Thus it is witnessed that the free model gives unrealistic results due to physically unreal overlapping and the inaccuracies increase with the increase of debonding damage.

7.1.3 Conclusions regarding the influence of debonding and multilayer delamination on dynamic behaviour of slabs

- Generally it was evident from all the analyses that debonding and interlayer delamination cause reduction in magnitudes of natural frequency of the GFRP slabs. Moreover, some vibration modes and accordingly the mode shapes are also noticeably changed.

- Furthermore, the results show that the presence of relatively small debonding or delamination has an insignificant effect on the natural frequencies and associated mode shapes of the GFRP plates considered in the present analysis. Interestingly, the free vibration characteristics are negligible for small debonds and delaminations, in the order of 1% of the plate area, for the plates considered in the analysis.

- The findings of the dynamic analyses with plates suggest that the debonding or delamination size and the end fixity of the plate are the most contributing factors in stiffness reduction due to debonding and delamination damage in composite laminates.

- The results also suggest that fastening the delamination region is an effective corrective measure in decreasing the natural frequency variation, hence improving its dynamic performance compared to the delaminated panel.

- It is discovered that the more the supports are restrained, the more the influence on free vibration behaviour due to debonding and interlayer delamination, specifically in terms of natural frequency reduction and influence on modes of vibration.

- It also follows from the results of the analyses that percentage increase in the debonding size results in the appearance of local modes even for the lower mode numbers. Hence, by the observation of such sudden variations in the modes, the severity of debonding may be appraised. This demonstrates the

feasibility of non-destructive methods to detect debonding and delamination damage in practical composite slabs.

7.1.4 Conclusions on the influence on dynamic seismic loading

- A reduction in natural frequencies occurs when GFRP slab panels are debonded, when compared to the reference building where the panels are fully bonded.

- The fall of natural frequencies with the increasing debonding damage is a direct result of the loss of stiffness of the buildings due to debonding.

- An increase in maximum vertical displacement in upper floors is observed in building configurations with substantial debonding. The loss of stiffness due to extensive debonding in GFRP slab panels causes an increase in downward displacement on the upper floors. Moreover it was observed that these variations are generally in the order of 6% (compared with reference building) for 50% debonding by area of the slab panels.

- Furthermore, it is observed that debonding for the building configurations considered for the present analysis does not noticeably influence the top lateral displacements.

- Most importantly, the results show that the presence of relatively small debonding in GFRP slab panels has no noticeable effect on the natural frequencies, associated mode shapes and interstorey drifts for the building configurations considered in the present analysis.

- Generally, lighter buildings having less mass and hence less inertia suffer less damage under seismic loading. Critical examination of the preliminary analyses points out that the flexibility and lightweight nature of GFRP slab panels favourably affect the seismic response of the buildings under consideration. Hence the replacement of heavyweight R/C slabs with lightweight GFRP slab panels would be a viable option to improve seismic response of buildings. An existence of substantial percentage of debonding causes a slight increase in the vertical displacements.

- Overall the work presented herein provides an insight regarding the effects of debonding on the seismic performance of R/C buildings upgraded with GFRP slab panels. Although the analysis has been conducted for a specific R/C building, the observations provide valuable insight relevant to similar structures.

7.1.5 Summary

The outcome of this research will make an important and fundamental contribution to the development of a deeper understanding of the dynamic behaviour of the novel GFRP beams and slabs subjected to debonding and delamination damage. The numerical results presented in this study will shed light on the vibration characteristics of single and laminated composite structures with damage, and they would be helpful in the development of vibration-based damage identification techniques for composite beams and slabs. Finally, the R/C buildings with GFRP slab panels subjected to seismic loadings presented in this report will pave the way for a feasible way of flooring to be considered as an engineered construction and a sustainable alternative to reinforced concrete flooring of mid-rise buildings.

7.2 Future work

Based on the findings of this research, the following listed areas are recommended for further study.

- In this study the debonding and delamination damage is assumed to be pre-existing before the vibrations start and to be constant during the free vibration period. The study can be extended to investigate the propagation of debonding through the free vibration duration to more realistically assess the dynamic performance. This investigation process is more complex and would need a more powerful FE software for the analyses.

- The current study considered rectangular and square shaped debonded for the dynamic analyses. This can be further extended to examine the dynamic

behaviour due to other shapes of debonds such as circular and triangular shapes.

- The present study examined the influence of seismic loading on debonding of GFRP slab panels. Another important aspect that can be considered for further study is impact loading. It will be of practical significance to study the effects of impact loading on the dynamic behaviour of debonded GFRP slab panels.

- For simplicity, the torsional effects attributed to seismic loading have been neglected in the current study, since comparative seismic response with and without debonded only is assessed. It is recommended to extend this study to focus on torsion effects on the dynamic behaviour of composite structures with and without debonds.

- Although the present study examined the dynamic behaviour of beams and slabs with debonds, it is worthwhile to extend the research to examine the dynamic behaviour of GFRP walls with debonds.

- The dynamic seismic analysis method adopted in this study is response spectrum analysis method. RSA is a linear dynamic statistical analysis method. To achieve greater accuracy of the seismic behaviour, dynamic non-linear time history analysis method can be adopted with a finite element software package capable of modelling the non-linear behaviour accurately.

- The seismic analysis in the current study has been carried out in accordance with AS1170.4 (2007). It would be of practical importance to perform similar analyses to other international design codes such as the International Building Code (IBC 2015) the Uniform Building Code (UBC 1997)

REFERENCES

Abeysinghe, C.M., Thambiratnam, D.P., & Perera ,N.J. (2013). Dynamic performance characteristics of an innovative Hybrid Composite Floor Plate System under human-induced loads. *Composite Structures*, 96, 590–600.

Abrate, S.(1997). Localized impact on sandwich structures with laminated facings. *Applied Mechanics Review*, 50**,** 62–82.

Agarwal, B.D., Broutman, L.J., & Chandrashekhara, K. (2006). *Analysis and Performance of Fibre Composites*, 3rd Edn, Wiley and sons, Inc.,Hoboken, New Jersey.

Alden A, Basic Map of Earth's Tectonic Plates, viewed 06 October (2013). http://geology.about.com/od/platetectonicmaps/ss/Basic-Map-Tectonic-Plates.htm.

Alhaddad M.S., Siddiqui, N.A., Abadel, A.A., Alsayed, S.H., & Al-Salloum, Y.A. (2012). Numerical Investigations on the Seismic Behavior of FRPand TRM Upgraded RC Exterior Beam-Column Joints. *Journal of Composites for Construction*, 16, 308-321.

Aravinthan, T. (2012). Research and Development of Fibre Composites in Civil Infrastructure - The Australian Experience. *KEY 06,Third Asia-Pacific Conference on FRP in Structures (APFIS2012)*, 2-4 February 2012, Hokkaido University Conference Hall, Sapporo, Japan.

Aravinthan, T., & Manalo, F. (2012). Field applications and case studies of FRP in civil infrastructure: the Australian experience:Proceedings of 6th Inter. Conf. on FRP Composites in Civil Engineering (CICE 2012), Rome, Section 11: Field Applications and Case Studies, Paper 210.

Aravinthan, T. (Ed.). (2008). *Fibre Composites in Civil Infrastructure Past, Present and Future.* Toowoomba, Queensland, Australia.

Arnold, C., Reitherman, R. (1982). *Building Configuration and Seismic Design*, Wiley,New York.

Awad, Z.K., Aravinthan, T., & Zhuge, Y. (2012a). Experimental and numerical analysis of an innovative GFRP sandwich floor panel under point load. *Engineering Structures*, 41, 126–135.

Awad, Z.K., Aravinthan, T., & Manalo, M. (2012b). Geometry effect on the behaviour of single and glue-laminated glass fibre reinforced polymer composite sandwich beams loaded in four-point bending. *Materials and Design*, 39, 93–103.

Awad, Z.K., Aravinthan, T., & Zhuge, Y. (2012c). Investigation of the free vibration behaviour of an innovative GFRP sandwich floor panel. *Construction and Building* Materials, 37, 209–219.

Bank, L.C. (2006). *Composites for construction*. John Wiley and sons, Inc., Hoboken, New Jersey.

Biggs, J.M. (1964). *Introduction to structural dynamics*, New York, McGraw-Hill.

Borst, R.D., Joris, Remmers, J. C. (2006). Computational modelling of delamination. *Composites Science and Technology*, 66, 713–722.

Buenett, J.(2006). *Forestry Commission Scotland - Greenhouse Gas Emissions Comparison - Carbon Benefits of Timber in Construction*, (Report No. ECCM-EM-196-2006), Edinburgh,
ECCM Ltd.

Bunsell, A.R., & Renard, J. (2005). *Fundamentals of fibre reinforced composite materials*, IOP Publishing Ltd, Bristol, UK.

Burlayenko, V.N., & Sadowski, T. (2010). Influence of skin/core debonding on free vibration behavior of foam and honeycomb cored sandwich plates. *International Journal of Non-Linear Mechanics*, 45(10), 959-968.

Burlayenko, V. N., & Sadowski, T. (2011). Dynamic behaviour of sandwich plates containing single/multiple debonding. *Computational Materials Science*, 50 (4), 1263-1268.

Burlayenko, V. N., & Sadowski, T. (2012). Finite element nonlinear dynamic analysis of sandwich plates with partially detached facesheet and core. *Finite Elements in Analysis and Design*, 62, 49-64.

Burlayenko, V.N., and Sadowski, T. (2014). Nonlinear dynamic analysis of harmonically excited debonded Sandwich plates using finite element modelling. *Composite Structures*, 108, 354–366

Chakrabarti, A., Sheikh, A.H. (2009). Vibration and Buckling of Sandwich Laminates having Interfacial Imperfections. *Journal of sandwich structure and materials*, 11, 313–328.

Chattopadhyay, A., Gu, H. (1994). A new higher order plate theory in modelling delamination buckling of composite laminates', *AIAA Journal*, 32. (8), 1709-1718.

Chattopadhyay, A., Radu, A.G., & Dragomir-Daescu, D. (2000). A higher order plate theory for dynamic stability analysis of delaminated composite plates. *Computational Mechanics*, 26, 302-308.

Chopra, A.K. (1995). *Dynamics of structures: Theory and applications to earthquake engineering.* Prentice-Hall, Englewood Cliffa, Nj.

Cripps, A. (2002). *Fibre-Reinforced Polymer Composites in Construction*. CIRIA, London.

Della, C.N., & Shu, D. (2005). Vibration of beams with double delaminations. *Journal of Sound and Vibration*, 282, 919-935.

Della, C.N., & Shu, D. (2007). 'Free vibration analysis of delaminated bimaterial beams', *Composite Structures*, 80, 212-220.

Dowrick D. J. (1977). *Earthquake Resistant Design*. John Wiley & Sons, Ltd.

Duggan, M., & Ochoa, O. (1992). Natural frequency behaviour of damaged composite materials. *Sound and Vibration*,158, 545-551.

Freeman, S.A. (2007). Response spectra as a useful design and analysis tool for practicing structural engineers, *ISET Journal of Earthquake Technology*, 44(1), 25–37.

Gallego, A., Moreno-Garcıa, P., & Casanova, C.F. (2013). Modal analysis of delaminated composite plates using the finite element method and damage detection via combined Ritz/2D-wavelet analysis. *Journal of Sound and Vibration*, 332, 2971–2983.

Gand, A.K., Chan, T.M., & Mottram,T. (2013). Civil and structural engineering applications, recent trends, research and developments on pultruded fiber reinforced polymer closed sections: a review Front. *Struct. Civ. Eng*., 7(3): 227–244.

Gibson, R.F. (2012). *Principals of composite materials mechanics*. CRC Press. NW.

Grouve,W.J.B., Warnet L, De Boer, A., Akkerman, R., & Vlekken J. (2008). Delamination detection with fibre bragg gratings based on dynamic behaviour. *Composite Science and Technology*, 68, 2418-2424.

Hall, J.F. (1995). *Parameter study of the response of moment resisting steel frame buildings to near surface ground motions.* SAC Report 95-08.

Hu, J.S., & Hwu, C. (1995). Free vibration of delaminated composite sandwich beams. *AIAA Journal*, 33(10), 1911-1918.

Hu, H., Belouettar, S., Potier-Ferry, M., & Daya, E.M. (2008). Review and assessment of various theories for modelling sandwich composites. *Composite Structures*, 84, 282-292.

Idriss, M., Mahi, A., Assarar, M., & Guerjouma, R. (2013). Damping analysis in cyclic fatigue loading of sandwich beams with debonding. *Composites: Part B*, 44, 597–603.

Islam, M.M., & Aravinthan, T. (2010). Behaviour of structural fibre composite sandwich panels under point load and uniformly distributed load. *Composite Structures*, 93, 206–15.

Jain, R., & Lee L. (2012), *Fiber reinforced polymer (FRP) composites for infrastructure applications.*

USA.

Ju F, Lee H.P., & Lee, K.H. (1995). Free vibration of composite plates with delamination around cutouts. Composite Structures, 31, 177–183.

Karbhari, V.M. (2004). Fiber reinforced composite bridge systems—transition from the laboratory to the field', Composite Structures, 66, 5–16.

Kappos, A.J. (2002). *Dynamic loading and design of structures* Spon press, London.

Karunasena, W., Aravinthan, T., & Manalo, A.C. (2009). Vibration of debonded laminated fibre composite sandwich *beams Proceedings of the APFIS 2009: Acia-Pacific Conference on FRP in Structures*, 9-12 December 2009, Seoul, Korea.

Karunasena, W. (2010). The effect of debonding on the natural frequencies of laminated fibre composite sandwich plates. *Proceedings of 6th Australasian Congress on Applied Mechanics, ACAM 6* , 12-15 December 2010, Perth, Australia.

Kim, H.S., Chattopadhyay, A., & Ghoshal, A. (2003a). Dynamic analysis of composite laminates with multiple delamination using improved layerwise theory. *AIAA Journal*, 41, (9), 1771-1778.

Kim, H.S., Chattopadhyay,A., & Ghoshal, A. (2003b). Characterisation of delamination effect on composite laminates using a new generalised layerwise approach. *Computers and Structures*, 81, 1555-1566.

Krueger,R., & Shell, A. (1999). 3D modeling technique for delaminations in composite laminates. Proceedings of American Society of Composites, 843–852.

Kulkarani, S.V. & Fredericks., D. (1971). Frequency as a parameter in delamination problem-A preliminary investigation. *Journal of composite materials*, .5, 112-119.

Kwon, Y.W., & Lannamann, D.L. (2002). Dynamic Numerical Modelng and simulation of Interfacial Cracks in Sandwich Structures for damage detection. *Journal of Sandwich Structures and Materials*, 4(2), 175–199.

Lee, J. (2000). Free vibration analysis of delaminated composite beams. *Computers and Structures*, 74,121-129.

Logan, D.L. (2012). *A first course in the finite element method*, 5th edn, Cengage Learning, Stamford, USA.

Manalo, A.C., Aravinthan, T., Karunasena, W., & Ticoalu, A. (2010a). A review of alternative materials for replacing existing timber sleepers. *Composite Structures*, 92 603–611.

Manalo, A.C., Aravinthan, T., Karunasena, W., & Islam, .M.M. (2010b). Flexural behaviour of structural fibre composite sandwich beams in flatwise and edgewise positions. *Composite Structures*, 92 (4), 984-995.

Manalo, A.C., Aravinthan, T., Karunasena,W. (2010c). Flexural behaviour of glue-laminated fibre composite sandwich beams Composite Structures, 92, 2703–2711.

Manalo, A.C. (2011). *Behaviour of fibre composite sandwich structures: a case study on railway sleeper application.* [Thesis (PhD/Research)].

Manalo, A. C., & Mutsuyoshi, H. (2012). *Behavior of fiber-reinforced composite beams with mechanical joints.* Journal of Composite Materials, 46 (4), 483-496.

Manalo,A.C., & Aravinthan, T., and Karunasena, W. (2013). *Mechanical properties characterization of the skin and core of a novel composite sandwich structure.* Journal of Composite Materials, 47 (14), 1785-1800.

McCue, K., Dent, V., & Jones, T. (1995). The Characteristics of Australian Strong Motion. Proceedings of the Fifth Pacific Conference on Earthquake Engineering, 71-80.

Mara ,V., Haghani, R., & Peter, H.(2014). Bridge decks of fibre reinforced polymer (FRP): A sustainable solution, *Construction and Building Materials*, 50, 190–199.

Margetan, F. (2011). Institute of physical research & technology, IOWA State University, viewed on 13 June 2013, http://www.cnde.iastate.edu/ultrasonics-and-composites/modeling-cracks-and-delaminations-carbon-fiber-composites-frank-margetan.

Meftah, S.A., Daya, E.M., & Tounsi., A. (2012). Finite element modelling of sandwich box column with viscoelastic layer for passive vibrations control under seismic loading, *Thin-Walled Structures,* 51, 174–185.

Mendelsohn, D.A., 2006, 'Free vibration of an edge-cracked beam with a Dugdale–Barenblatt cohesive zone', *Journal of Sound Vibration*, 292, 59–81.

Mittal R.K. & Prashanth P. (2012). Response Spectrum Modal Analysis of Buildings using Spreadsheets. *International Journal of Modern Engineering Research (IJMER)*, 2, (6), 4207-4210.

Mousa, M.A., & Uddin, N. (2012). Structural behaviour and modelling of full-scale composite structural insulated wall panels. *Engineering Structures*, 41, 320-334.

Mujumdar, P.M., & Sunyanarayan, S. (1988). Flexural vibration of beams with delaminations. *Journal of Sound and Vibration*, 25(3), 447–461.

Penelis, G., & Kappos, J. (1997). *Earthquake resistant concrete structures*. E & FN Spon, London.

Pisano, A.A., & Fuschi, P., 2011, " Mechanically fastened joints in composite laminates: Evaluation of load bearing capacity" Composites PartB: Engineering, 42, 949–961.

Qiao, P., Lestari, W., Shah, M.G., & Wang,J., 2007, 'Dynamics-based Damage Detection of Composite Laminated Beams using Contact and Noncontact Measurement Systems', *Journal of Composite Materials*, 41(10), 1217–1252.

Reddy, .J.N., & Miravete, .,A 1995, *Practical analysis of composite laminates*, CRC press.

Reddy,J. N. (2003). *Mechanics of laminated composite plates and shells: theory and analysis*. CRC Press.

Reid, S.R., & Zhou, G. (2000). *Impact behaviour of fibre-reinforced composite materials and structures*. Woodhead Publishing Ltd, USA.

Reinhart, T.J. (1998). Overview of Composite Materials. *In*: S. T. PETERS, ed. *Handbook of Composites*. London: Chapman and Hall.

Roeder, C.W. (1998). Development of hybrid and composite systems for seismic design in the United States, *Engineering Structures*, 20(4), 355-63.

Ronagh, H.R., & Eslami, A. (2013). Flexural retrofitting of RC buildings using GFRP/CFRP- A comparative study. *Composites; Part B*, 46,188-196.

Schwarts-Givil, H, Rabinovich, O., & Frostig, Y. (2007). Free vibrations of delaminated unidirectional sandwich panels with a transversely flexible core-a modified Galerkin approach. *Journal of Sound and Vibration*, 301, 253-277.

Scawthorn,C .,& Chen, W.F. (2002). *Earthquake engineering handbook*. CRC press.

Schwarts, G.H., Rabinovich, O., & Frostig,Y. (2008). Free vibration of delaminated unidirectional sandwich panels with a transversely flexible core and general boundary conditions - A high-order approach', *Journal of Sandwich Structures & Materials*,10, 99-131.

Shanmugam, V., Penmetsa, R., Tuegel, E., & Clay, S. (2013). Stochastic modeling of delamination growth in unidirectional composite DCB specimens using cohesive zone models. *Composite Structures*, 102, 38–60.

Shu, D., & Fan, H. (1996). Free vibration of a bimaterial split beam. *Composites: Part B*. 27(1), 79-84.

Sinadinovski, C., McCue, K.F., and Somerville, M. (2000). Characteristics of strong ground motion for typical Australian intra-plate earthquakes and their relationship with the recommended response spectra. *Soil Dynamics and Earthquake Engineering*, 20,101-110.

Smith, S.S., & Coull, A. (1991). *Tall building structures*: *Analysis and design*. New York: John Wiley & sons.

Stewart, R. (2011). Composites in construction advance in new directions. *Reinforced plastics*, 55 (5), 49-54.

STRAND7. (2010). *Strand7 finite element analysis FEA software*. Release 2.4.1, Sydney, Australia (website: www.strand7.com).

STRAND7. Software. (2005). *Theoretical Manual: Theoretical background to the Strand7 finite element analysis system*. Strand7 Pty Ltd Sydney NSW Australia.

STRAND7. Web notes-Applications/Structural (2015). ST7-1.40.35.22 AS1170.4-2007 Earthquake Analysis in Strand7. Strand7Pty Ltd, www.strand7.com

Tan, S.C. (1992). *Analysis of bolted and bonded composite joints*. Wright Materials Research 3591 Apple Grove Dr. Beavercreek, OH 4543.

Tenek, L.H., Henneke, E.G., & Gunzburger, M.D. (1993). Vibration of Delaminated Composite plates and Some Applications to Nondestructive Testing. *Composite Structures*, 23(3), 253-262.

Thambiratnam. D., and Y. Zhuge. (1996). Free vibration analysis of beams on elastic foundation. *Computers & Structures* , 60, 971-980.

Thambiratnam, D. (1997). *Analysis & design of buildings subjected to earthquakes*. Lecture notes, The structural Branch of The Institution of Engineers Australia, Barden Professional Centre, Brisbane.

Ticoalu, A., Aravinthan, T., & Cardona, F. (2010). A review of current development in natural fiber composites for structural and infrastructure Applications. *Proceedings of the Southern Region Engineering Conference*11-12 November 2010, Toowoomba, Australia.

Tracy, J.J., & Pardoen, G.C. (1992). Effect of delamination on the natural frequencies of composite laminates. *Journal of Composite Materials*, 23(12), 1200–1215.

Treviso, A., Mundo, D., & Tournour, M. (2017). Dynamic response of laminated structures using a refined zigzag theory shell element. *Composite Structures*, 159, 197-205.

Van Erp,G., Cattell, C., & Heldt, T. (2005). Fibre composite structures in Australia's civil engineering market: an anatomy of innovation *Progress in Structural Engineering Materials*, 7, 150-160.

Van Erp, G., Cattell, C., & Ayers, S. (2006). A fair dinkum approach to fibre composites in civil engineering. *Construction and Building Materials*, 20, 2-10.

Van Erp, G., and Rogers, D. (2008), A highly sustainable fibre composite building panel. In: *Proceedings of the International Workshop on Fibre Composites in Civil Infrastructure – Past, Present and Future*, University of Southern Queensland, Toowoomba, Queensland, Australia, December.

Van-Erp, G. (2010,). Commercialisation of fibre composites in Australia?s civil engineering market', paper presented to 21st Australasian Conference on the

Mechanics of Structures and Materials: Incorporating Sustainable Practice in Mechanics of Structures and Materials (ACMSM21), Melbourne.

Wang, J.T.S., Lin, Y.Y., & Gibby, J.A. (1982). Vibration of split beams. *Journal of Sound and* Vibration, 84 (4),491–520.

Wilson, E.L. (2002). *Three-dimensional static and dynamic analysis of structures*, Computers and Structures, Inc, Berkeley, California, USA.

Yam, L.H., Wie Z, Cheng ,Z., & Wong, W.O. (2004). Numerical analysis of multi-layer composite plates with internal delamination. *Computers and Structures*, 82, 627–637.

Zenkert, D. (1991). Strength of sandwich beams with interface debondings. *Composite Structures*, 17(4), 331-350.

Zhoudao, L.U., Lei, S.U., & Jiangtao, Y.U. (2011). Experimental Study on the Seismic Behaviour of Strengthened Concrete Column-Beam Joints by simulated earthquake. *Procedia Engineering*, 14, 1871-1878.

APPENDIX A

Table 1 Mass participation factors for the 128 modes considered for the reference building model

MODAL EXCITATION

Mode	Spectral Value	Excitation	Amplitude	Participation (%)
1	1.826785E+00	1.296172E+04	2.812133E+02	39.918
2	2.448255E+00	8.032792E+03	1.307523E+02	15.331
3	3.454157E+00	8.655314E+03	9.844828E+01	17.800
4	3.680000E+00	5.713739E+03	2.777435E+01	7.757
5	3.680000E+00	5.399504E+02	1.070807E+00	0.069
6	3.680000E+00	2.675332E+02	5.168769E-01	0.017
7	3.680000E+00	4.800862E+02	9.035400E-01	0.055
8	3.680000E+00	1.935832E+03	3.506618E+00	0.890
9	3.680000E+00	2.382891E+03	4.242908E+00	1.349
10	3.680000E+00	2.778795E+03	4.845093E+00	1.835
11	3.680000E+00	2.545862E+03	4.232540E+00	1.540
12	3.680000E+00	4.920571E+03	4.795455E+00	5.753

13	3.680000E+00	1.448950E+03	1.376041E+00	0.499
14	3.509060E+00	1.247230E+03	9.550781E-01	0.370
15	3.480764E+00	1.380913E+03	1.022221E+00	0.453
16	3.387237E+00	3.665589E+02	2.418906E-01	0.032
17	3.314619E+00	1.199064E+02	7.213534E-02	0.003
18	3.195870E+00	3.595274E+02	1.846820E-01	0.031
19	3.182371E+00	2.758268E+02	1.390862E-01	0.018
20	3.180019E+00	2.156216E+02	1.083759E-01	0.011
21	3.161742E+00	2.283648E+02	1.119131E-01	0.012
22	3.137922E+00	2.493807E+02	1.182077E-01	0.015
23	3.129528E+00	9.190106E+01	4.304906E-02	0.002
24	3.115560E+00	1.018283E+02	4.676403E-02	0.002
25	3.108429E+00	1.832227E+01	8.329323E-03	0.000
26	3.101617E+00	1.358635E+02	6.116486E-02	0.004
27	3.096584E+00	1.795199E+02	8.023741E-02	0.008
28	3.077290E+00	7.321814E+00	3.182661E-03	0.000

29	3.070756E+00	3.366304E+01	1.449447E-02	0.000
30	3.049738E+00	5.186653E+02	2.165620E-01	0.064
31	3.045672E+00	8.793717E+01	3.649785E-02	0.002
32	3.036341E+00	1.018758E+02	4.170404E-02	0.002
33	3.017223E+00	5.620476E+02	2.236248E-01	0.075
34	3.014424E+00	4.372263E+02	1.732343E-01	0.045
35	3.005547E+00	1.082531E+03	4.232313E-01	0.278
36	3.003192E+00	1.796816E+03	7.000034E-01	0.767
37	2.995603E+00	8.803566E+01	3.390610E-02	0.002
38	2.973927E+00	1.189368E+03	4.432065E-01	0.336
39	2.957821E+00	1.489470E+02	5.414589E-02	0.005
40	2.931171E+00	3.434224E+02	1.197719E-01	0.028
41	2.925463E+00	1.968299E+02	6.803404E-02	0.009
42	2.924216E+00	2.215658E+01	7.643387E-03	0.000
43	2.910632E+00	4.657921E+02	1.572745E-01	0.052
44	2.898623E+00	3.181395E+02	1.053873E-01	0.024

45	2.882174E+00	2.674461E+02	8.628816E-02	0.017
46	2.810921E+00	1.328117E+02	3.811135E-02	0.004
47	2.779535E+00	1.204249E+03	3.276615E-01	0.345
48	2.741417E+00	3.725631E+00	9.489447E-04	0.000
49	2.699961E+00	2.695748E+02	6.379038E-02	0.017
50	2.678539E+00	1.492465E+03	3.397245E-01	0.529
51	2.664825E+00	3.787191E+02	8.406717E-02	0.034
52	2.618977E+00	1.835127E+02	3.739028E-02	0.008
53	2.589559E+00	7.648317E+02	1.472856E-01	0.139
54	2.583819E+00	2.057311E+03	3.917923E-01	1.006
55	2.568843E+00	9.568065E+02	1.769554E-01	0.218
56	2.564089E+00	2.929876E+02	5.368137E-02	0.020
57	2.519298E+00	1.823403E+02	3.053993E-02	0.008
58	2.501613E+00	1.027505E+02	1.659661E-02	0.003
59	2.463323E+00	9.341456E+00	1.392589E-03	0.000
60	2.444846E+00	5.301812E+01	7.597254E-03	0.001

61	2.423249E+00	2.163019E+02	2.957311E-02	0.011
62	2.414607E+00	1.484990E+03	1.992047E-01	0.524
63	2.406420E+00	5.064575E+02	6.671762E-02	0.061
64	2.399991E+00	1.026517E+01	1.333031E-03	0.000
65	2.388495E+00	5.151866E+01	6.519712E-03	0.001
66	2.381464E+00	3.003670E+01	3.741162E-03	0.000
67	2.381204E+00	2.868015E+01	3.570096E-03	0.000
68	2.377043E+00	2.122217E+01	2.616856E-03	0.000
69	2.369841E+00	9.733426E+01	1.180618E-02	0.002
70	2.366830E+00	5.195433E+01	6.258429E-03	0.001
71	2.360042E+00	1.253205E+01	1.486190E-03	0.000
72	2.357499E+00	1.762748E+01	2.078205E-03	0.000
73	2.355537E+00	1.241480E+02	1.457012E-02	0.004
74	2.353092E+00	9.707622E+01	1.132845E-02	0.002
75	2.340706E+00	2.406058E+02	2.727693E-02	0.014
76	2.337530E+00	3.059991E+02	3.443224E-02	0.022

77	2.336472E+00	1.136685E+02	1.275857E-02	0.003
78	2.329026E+00	4.176765E+02	4.606310E-02	0.041
79	2.322360E+00	3.676673E+02	3.990971E-02	0.032
80	2.320314E+00	7.214014E+02	7.792512E-02	0.124
81	2.318303E+00	2.893773E+02	3.110821E-02	0.020
82	2.308000E+00	1.810726E+02	1.898874E-02	0.008
83	2.295300E+00	1.694969E+02	1.723439E-02	0.007
84	2.292292E+00	3.120519E+01	3.149646E-03	0.000
85	2.285371E+00	8.661803E+01	8.595105E-03	0.002
86	2.281467E+00	8.693051E+01	8.543277E-03	0.002
87	2.279113E+00	7.616109E+01	7.441335E-03	0.001
88	2.274667E+00	1.194597E+01	1.154351E-03	0.000
89	2.271133E+00	7.211530E+01	6.907378E-03	0.001
90	2.269715E+00	1.467054E+01	1.400206E-03	0.000
91	2.263121E+00	8.439981E+01	7.923135E-03	0.002
92	2.259601E+00	3.135460E+02	2.917433E-02	0.023

93	2.257858E+00	5.416627E+02	5.017808E-02	0.070
94	2.254977E+00	5.414915E+02	4.979733E-02	0.070
95	2.249882E+00	6.711375E+01	6.092522E-03	0.001
96	2.245240E+00	9.745612E+01	8.742644E-03	0.002
97	2.243147E+00	1.563111E+02	1.394738E-02	0.006
98	2.236592E+00	3.978275E+01	3.490348E-03	0.000
99	2.235540E+00	2.758505E+02	2.413609E-02	0.018
100	2.228462E+00	2.163414E+02	1.858484E-02	0.011
101	2.224609E+00	1.099594E+02	9.351668E-03	0.003
102	2.220649E+00	7.594958E+02	6.392629E-02	0.137
103	2.215374E+00	2.169916E+02	1.801247E-02	0.011
104	2.212131E+00	7.776678E+01	6.400371E-03	0.001
105	2.208395E+00	3.752261E+02	3.057780E-02	0.033
106	2.204444E+00	1.812321E+02	1.461452E-02	0.008
107	2.202538E+00	1.387915E+02	1.113536E-02	0.005
108	2.196904E+00	2.319005E+01	1.832696E-03	0.000

109	2.195797E+00	3.065893E+02	2.415766E-02	0.022
110	2.194939E+00	1.332885E+02	1.047822E-02	0.004
111	2.187772E+00	1.088695E+02	8.394562E-03	0.003
112	2.183889E+00	1.478786E+01	1.128281E-03	0.000
113	2.180933E+00	1.384587E+02	1.047935E-02	0.005
114	2.175550E+00	5.471666E+01	4.080716E-03	0.001
115	2.170117E+00	5.631530E+02	4.137622E-02	0.075
116	2.159382E+00	2.127157E+02	1.517009E-02	0.011
117	2.155043E+00	5.606906E+01	3.950401E-03	0.001
118	2.146117E+00	1.510460E+02	1.037791E-02	0.005
119	2.142431E+00	1.793907E+02	1.219726E-02	0.008
120	2.137722E+00	1.462470E+02	9.811260E-03	0.005
121	2.136784E+00	5.114969E+01	3.422289E-03	0.001
122	2.131821E+00	2.254999E+02	1.487451E-02	0.012
123	2.129111E+00	3.284127E+02	2.149465E-02	0.026
124	2.127100E+00	1.858604E+02	1.209419E-02	0.008

125	2.124596E+00	2.428951E+02	1.569149E-02	0.014
126	2.123311E+00	1.211642E+02	7.798334E-03	0.003
127	2.117800E+00	7.124103E+02	4.512283E-02	0.121
128	2.112923E+00	2.096543E+02	1.309099E-02	0.010

TOTAL MASS PARTICIPATION 99.432%